

**Impact of Particle Morphology on the
Rheology of PCC-Based Coatings**

A Thesis
Presented to
The Academic Faculty

By

Enrique Michel-Sanchez

In Partial Fulfillment
Of the Requirements for the Degree
Master of Paper Science Engineering in the
School of Chemical and Biomolecular Engineering

Georgia Institute of Technology
August 2005

Impact of Particle Morphology on the Rheology of PCC-Based Coatings

Approved by:

Dr. Victor Breedveld
School of Chemical and Biomolecular Engineering
Georgia Institute of Technology

Dr. Timothy Patterson
School of Mechanical Engineering
Georgia Institute of Technology

Dr. Yulin Deng
School of Chemical and Biomolecular Engineering
Georgia Institute of Technology

Dr. Cyrus Aidun
School of Mechanical Engineering
Georgia Institute of Technology

Date approved: April 29, 2005

To GOD, the owner of my life and the
light that guides me everyday

To my beloved parents, brother, and sister
Alfredo, Lupita, Alfredo, and Gaby
Thank you for your love and support, you make me want to be better

To my beloved grandma Josefina a treasure that I have the privilege to have and to my
grandparents Enrique, Alfredo, and Hortensia
You are always in my heart

To my friend Sharon
You brightened my life

ACKNOWLEDGEMENTS

My experience at Georgia Tech has been excellent because of the great professionals I have met and worked with. They all have different visions, thus, ways of thinking that have provided me with a rich academic and social atmosphere. I had the great opportunity of learning from them. I want to thank my advisors, Dr. Victor Breedveld and Dr. Tim Patterson, for all the guiding, dedication, and hard work they put into my project. Also, my appreciation to the Institute of Paper Science and Technology for the graduate fellowship that made possible my studies.

Special thanks to my friends and two of the most brilliant chemical engineers I have met, Dr. Raymond Tu and future doctor Jun Sato, for all the helpful teaching and discussions. Also thanks to the complex fluids research group Ryan, Katie, Tori, Byron, Haris, and Jae Kyu.

Thanks to Dr. Yulin Deng, Dr. Cyrus Aidun, Michael Schaepe, Kennisha Collins, Tuwanda Strowbridge, and Andy De Maio for their expertise and technical support in crucial stages of my research. Thanks to my friend and awesome former officemate Susan Fernandez for all her support and advice during the writing of my thesis.

All my appreciation to my friends that made my life at Atlanta an enjoyable great experience during both, good and tough moments, thanks to Sigi, Mike, Alexs, Faram, Ritika, Rocio, Katie, Jacobo, Luz, Ana, Eduardo, Charlene, Jun, Elise, and Ray.

TABLE OF CONTENTS

Acknowledgements	iv
List of Tables	viii
List of Figures	ix
Summary	xiv
Chapter 1 Introduction	1
1.1 Innovation Opportunity	2
1.2 Research Description	4
Chapter 2 Background	6
2.1 Coating Process Description	6
2.1.1 Factors Affecting the Run-ability of a Coating Operation	7
2.1.2 Improvement Opportunities by Manipulating Coating Rheology	8
2.2 Rheology	9
2.2.1 Rheological definitions	9
2.2.2 Measurements: Flow-Curves Qualitative Features	11
2.2.3 Models	13
2.2.3.1 Einstein/Batchelor for Suspensions	13
2.2.3.2 Krieger-Dougherty for Concentrated Suspensions	14
2.2.4 Rheology of Paper Coatings: Characteristic Shear Rates	15
2.3 Coating Formulations	15
2.3.1 Pigments	16
2.3.1.1 Kaolin	18

2.3.1.2	Precipitated Calcium Carbonate	20
2.3.2	Binders	23
2.3.2.1	Binding Strength	25
2.3.2.2	Binder Demand	26
2.3.2.3	Natural Binders	27
2.3.2.4	Synthetic Binders	31
2.3.3	Additives	33
2.4	Flow Behavior	35
2.4.1	Main Factors Affecting Coating Rheology	38
2.4.1.1	Particle Size	38
2.4.1.2	Particle Shape	41
2.4.2	Interactions between the Coating Components	43
Chapter 3	Objective	45
Chapter 4	Materials and Methods	47
4.1	Coating Formulation Used for the Experimental	47
4.2	Experimental Program	54
4.3	Rheometry	56
4.4	Procedure for Rheological Data Collection	62
4.5	Coated Paper Testing	64
Chapter 5	Results and Discussions	71
5.1	Coating flow-curves	68
5.2	Viscosity of Coating Mixtures with Pigments of Same Shape	72
5.3	Viscosity of Coating Mixtures with Pigments of Different Shape	84

5.4 Paper Testing Results	95
5.5 Results Modeling	99
Chapter 6 Conclusions	107
Chapter 7 Future Research	109
References	113

LIST OF TABLES

Table 2.1	Values of C.P.V.C. for Different Pigments	27
Table 4.1	Pigments Used in tested Coating Formulations	48
Table 4.2	Single Pigment Coatings Preparation	52
Table 4.2	(Continued) Single Pigment Coatings Preparation	53

LIST OF FIGURES

Figure 2.1	Coating Process and its Four Sections	6
Figure 2.2	Description of Equation 2.1	10
Figure 2.3	Scheme of Types of Rheometers: Measurements and Geometries	11
Figure 2.4	Flow-Curves of the Different Flow Behaviors	12
Figure 2.5	Qualitative Feature of a Flow-Curve	13
Figure 2.6	SEM Image of Calcite PCC Pigment	21
Figure 2.7	SEM Image of Aragonite PCC Pigment	21
Figure 2.8	Synthetic Latex Binding Resin Particles	24
Figure 2.9	Molecular structure of Amylose (top) and Amylopectin (bottom)	28
Figure 2.10	Hydroxyl-ethyl Ether of Starch	30
Figure 2.11	Attraction and repulsion Forces Between Particles	37
Figure 2.12	A Schematic Diagram of Viscosity as a Function of Shear Rate for Suspensions with Different Particle Sizes	39
Figure 2.13	Relative Viscosity for Volume Fractions of Uni-modal, Bi-modal, and Tri-modal Systems	40
Figure 2.14	Effect of the Relative Amount of Large Particles in a Bimodal Suspension Containing 0.68 and 0.21 μm Particles, on the Viscosity at a Shear Stress Level of 1.0 dyn/cm	41
Figure 2.15	Viscosity as a Function of Volume Fraction for Different Particles Geometries	42

Figure 4.1	SEM of PCC Pigments	49
Figure 4.2	Base Fluid of Experimental Coating Formulation at 20 °C	51
Figure 4.3	Scheme for the Combination of Coatings Based on Pigments with Same Shape but Different Particle Size	55
Figure 4.4	Scheme for the Combination of Coatings Based on Pigments with Different Shape and Different Particle Size	56
Figure 4.5	Cone and Plate and Couette Cylinders	57
Figure 4.6	Cone and Plate: Flow-curves for Different Time Settings at 23.5 °C	59
Figure 4.7	Couette Cylinders: Flow-curves for Different Time Settings at 23.5 °C	59
Figure 4.8	Hysteresis of Cone and plate vs Couette Cylinders	61
Figure 4.9	Three Experimental Runs for the Opacarb:Albagloss XL 90:10 Coating and Data Points Selection at Two Different Shear Rates Relevant to the Industry	63
Figure 4.10	Three Roll Super-Calender Used for the Experiments	65
Figure 5.1	Flow-Curves for each Single Pigment Coating from Low to High Shear Rates (0.001 to 3000 s ⁻¹)	69
Figure 5.2	Flow-Curves for Albagloss S (0.6 μm) and Albagloss XL (2.4 μm) Coatings	71
Figure 5.3	Relative Viscosity for Albagloss S: Albagloss XL combination at 1.73 s ⁻¹ for the Three Experimental Runs	73
Figure 5.4	Relative Viscosity for Albagloss S: Albagloss XL combination at 1420 s ⁻¹ for the Three Experimental Runs	74
Figure 5.5	Reproducibility of the First Experimental Run for Albagloss S: Albagloss XL at 1.73 s ⁻¹	74

Figure 5.6	Reproducibility of the First Experimental Run for Albagloss S: Albagloss XL at 1420 s^{-1}	75
Figure 5.7	Relative Viscosity for Albagloss S: Albagloss M combination at 1.73 s^{-1} for the Three Experimental Runs	75
Figure 5.8	Relative Viscosity for Albagloss S: Albagloss M combination at 1420 s^{-1} for the Three Experimental Runs	76
Figure 5.9	Reproducibility of the First Experimental Run for Albagloss S: Albagloss M at 1.73 s^{-1}	76
Figure 5.10	Reproducibility of the First Experimental Run for Albagloss S: Albagloss M at 1420 s^{-1}	77
Figure 5.11	Comparison of Relative Viscosity of Silica Particles Suspension at 50 vol. % with Average Sizes 0.6 and $0.85 \mu\text{m}$ and PCC Albagloss S and M Suspension at 48 vol.% with Average Sizes 0.6 and $1.0 \mu\text{m}$ at 1000 s^{-1}	79
Figure 5.12	Comparison of Fluidity limit and Dry Random-Close-Packing Fraction for Bidisperse Suspensions with Particle Size Ratios of 2:1 and 4:1	81
Figure 5.13	Absolute Viscosity of Albagloss S: Albagloss M Coating (blue triangles) and Albagloss S: Albagloss XL Coating (red squares) at 1420 s^{-1} for the First Experimental Run	82
Figure 5.14	Hysteresis in the Third Experimental Run for the Two Pigment Combinations of Different Size at 1420 s^{-1}	83
Figure 5.15	Relative Viscosity for Opacarb : Albagloss XL combination at 1.73 s^{-1} for the Three Experimental Runs	84
Figure 5.16	Relative Viscosity for Opacarb : Albagloss XL combination at 1420 s^{-1} for the Three Experimental Runs	85

Figure 5.17	Reproducibility of the First Experimental Run for Opacarb : Albagloss XL at 1.73 s^{-1}	85
Figure 5.18	Reproducibility of the First Experimental Run for Opacarb : Albagloss XL at 1420 s^{-1}	86
Figure 5.19	Relative Viscosity for Opacarb : Albagloss S combination at 1.73 s^{-1} for the Three Experimental Runs	86
Figure 5.20	Relative Viscosity for Opacarb : Albagloss S combination at 1420 s^{-1} for the Three Experimental Runs	87
Figure 5.21	Reproducibility of the First Experimental Run for Opacarb : Albagloss S at 1.73 s^{-1}	87
Figure 5.22	Reproducibility of the First Experimental Run for Opacarb : Albagloss S at 1420 s^{-1}	88
Figure 5.23	Absolute Viscosity of the Four Pigments Coatings Combinations in the First Experimental Run at 1420 s^{-1}	90
Figure 5.24	Hysteresis for the Third Experimental of Two Pigment Coating Combinations of Different Shape and Size at 1420 s^{-1}	91
Figure 5.25	Absolute Viscosity of the Coatings at 1.73 s^{-1}	93
Figure 5.26	Absolute Viscosity of the Coatings at 1420 s^{-1}	93
Figure 5.27	Decrease in Viscosity by Using Opacarb / Albagloss XL (90/10) Combination	94
Figure 5.28	Decrease in Viscosity by Using Albagloss S / Albagloss XL (90/10) Combination	94
Figure 5.29	Glossiness test	95
Figure 5.30	Roughness Test	96

Figure 5.31	Porosity Test	96
Figure 5.32	ISO-Brightness	97
Figure 5.33	Comparison between the observed relative viscosity and predicted values from the Farris and D’Haene and Mewis model for 50 vol% bidisperse silica suspensions containing 0.6 and 0.85 μm silica particles at a shear rate level of 1000 s^{-1} at $25 \text{ }^\circ\text{C}$	99
Figure 5.34	Ratio of Absolute Viscosities of Opcarb:AlbaglossXL and Albagloss S and Albagloss XL at Two Different Shear Rates	103
Figure 5.35	Model for the Prediction of Viscosity Values at Volume Fraction of 0.48 at 1420 s^{-1}	105
Figure 5.36	Model for the Prediction of Viscosity Values at Volume Fraction of 0.48 at 1.73 s^{-1}	106
Figure 7.1	MD1074 PCC	111
Figure 7.2	Immobilization Cell from Paar Physica	112

SUMMARY

The impact of particle size, size distribution, and shape on the rheology of precipitated calcium carbonate (PCC) based coatings was studied. Evaluating the interactions between different particles sizes and shapes leads to a better understanding of the packing fraction of PCC. High packing fraction is desirable because of the positive impact on the fluidity of suspensions. Suspensions with higher levels of fluidity can potentially load larger amounts of solids while keeping low viscosities. In the paper coatings industry, high solids suspensions are key factors to improve the efficiency, and thus, the business profitability. Common issues in this sector are the high energy consumption and coating machine down-time caused by coatings formulations with high viscosities and low volume fraction of solids. To address this issue, PCC pigments of different sizes and shapes were mixed in different ratios to find mixtures with higher packing fractions that could result in coatings with lower viscosity. Two of the coatings combinations yield interesting behaviors when 90% by weight of small particles are mixed with 10% of large particles. Viscosity decreased by approximately 50% in some cases in comparison to the formulation with 100% of small particles. By testing the dry coating, it is suggested that the coatings presenting the most dramatic changes in viscosity also have the highest packing fractions. Future research related to investigating the packing fractions of coatings with different PCC pigments in more detail and modeling coating rheology as a function of solids volume fractions is discussed.

CHAPTER 1

INTRODUCTION

Industries are in the continuous search for more profitable business areas or processes. A company can achieve this by investing either in technology or in new markets. Along these lines, the paper industry is looking for new products and ways to improve existing ones. The paper coating industry could be one of the most profitable business units of the paper industry after the tissue business. This is because of the added-value in their final products. The principal added-value is the improvement of printing properties (smoothness, absorbance, porosity) and optical properties (brightness, color, gloss) due to surface coating, for example for printed board, magazine, photographic, wrapping, and wallpaper. The other role of paper coatings is as protective agents. The food industry uses wax as a coating for the packaging of fresh meat and fish in order to prevent the wetting of the board box. This represents a recycling problem, because the wax is not easily removed from the fibers and any wax that remains in the process will degrade future paper quality. A water-repellant functionalized coating could help to solve this problem. However, these applications are not specifically considered in the current work.

In recent years, the performance of the paper coating industry has been below that of many other industries. The industry's average return on assets was about four percent in the early to mid nineties.¹ Investors have others investment opportunities that provide

better returns at considerably less risk. The paper coating industry can be made more attractive to investors by implementing new technology or by improving existing processes to increase productivity and thus decrease the manufacturing cost. However, implementing new technology, in particular coating machines that are able to coat paper at higher speeds, is capital-intensive and does not necessarily provide a solution to the underlying technological issues. These issues include paper rupture due to high machine speeds, high energy consumption, and long coating deposition times due to viscous coatings formulations. The general goal of this project is to investigate and improve the coating process by focusing not on where the problem occurs (the machine) but on where the problem arises: the coating formulation and its flow properties.

In the paper industry, coating formulations are considered trade secrets, because the same components can give rise to very different product properties depending on their relative amounts, physical properties, and mixing order. A typical coating formulation has three components: pigments, binders, and additives. The interactions between these components are at the root of many problems with the coating machine run-ability. By systematically studying the flow properties of coating formulations, this study aims to provide new insight into the nature of these interactions, and ultimately improve the properties of coatings formulations.

1.1 Innovation opportunity

How can coating-flow behavior influence the manufacturing cost of the process? Many factors affecting the process profitability can be correlated directly with flow phenomena.

First, when the paper breaks on the coater because of its high coating speed, there is a delay while the process is re-started. This downtime results in decreased plant productivity and directly affects the manufacturing cost. Why does the paper break on the coater? In all coating technologies (blade, rod, air-knife coaters, etc...), there is a dramatic deformation of the coating in the application section due to a sudden change in flow speed. From an almost stationary state, the coating is accelerated to the speed of the paper web in the coater, which can be greater than 1500 m/min. When the viscosity of the coating formulation is high, the fluid cannot deform fast enough to spread the coating evenly across the paper surface, eventually causing sheet failure due to fluid accumulation between the coating device and the paper surface. A high viscosity coating requires an increase in the deposition time and thus a decrease in the machine speed. Secondly, the principal source of energy consumption in a coating facility is the drying section, where the remaining water in the coated paper is removed. A typical coating formulation contains 35 percent of water by weight. If the amount of pigment solids can be increased, the water content decreases, so that the drying section requires less energy. Can the amount of water in coating formulations be decreased without affecting their flow behavior? The viscosity of a suspension depends to a large degree on the particles in the suspension. Favorable interactions between particles could lead to a higher maximum packing fraction with less void space between particles. The maximum packing fraction and interactions between pigment particles can be used to manipulate the coating viscosity. In summary, the interactions between the different components in a coating formulation determine the coating viscosity and play a key role in the coating process. As a consequence, there are opportunities to improve the process efficiency and

productivity, and therefore manufacturing cost, by focusing on the flow properties and composition of coating formulations. This work characterizes the effect of particle properties on the flow behavior of various coating formulations. Rheology is used as the main characterization technique.

1.2 Research Description

The purpose of this systematic rheological study was to assist the paper coating industry in optimizing their processes by evaluating the interactions between different pigment sizes, size distributions (PSD), and shapes in coating formulation. Different particles sizes and shapes with narrow PSD, that are currently available in the industry, were examined by evaluating their effects on both coating rheology and coated paper properties. Finally, pigment geometry combinations were evaluated to optimize the rheology for coating applications.

Our study used materials which are available from coating suppliers and therefore the results should correlate with what would be expected in an industrial implementation. The pigment raw material included calcite and aragonite precipitated calcium carbonate (PCC). Aragonite PCC of a rhombohedra shape with aspect ratio of 3 to 4, and calcite PCC with an ovoid shape of low aspect ratio ~ 1.5 . Calcite PCC has a size of ($D_{50}=0.4 \mu\text{m}$) and Aragonite has three sizes: $D_{50}=0.6 \mu\text{m}$, $D_{50}=1.0 \mu\text{m}$, and $D_{50}=2.0 \mu\text{m}$ respectively. Most notably most of the used materials (pigments) are available, thus allowing for immediate implementation of this technology in the coatings industry.

A more detailed explanation of coating processes, coating rheology, and coating formulations will be given in Chapter 2. In Chapter 3, the objectives of our research are formulated. Procedures, equipment and materials specifications are provided in Chapter 4. Chapter 5 presents the results and detailed discussion of the rheological data for the various coating formulations, as well as analysis of coated paper properties for selected coating formulations. Chapter 6 offers suggestions on pigment combinations that optimize the rheological behavior suitable for coating operations. Finally, in Chapter 7, research ideas are presented that could be expanded or developed based on this study.

CHAPTER 2

BACKGROUND

2.1 Coating Process Description

Paper coatings improve the printing properties of paper substrates and can be used as protective agents. The added-value of paper coatings comes from the formation of a smoother, glossier, brighter, and more opaque paper surface. In a regular coating process, the ratio of base-stock paper to coating is 80:20 in terms of weight. The coating can be deposited on one or both sides of the base-sheet.

A coating process typically includes four sections: application, metering, drying, and super-calendering. Figure 2.1 shows a basic coating process.

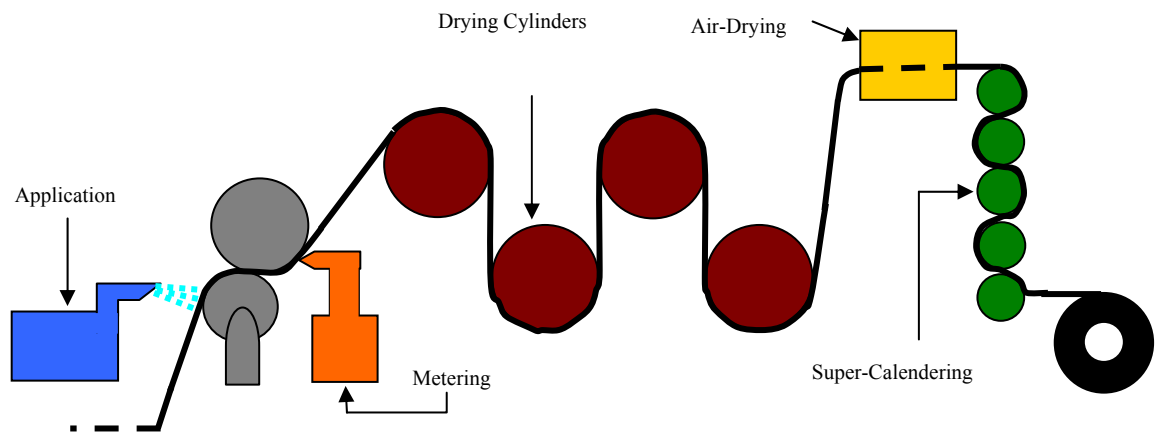


Figure 2.1 Coating Process and its Four Sections

In the application section, the coating is deposited on the paper surface. Three application systems predominate: single-roll, two-roll, and three roll. The most prevalent, single-roll, rotates in the web direction at 10 to 40 % of the web speed, picking up a controlled amount of coating and applying it in excess to the web. The web speed is usually in the range of 1500 to 3000 m/min.² The metering section follows the application section. The metering section regulates the amount of coating that is applied to the paper using one of three possible devices: metering blade, air-knife, or rod coater. For example, in a blade coater, the blade forms a nip with the backing roll. As the sheet passes through this nip, the pressure exerted on the blade is used to regulate the amount of coating that is metered off. Excess coating is recycled to the application section. The drying cylinders remove most of the water in the coating formulation by direct contact with a hot surface. The air-drying section removes most of the remaining moisture in the coated paper. The last phase of a coating process is the super-calendering section which gives a glossier and smoother finishing to the paper surface by reducing the roughness of the paper. In the super calendering step, pressure is applied to the coated paper between rolls with and extremely smooth surfaces, some of which are heated. The result is compression of the sheet and coating layer which re-aligns coating particles and densifies thicker sections of the web to produce a sheet of uniform thickness and surface roughness.

2.1.1 Factors Affecting the Run-Ability of a Coating Operation

Run-ability refers to the smoothness of a coating operation, i.e. the ease with which the productivity and product quality can be maintained. Poor run-ability is characterized by a large number of sheet breaks, poor product quality, and high energy consumption.⁴ A

variety of factors produce machine-related problems, for example web breaks, scratches, and loss of coat-weight profile.³ Those factors can be correlated with the base-stock paper characteristics (porosity, roughness, sizing degree, etc...), and the application method (rolls, blade, etc...). However, the main factors affecting run-ability arise from the coating formulation itself: rheology, solids content, and water retention.

2.1.2 Improvement Opportunities by Manipulating Coatings Rheology

Paper coatings have complex rheological characteristics. This is due to the presence of solid particles (pigments) at high volume concentrations and the interactions that occur between coating components.⁴ Coating formulations can be manipulated to optimize their flow characteristics and improve machine run-ability. For example, as machine speed increases, poor run-ability manifests itself as blade bleeding, the accumulation of coating in the metering section of the coating process.⁵ This occurs when the viscosity of the coating is too high and the coated layer does not deform fast enough, producing poor deposition and accumulation on the blade. By decreasing the viscosity of the coating, web breaks can generally be avoided.

The drying section of a coating machine is the portion consuming most of the energy in the process. Drying time can be decreased by decreasing the amount of water in the wet coating formulation. However, high solids loads generally lead to high viscosity, which can adversely affect machine run-ability as explained above. Therefore, the goal would be to achieve higher solids loads while maintaining a low viscosity. Also, lower viscosity fluids provide an energy savings by reducing pumping power.

2.2 Rheology

Most industrial processes that involve fluids use rheology as a characterizing tool. Besides characterization, it can be used as an optimization tool to determine the fluid characteristics that will make the process run smoother, and more efficiently.

2.2.1 Rheological Definitions

Rheology is the science that studies the deformation and flow of matter. The important mechanical properties routinely evaluated or manipulated are viscosity and elasticity. An elastic material is capable of storing energy while a viscous material dissipates it into heat. All materials have a viscous and an elastic modulus. Temperature and time affect rheology. Most fluids become less viscous when exposed to higher temperatures, and the time-scale associated with the energy dissipation decreases. Glass has a long time-scale of deformation (hundreds of years). In comparison to glass, paper coatings have an extremely short deformation time scale.

Viscosity is the flow resistance of a fluid due to frictional forces between molecules.⁶ The more viscous a fluid is the more resistance it shows to flow. Viscosity is simply defined as:

$$\eta = \frac{\tau}{\dot{\gamma}} [=] Pa \cdot s \quad (2.1)$$

where τ is the shear stress and $\dot{\gamma}$ is the shear rate. Kinematic viscosity is the ratio of the shear viscosity to the density of the fluid, ρ , and is sometimes used as well:

$$v = \frac{\eta}{\rho} \left[\frac{m^2}{s} \right] \text{ (or Stokes)} \quad (2.2)$$

The principle for measuring viscosity is as follows: in a well-defined geometry, a known deformation is applied and the required force measured (controlled strain) or a known force is applied and the resulting deformation measured (controlled stress)

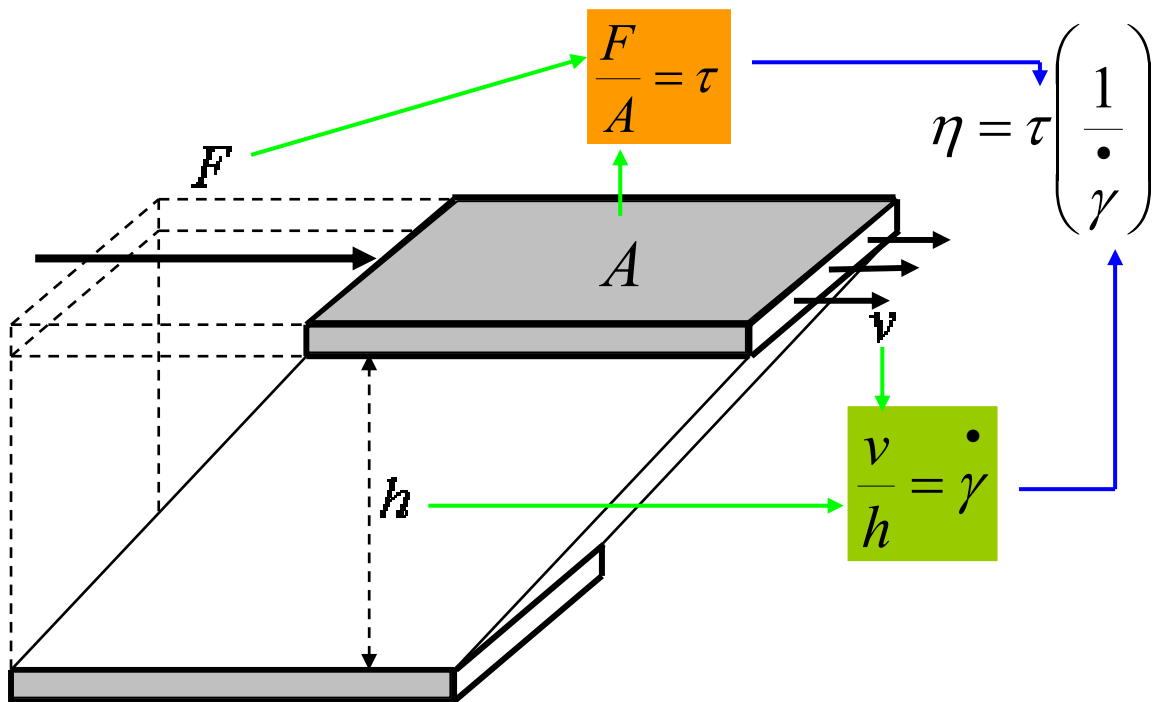


Figure 2.1 Description of Equation 2.1

The simplest flow geometry is the flow between infinite parallel plates. In rotational rheometers this simple shear flow can be mimicked with a variety of geometries, i.e., plate-and-plate, cone-and-plate, and Couette cylinders. Capillary viscometers are very useful to measure viscosity at high shear rates.

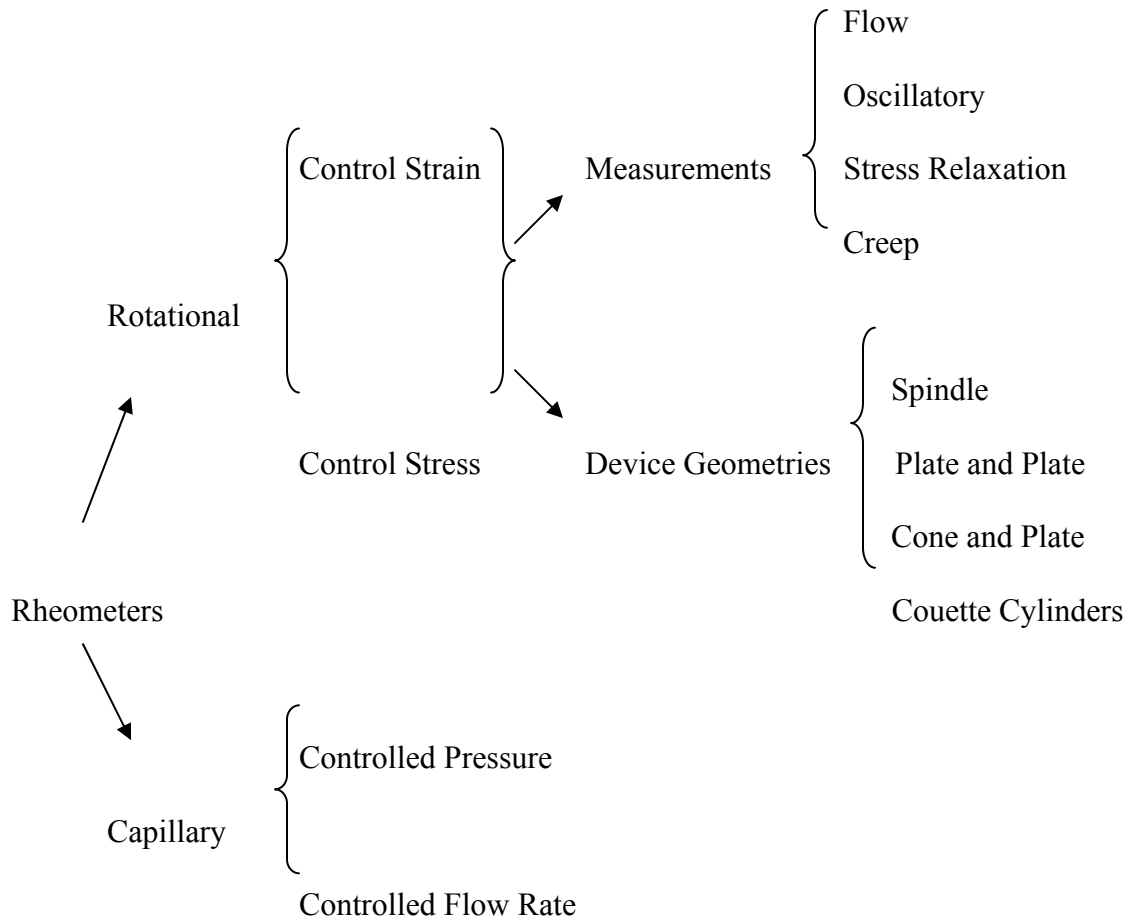


Figure 2.2 Scheme of Types of Rheometers: Measurements and Geometries

2.2.2 Measurements: Flow-Curves Qualitative Features

Flow-curves are used to present data from rheological measurements. Flow-curves show viscosity data (Y-axis) against shear rate (X-axis), usually on a logarithmic scale. By analyzing these kinds of graphs, fluid behavior at different shear rates can be investigated. Figure 2.4 shows different classes of typical flow behavior exhibited by coating components or coating formulations. For example, water is a Newtonian fluid, its viscosity being constant regardless of the shear rate applied; the other components of a

coating are usually non-Newtonian, meaning that they can show a shear-thinning (pseudo-plastic), shear thickening (dilatant), or Bingham plastic behavior. Figure 2.4 shows these behaviors.

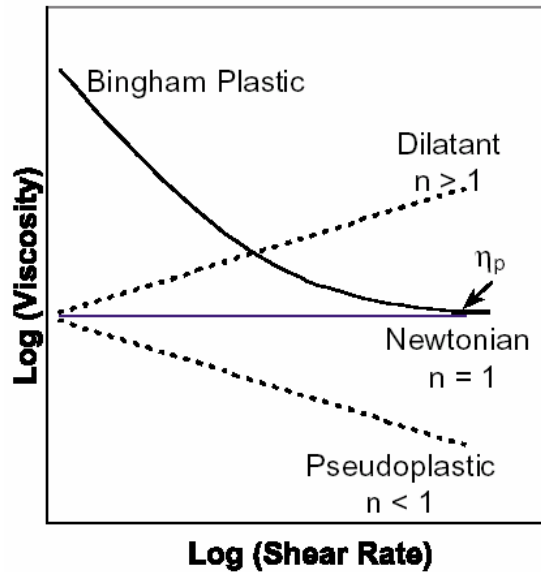


Figure 2.3 Flow-Curves of the Different Flow Behaviors²

The qualitative features of a flow-curve for a typical coating are shown in Figure 2.5: (1) Low-shear plateau, usually found at low shear rates. (2) Shear-thinning behavior due to alignment of particles in the flow. (3) High-shear plateau, usually occurs because the particles in the suspension are well-aligned. (4) Shear thickening behavior at very high shear rates. Shear thickening occurs because particles that are aligned in layers start to become disoriented and therefore interact with neighboring layers, which produces a sudden rise of viscosity.

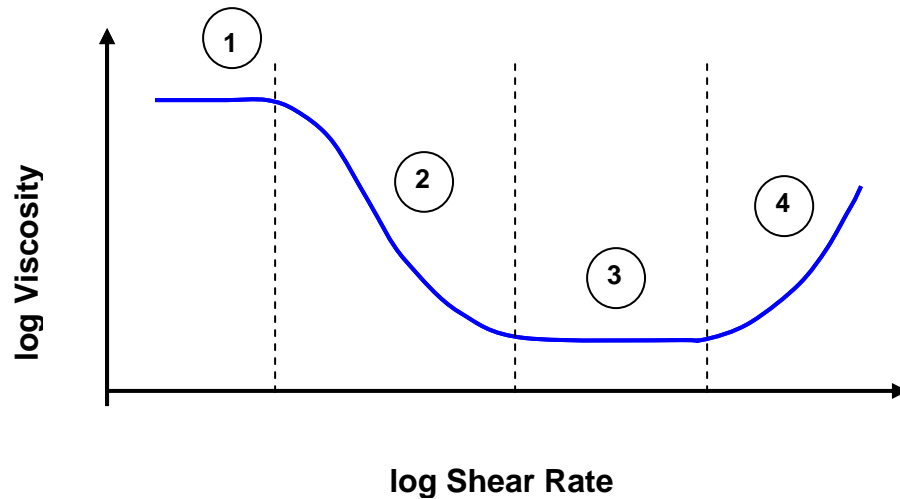


Figure 2.4 Qualitative Feature of a Flow-Curve

2.2.3 Models

2.2.3.1 Einstein/Batchelor for Suspensions

In dilute suspensions of hard spheres, it is well-known that viscosity depends only on the volume fraction of the particles. A suspension is considered dilute when the distance between the particles in suspension is larger than the average mean free path due to Brownian motion of a single particle. Einstein⁷ derived the following relation between suspension viscosity and particle volume fraction at zero shear rate:

$$\frac{\eta_o}{\eta} = 1 + 2.5\varphi \quad (2.3)$$

where η_o is the zero-shear viscosity of the suspension, η is the viscosity of the suspending fluid, and φ is the volume fraction of the particles. The ratio of the viscosity of the suspension to the viscosity of the base fluid is called relative viscosity. Einstein's equation can be used in suspensions having solids volume fractions of up to 0.1.

Batchelor⁸ derived an extension of Einstein's equation. He added a term to account for the hydrodynamic interactions between particles and the direct and indirect contributions to the bulk stress due to Brownian motion. In magnitude, these contributions are of the order of ϕ^2 . The Einstein-Batchelor equation is therefore valid for suspensions having solids volume fractions up to 0.20:

$$\eta_{rel} = \frac{\eta_o}{\eta_s} = 1 + 2.5\phi + 6.2\phi^2 \quad (2.4)$$

Paper coating formulations are highly concentrated suspensions with volume fractions above 0.40, but the Einstein-Batchelor equation tells us that there is a direct relation between viscosity and volume fraction. This is also true at higher coating concentrations, but more complicated models must be used.

2.2.3.2 Krieger-Dougherty for Concentrated Suspensions

For the paper coatings industry, a useful model is the Krieger-Dougherty equation for medium-to-high concentrated suspensions, which relates the viscosity of a suspension to a maximum packing fraction (volume fraction) of the particles:

$$\eta_{rel} = \frac{\eta_o}{\eta_s} = \left(1 - \frac{\phi}{\phi_m}\right)^{-2} \quad (2.5)$$

where ϕ_m is the maximum volume fraction that varies according to particle geometry. This parameter is a function of particle size distribution and particle deformability as well as flow conditions.⁹ The Krieger-Dougherty equation has been found to be valid for a wide range of shear rate.

2.2.4 Rheology of Paper Coatings: Characteristic Shear Rates

In the paper coating process, the coating formulation experiences a range of shear rates during common handling and process steps:

- From 0.1 to 1000 s⁻¹, low to moderate shear rate. Storage, pumping, and mixing operations take place in this range. Typical time scales range from a few seconds to several minutes. In Figure 2.5, zone 1 and 2 describe the flow behavior in this range where low shear plateau and shear-thinning behavior are commonly observed.
- From 1000 to 100 000 s⁻¹, moderate to high shear rates. Application of paper coating on the base-stock. This process lasts a few milliseconds. In Figure 2.5, zone 3 represents the high-shear plateau in this shear rate regime.
- From 100 000 to 2 000 000 s⁻¹, high to ultra-high shear rates. Process during final metering of the coating. Duration is very short, on the order of few microseconds.² Zone 4 in Figure 2.5 shows the potential behavior at these high and ultrahigh shear rates.

2.3 Coating Formulations

Paper coatings have three distinctive groups of components: pigments, binders, and additives. Any mixture not containing one of these elements is not a true paper coating,

although it can be used as a size press solution, water box solution, or a wash coat.¹⁰ The purpose of a coating is to provide a functional surface that will enhance the performance of the product.¹¹

A typical coating formulation will have 100 parts of pigment, 5-20 parts of binder, and 1-10 parts of additives by dry weight. Depending on the amount and type of each component in the coating formulation, the coated paper will have different final characteristics: brightness, smoothness, glossiness, and opacity. The brightness, opacity, and smoothness of a coated paper will mostly depend on the pigment and additives while the binders have a greater impact on the strength and glossiness.

Dry solids contents in coating formulations prior to application can be up to 70 percent by weight, the rest being water. The amount of dry solids is limited by the packing efficiency of the pigment particles. Each coating formulation has a maximum packing fraction, above this fraction the coating will not flow because particles can no longer move past each other. The higher the maximum packing fraction (i.e., more efficient packing of solids particles), the higher the solids concentration of the coating formulation can be.

2.3.1 Pigments

In today's paper industry, the most popular pigments are kaolin and precipitated Calcium Carbonate (PCC) due to the characteristics that they can provide to the final product and their cost. Other specialty pigments such as titanium di-oxide (TiO₂),

calcined clay, and synthetics are sometimes used in smaller amounts.¹ Pigment accounts for approximately 80 to 95 percent of dry coating weight. From a rheological viewpoint, a more important quantity is the pigment volume fraction, which is approximately 50 %.

Basic pigment properties are: particle size, particle size distribution, particle shape, refractive index, light scattering and absorption characteristics, and density. We refer to these properties as basic because they play a major role in determining the characteristics of the coated paper sheet:

- Glossiness increases with decreasing surface roughness; as a result plate-like shapes and small particle sizes give the best result
- Opacity increases with higher refractive indices
- Brightness depends on the light absorption characteristics of the pigment.
- Viscosity and porosity decrease with higher maximum particle packing fraction and by mixing of particles shapes

Another factor affected by the chemical and physical nature of the pigments is the stability of the dispersion. Pigments can have an electrostatic charge on their surfaces. This charge may change with location on the particle's surface, edges and faces of plate-like particles can have different charges. The interaction between charged particles can either prevent (like charge) or cause (opposite charge) particle aggregation, which would lead to sedimentation of the suspended pigment. Strong repulsions between charged particles will increase viscosity; ionic species can be added to the suspension in to control particle interactions.

An ideal pigment would have the following properties: high brightness, good opacity, appropriate particles size and particle size distribution, colloidal stability, small binder demand, low density, low water absorption, good glossiness, low price, and good compatibility with other pigments.² The criteria for choosing a pigment are based on the specifications required by the customer and cost of manufacturing. Industry will select the pigment or a combination of pigments to achieve required coating properties at minimum manufacturing cost.

This study primarily used PCC. During early stages of the research project, kaolin clay was used to select the rheometer geometry for experimental work.

2.3.1.1 *Kaolin*

Kaolin clay is a widely occurring mineral but deposits of significant quality for paper coating applications are limited.¹² Kaolinite $[Al_2 Si_2 O_3 (OH)_4]$ is the most important kaolin mineral for the paper industry, its annual consumption in North America is approximately 4.2 million tons.¹³ Most of the kaolin clay used for paper coating in the United States comes from the Georgia and South Carolina deposits. Other commercially important deposits in the world are located in southwest England, and Brazil. Kaolin clay is also used in paints, ceramics, ink, fiberglass, and cracking catalysts, and as filler in plastics and rubber. It is widely used because of its low cost and availability. Kaolin clays from different regions share the same desirable characteristics: non-toxicity, fine particle size for good opacity and smoothness, easy dispersion in water at high solids

fraction (~65 wt %), plate-like particle shape for good ink receptivity and print quality, and inertness.

Kaolin clays are white or near white in color and can present good flow properties at high solids content. Individual particles have the shape of a hexagonal plate. Kaolinite theoretical composition is 39.8% alumina, 46.3% silica, and 13.9% water. Its brightness ranges from 84 to 87 % according to ISO-Brightness from TAPPI Standards . Its refractive index is 1.576 for pure kaolinite and may vary from 1.542 to 1.576 depending on impurities due to metal oxides and processing for commercialization. Physical clay characteristics such as brightness, PSD, viscosity, and chemicals oxides content (i.e. Fe_2O_3 and TiO_2) vary according to geographical origin.

The processing of kaolin clays is done by air-float or wet processing. Air-float clays are primarily as filler and have a minor role in coatings because of their grit content (non-kaolin particles) and low brightness. For paper coatings, wet-processed clays are used, which are classified from numbers 1 to 4 depending on the percent of pigments smaller than $2\ \mu\text{m}$.² In terms of particle size distribution they are classified as follows:

- No. 1, 90 to 95 % of particles smaller than $2\ \mu\text{m}$
- No. 2, 80 to 89 % of particles smaller than $2\ \mu\text{m}$
- No. 3, 70 to 79 % of particles smaller than $2\ \mu\text{m}$
- No. 4, 65 to 70 % of particles smaller than $2\ \mu\text{m}$ (Coarse)

Delaminated clays offer good paper surface coverage and high ink gloss but low sheet gloss. These are primarily used for light weight coated paper (LWC) because of their coverage with a low coating weight. Properties of kaolin coatings such as porosity, glossiness, ink drying rate, surface smoothness, and coating picking are strongly influenced by particle size, particle size distribution, and shape. To optimize these, commercial kaolin is “engineered” by the manufacturers to improved particle size distributions and aspect ratios.

2.3.1.2 *Precipitated Calcium Carbonate*

Calcium carbonate is the most common mineral on the earth’s surface besides quartz.² Precipitated calcium carbonate (PCC) has been gaining popularity in recent years in North America due to its manufacturing cost, availability, and brightness. There are three different forms: calcite (see Figure 2.6), aragonite (see Figure 2.7), and vaterite.

PCC pigments particles commonly contain 97 % CaCO_3 and 1 to 2 % MgCO_3 and other minor impurities. ISO-brightness ranges from 93 to 96 % and suspension pH ranges from 8.5 to 10.5, the higher pH being indicative of the presence of un-reacted lime (CaO). Physical properties vary depending on the preparation method. PCC pigments available on the market range from 0.4 to 3 μm in average particle size and the corresponding surface area varies from 3 to 13 g/m^2 . By using particle sizes in the provided range the paper coatings industry can address gloss issues. PCC requires low amounts of dispersant, between 0.5 and 3 by weight percent of pigment, which increases with decreasing particle size.

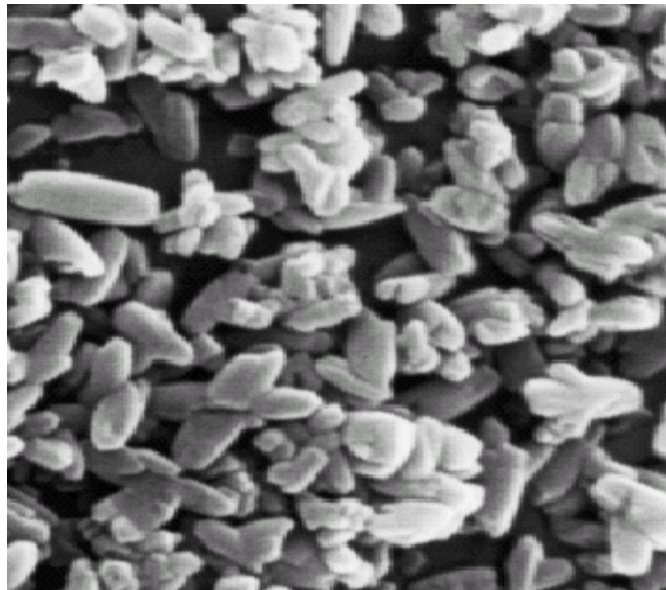


Figure 2.5 SEM Image of Calcite PCC Pigment¹⁷

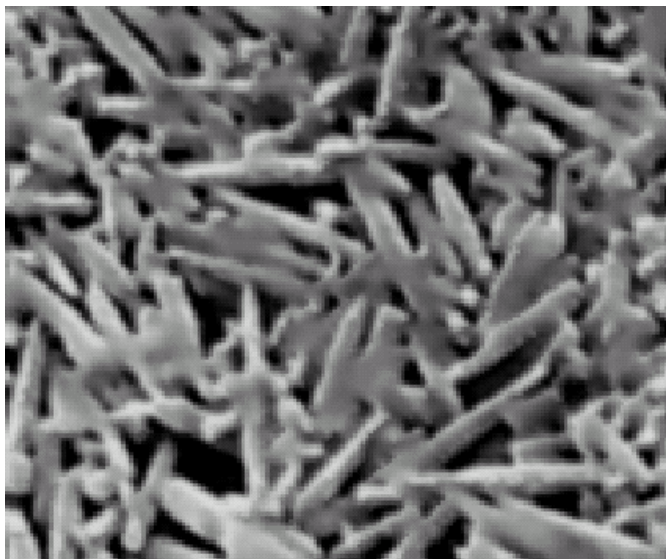
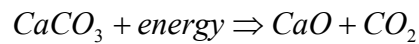


Figure 2.6 SEM Image of Aragonite PCC Pigment¹⁷

The precipitated form of calcium carbonate (PCC) is available in different sizes and shapes. Coarser grades are usually used in size press formulation or as fillers. New PCC pigments introduced in the market in the mid 80's provided improvements in smoothness,

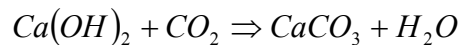
porosity control, printing properties, coating rheology, and machine run-ability because of narrower particle size distributions and more appropriate shapes.¹⁴ Calcite, the most stable form of PCC, has rhombohedra or octahedral structure. Aragonite and vaterite have an orthorhombic structure that because of its meta-stability will remain orthorhombic only at temperatures below 400 °C.

High purity limestone (95 % CaCO₃) is calcined at 1000 °C in a kiln to produce carbon di-oxide gas and calcium oxide (CaO - lime). The next step is to react the CaO with water to yield a slurry of Calcium hydroxide (Ca(OH)₂ - slake):

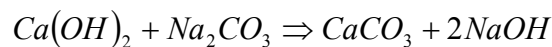


The slake is screened or filtered to remove un-reacted lime.

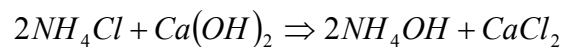
The three methods to manufacture PCC from calcium hydroxide are: lime/CO₂ process, also called carbonation, the lime/soda process, and the ammonium chloride process:



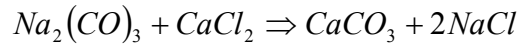
or,



or,



In the last process, calcium chloride is subsequently reacted with the sodium carbonate solution to produce calcium carbonate:



Factors such as concentrations, pH, and reaction time and temperature can be modified in order to vary the final morphology or particle size and size distribution of the resulting calcium carbonate.

PCC particle size and size distribution affect directly the gloss of the coated paper through particle packing. More efficient packing decreases porosity, thus, increases glossiness. Opacity increases by using smaller particles because of the larger number of scattering surfaces.¹⁸ Rheology is also affected by particle size and particle size distributions and this aspect is at the core of the current study. Shipments of dry PCC for coatings can have poor dispersion when water is added. Without proper dispersion, optical and physical properties of the coated sheet will be compromised. Dispersing agents such as poly-acrylates, or poly-phosphates are used to decrease aggregation and sedimentation.

2.3.2 Binders

Binders form the second largest category of coating components. Their function is to bind the pigments to the base-sheet, fill the void volume between pigments, bind pigments to each other, and decrease coating viscosity. Figure 2.8 illustrates how latex particles bind together and fill the void volume between particles. There are two main binder types of binders: natural and synthetic. Among the natural binders, starch is by far

the most abundant with soy protein being second. Corn starch is the most common in the North American paper industry because of its availability, cost, and properties. These binders are mostly supplied in the form of granular powder and have to be cooked at the mill. Natural binders are usually chemically modified to improve their binding and rheological properties.

Of the synthetic binders, co-polymer of styrene and butadiene latex is the most popular followed by poly-vinyl acetate, vinyl-acrylic, and poly-vinyl alcohol.¹⁰ Binder strength is a key factor.

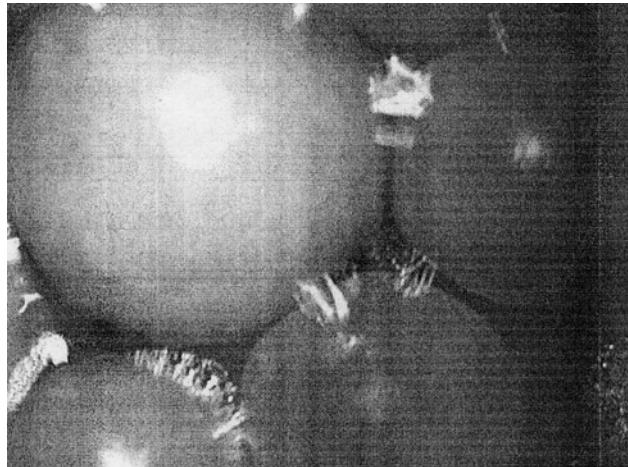


Figure 2.7 Synthetic Latex Binding Resin Particles¹⁵

Binder selection criteria are based on the customer needs and requirements. Four basic criteria for choosing a binder are:

1. Compatibility with chosen pigments as required for coated paper grade specified by the customer.

2. Availability of suitable application equipment, storage tank, cooking facilities, and pumping equipment available.
3. Optimization of coating rheology.
4. Cost of binder.¹⁶

An ideal binder should have good binding power, water retention, compatibility with coating components, should be easily dissolved or dispersed in water, have desired effect on viscosity, chemical and mechanical durability, be harmless to health, non-odorous, have low tendency to foam, be resistant to bacterial attack, low price, availability, and should have good optical properties. Combination of binders are often used to optimize coating properties, principally to adjust rheology and water retention. In the binder mix, the minor component is usually referred to as co-binder.

2.3.2.1 Binding Strength

Binding strength is probably the most important characteristic of a binder. It can be expressed as the relative amount of binder needed to obtain the same coating strength as obtained with the highest binding strength binder.² For example, binding strength of poly-vinyl alcohol (PVA) is 1 and binding strength of styrene-butadiene (SB-latex) is 2 to 2.5., meaning that if PVA is replaced by SB-latex in a coating formulation, the amount of SB-latex has to be 2 to 2.5 times higher than the original amount of PVA to obtain the same binding strength. The strength can be tested by performing a wax-picking test (T-459 TAPPI Standards).

2.3.2.2 Binder Demand

In general, binders are among the most expensive components of a coating formulation. To optimize its use only the amount required to achieve the minimum strength should be used. Two pigment properties that directly affect binder demand are: dispersion and packing fraction. When the pigment is well-dispersed and the pigment packing fraction is high, the binder demand will be lower. Binder demand can be estimated by calculating the void volume between particles which is given by:

$$V_V = 1 - \frac{1}{S_R} \quad (9)$$

where V_V is the void volume fraction and S_R is the relative sediment volume which is the ratio of the volume of the sediment to the total sample volume.¹⁷ As packing fraction increases due to changes in pigment shape, there is a decrease in binder demand.

Particle size distribution and particle shape are important for the pigment packing which directly affects the rheology of the formulation. Pigment volume concentration (P.V.C.) is obtained by using the following equation:

$$P.V.C. = \frac{\text{Volume of pigment}}{\text{Volume of pigment} + \text{Volume of Binder}} \cdot 100\% \quad (8)$$

Critical pigment volume concentration C.P.V.C. is the volume concentration at which the binder fills the void volume between pigment particles. When P.V.C. is higher than C.P.V.C. the binder only partially fills the void volume between the pigments. When P.V.C. is lower than C.P.V.C., there is excess binder. Table 2.1 shows C.P.V.C. values of some pigments according to their shapes.³

Table 2.1 Values of C.P.V.C. for Different Pigments

Pigment	Shape	C.P.V.C.
Coarse Kaolin	Plate-like	50 %
PCC	Sphere-like	50 %
TiO ₂	Octahedron-like	51 %

2.3.2.3 *Natural Binders*

Natural binders include starches and proteins usually chemically modified to improve their binding and rheological properties.

The main sources of commercial starch are corn, wheat, potatoes, and waxy maize.¹⁸ Corn is the dominant source for starches used in the paper industry.¹⁹ In addition to the binding properties, starch also contributes to the rheological properties of the coating formulation: it acts as a flow modifier and provides water retention. Today, most of the starches used in coating formulations are chemically modified to prevent spoilage and to enhance physical and chemical properties.

Starch is a natural high-molecular-weight polymer that can be considered a condensation polymer of glucose. Most starches consist of two types of molecules: amylopectin (70-80%) and amylose (20-30%).²⁰ Both of them consist of polymers from α -D-glucose units. Amylose is a linear molecule, and amylopectin, is a highly branched polymer. Figure 2.9 show the partial structures of amylopectin and amylose.

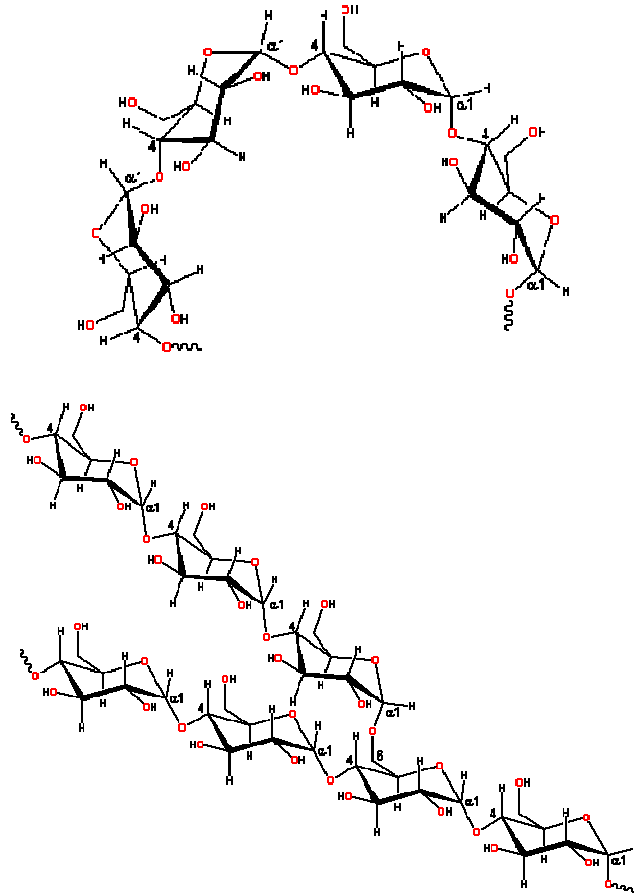


Figure 2.8 Molecular structure of Amylose (top) and Amylopectin (bottom)²⁶

Starch granules are insoluble in cold water due to the organization of the hydrogen bonds. When aqueous suspensions of starch are heated to a critical temperature, the starch granules begin to swell, causing a large increase in viscosity – this critical temperature is also known as pasting or gelatinization temperature.¹⁸

In a coating formulation, starch is used as a co-binder in amounts up to five percent by weight of the total amount of pigment. The exact amount is determined by the

requirements for optimal binding and structure film strength. It can also be used in amounts close to one percent by weight of pigment when used as a flow modifier.

Of the two main components of starch, amylose has the most useful functions as a hydrocolloid, i.e., a substance that forms a gel with water. Extended conformation of the amylose causes the high viscosity of water-soluble starch. Stickiness and gel firmness will depend on the amylose concentration. Starches high in amylopectin do not gel or precipitate upon cooling.

The gel and film forming ability of starch depends also on the molecular weight of the polymer. A high-molecular-weight polymer will give a flexible and more continuous film compared to one produced from a low-molecular weight polymer. Association and crystallization during cooling and storage decreases the stability by causing shrinkage and the release of water.

There are three types of chemically modified starch used in coating formulations oxidized, hydroxyl-ethylated, and cationic starch. Oxidized starch is prepared using a solution of sodium hypochlorite (with 6 to 9% available chlorine) or hydrogen peroxide. The solution is added to the starch slurry in the reactor, and once the desired reduction is achieved, the reaction is neutralized with acid. Then, sodium bisulphate is added to remove the free chlorine. The stability of the starch slurry improves and the viscosity decreases as a result of the oxidation process. Oxidized starch has an anionic character.

Hydroxyl-ethylated starch is also known as ethylated starch. It is prepared by reacting starch with ethylene oxide. Some salts are added in this process to prevent starch from being solubilized by the alkalinity of the reaction.

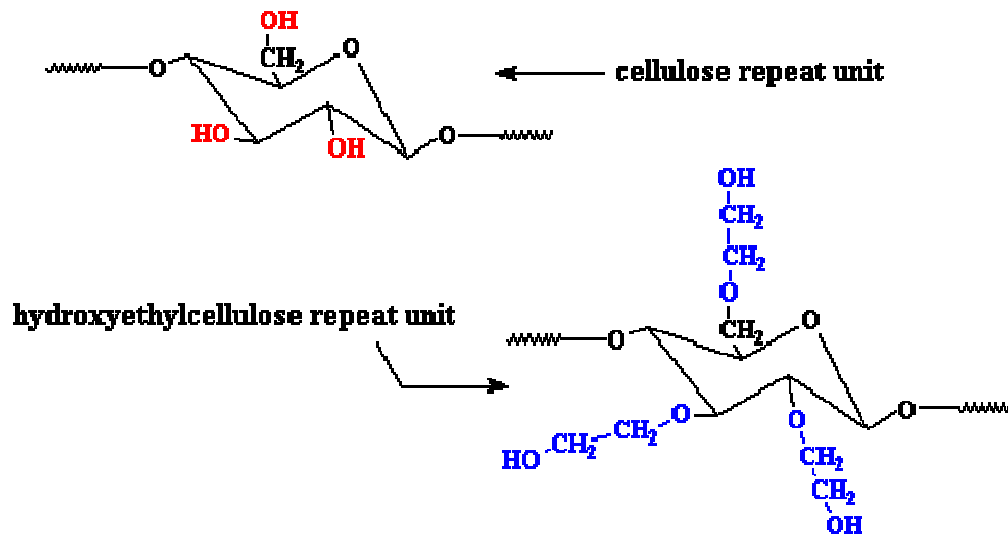


Figure 2.9. Hydroxyl-ethyl Ether of Starch²¹

Hydroxyl-ethyl groups do not allow the polymer to crystallize and show a great tendency to swell and disperse into an aqueous phase. Once ethylated, the starch can remain stable for a long period since the hydroxyl-ethyl groups are also hydrophilic. A higher degree of hydroxyl-ethylation produces a lower gelatinization temperature, greater stability, and higher water binding capabilities.

Cationic starch is another type of starch and was the starch used in this study. The choice was dictated primarily by spoilage resistance. It is prepared by reacting starch with agents that will substitute hydroxyl groups on the polymer with cationic groups,

usually a tertiary amino group. The positive charge of the polymer has an impact on strength, rheology, and water retention. As the charge increases, so does the viscosity and water holding.

2.3.2.4 Synthetic Binders

Synthetic binders can be divided into two groups: water-soluble polymers and emulsions (latex). Soluble-in-water synthetic binders such as poly-vinyl alcohol (PVA) have been gaining acceptance in recent years due to its excellent film strength and barrier properties in the presence of grease and oil, though its usage in North America is small due to high viscosity and cost. Styrene-butadiene co-polymers latices are the most prevalent in the paper coatings industry, due to their binding strength, rheology, and cost. Styrene-butadiene latex was the synthetic binder used in this research and is therefore the only binder discussed in this section.

Latex is a water emulsion of a synthetic rubber or plastic particles obtained by polymerization. The polymer is suspended in an aqueous phase. Latices used in paper applications are mainly based on butadiene, styrene, acrylics and acetates. When latex is used in the manufacturing of coated paper, improvement in properties such as film uniformity, strength, and stiffness result from the chemical nature of the polymer, in particular its stability, viscosity, and capability to form homogeneous polymer films.²² In addition to functioning as binders, certain latices are also used as specialty pigments.

Latices are usually characterized by their composition, particle size, pH, and glass transition temperature (T_g). For paper coatings, other important characteristics are molecular weight and particle surface charge. Particle sizes range from 10 to 1000 nm and particle size distributions are typically very narrow.

Styrene-butadiene latices are designed to be used over a wide range of applications. They must be mechanically and chemically stable in order to show a positive response to the shear forces encountered in the coating process and to be compatible with various pigments, starches, proteins, insolubilizers, thickeners, and other additives. Styrene-butadiene latices range from 48 to 52 % of solids in the emulsion. Particle size is generally in the range of 1000 to 2000 Å with narrow particle size distributions.²³

In this co-polymer, styrene is the “hard” monomer and butadiene is the “soft” monomer, which internally plasticizes the hard monomer to achieve desired pigment binding and film forming. The ratio of styrene to butadiene can be tuned to produce an acceptable binder for paper coatings. Both at high and low styrene content film strength is poor. At low styrene content, there is an excess of soft polymer (butadiene) making the resulting polymer weak as a pigment binder. At high styrene concentrations, the polymer is too hard to allow for the film formation that is necessary for pigment binding. Gloss increases with styrene content because of the elasticity that it provides at the surface. In paper coatings, the styrene-butadiene latices typically have 50 to 60 % styrene content. The addition of vinyl acid in amounts of 0 to 15 parts by dry weight is one of the most significant changes in the latex chemistry and this process is called carboxylation. The binding strength of carboxylated latices is increased because of the greater polarity

induced by the acid.²⁴ Dry pick strength, the strength of the substrate-coating interface, is increased by using a latex with small particle and by increasing the degree of carboxylation.

2.3.3 Additives

Coating additives form a large group of compounds that enhance the performance of paper coatings. Coating additives are classified in the following categories:¹⁰

- Dispersants
- Flow modifiers
- Lubricants
- Cross-linkers or insolubilizers
- Biocides
- pH controllers
- Repellents
- Optical brighteners
- Dyes
- Foam control agents

Since dispersants and flow modifiers are the most commonly encountered in coating formulations and are the principal additives contributing to coating rheology, a brief explanation will be given of only those additives.

Dispersants are used to prevent aggregates from forming, and to avoid sedimentation. They prevent aggregation by imparting electrical repulsive forces to individual pigment particles. Tetra sodium poly-phosphates and sodium poly-acrylate are widely used as dispersants for paper coating pigments. Poly-acrylates are stable at elevated temperatures and for extended periods. Pigment chemistry, coatings preparation method, and coatings drying influence the selection of dispersants. It has been shown that inorganic dispersants (poly-phosphates) break down rapidly at temperatures in the range of 60 to 65 °C and more slowly between 32 to 38 °C. Organic dispersants (poly-acrylates) offer great advantages over inorganic dispersants in terms of stability since they are unaffected by temperatures in this range.²⁵ Dispersants are usually included in the pigment slurry provided by the pigment manufacturer in amounts ranging from 0.1 to 1 % by dry weight of pigment.

Flow modifiers are also called viscosity modifiers. They are used in combination with synthetic binder to increase water retention, and have an impact on the viscosity of the system. The most commonly used flow modifiers are: carboxy-methyl cellulose, hydroxyl-ethyl cellulose, sodium alginate, cationic starch, and acrylic responsive thickeners. They are used in amounts of 1 to 5 % by dry weight of pigment.

2.4 Flow Behavior

As explained in the previous section, paper coatings have three main components: pigment, binder, and additives. Both by weight and volume percent, pigments are the most abundant component in a formulation. Pigments are rigid particles that can only

move through the fluid at a single velocity, and thus velocity gradients cause the particles to rotate. Energy used for rotation decreases the energy available for fluid flow and as a result, suspensions are more viscous than the pure suspending fluid.²⁶ Non-Newtonian behavior of paper coating formulations is mostly due to the presence of pigment particles. Binders and additives (base fluid) contribute to coating viscoelastic properties to a lesser degree.

The viscosity of a suspension depends on the balance between the particle interaction forces, thermal diffusion, and hydrodynamic interactions. Thermal diffusion causes the particles in the dispersion to move freely with no specific order (Brownian motion). As particle number increases, the frequency of particle-to-particle contact also increases. At sufficiently high concentrations, particle interaction forces dominate the flow properties. The increase of these interactions is directly related to the change in volume fraction. Relative viscosity increases as volume fraction increases until reaching the maximum packing or maximum volume fraction at which the fluid starts to behave as a solid. A suspension where colloidal and hydrodynamic forces predominate without reaching a solid structure being developed is considered concentrated.

In concentrated suspensions (i.e. paper coatings), there are four dominant interaction forces between particles: hard-sphere, electrostatic, steric, and van der Waals. Hard-sphere interactions are due to the fact that solid particles cannot overlap. There is a large repulsive potential developed at the inter-particle contact point. When particles are not touching, hard-sphere interactions play no role.

Electrostatic interaction is found in systems where there is a significant electrical double layer at the particle surface. The electrical double layer describes the variation of electric potential near a surface and it originates from the interaction of interfacial charges (i.e. ions), and electrostatic interaction of interfacial molecules. For particles with thick double layers it is essential to define an effective radius, which is the radius of the particle plus the double layer thickness since this reflects the distance at which particles interact with each other due to their repulsive electrostatic forces. Therefore, particles with large effective radius due to thick double layers will increase the effective volume fraction of the suspension. The double layer extension depends on the electrolyte concentration of the suspension and can be obtained by estimating the reciprocal of the Debye-Hückel parameter.³⁵ As the amount of electrolytes is increased, the thickness of the double layer decreases due to shielding of the surface charge. By modifying the double layer thickness, the suspension rheology can be controlled, since it is equivalent to changing particle concentration.

Steric interaction forces occur when particles contain adsorbed layers of non-ionic surfactants or macromolecules. These forces result from the loss of configurational entropy of the surface layers when they experience compression during particle-to-particle approaches. A secondary contribution to the potential can come from the free energy of mixing between the polymer layers.

Van der Waals interaction forces between particles are attractive and originate from the charge fluctuations within an atom or molecule due to the motion of its electrons.²⁷

The combination of all previously mentioned forces results in an energy-distance curve that determines the stability of the suspension (see figure 2.11). If the energy minimum in the graph becomes too deep (compared to thermal energy $k_B T$), particles will tend to aggregate.

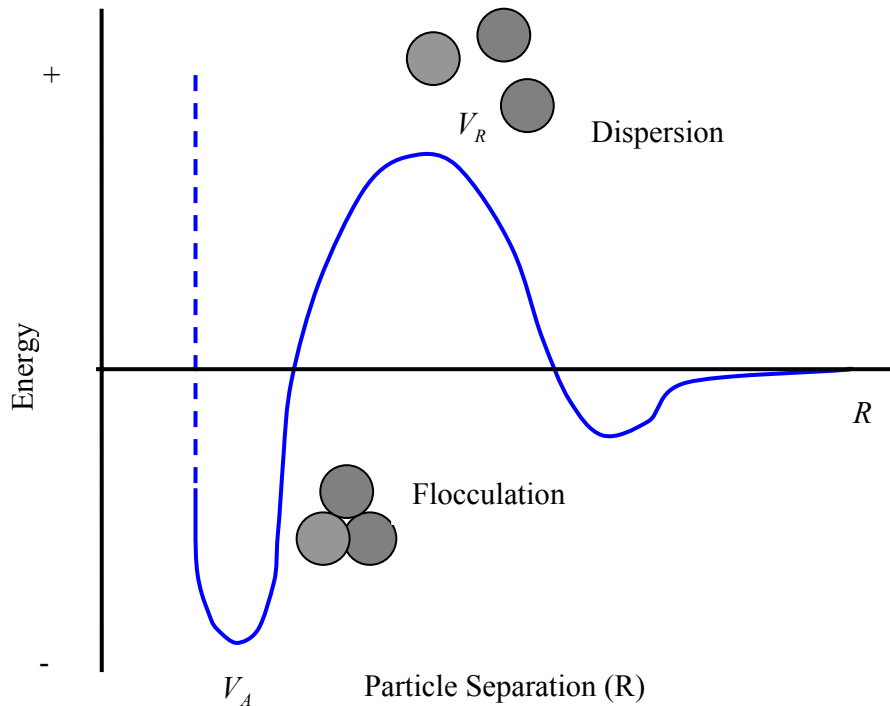


Figure 2.10 Attraction and repulsion Forces Between Particles

In a suspension, the fluidity limit is defined as the concentration or volume fraction of solids below which the suspension behaves like a liquid in the sense that an applied shear stress induces velocity gradients in the mixture.²⁸ When the volume fraction of the suspended solid particles exceeds this limit, the mixture will behave like a solid. Since

the viscosity is directly affected by the volume fraction, the factors influencing volume fraction will be described.

2.4.1 Main Factors Affecting Coating Rheology

2.4.1.1 *Particle Size*

Particle size and particle size distribution of pigments play an important role in determining the rheology of paper coatings. Coatings with small size particles will be more viscous than coating containing larger size particles provided that both have narrow PSD. Shear thinning behavior is easier for large particles where Brownian motion is less effective and the hydrodynamic forces are more important. The effect of Brownian motion is more pronounced for small particles, thus, higher values of shear rate are needed to achieve the same amount of shear thinning. These effects can be explained by analyzing the Péclet number. Péclet number is the ratio of the hydrodynamic to the thermal forces and is defined as:

$$Pe = \frac{a^3 \eta \dot{\gamma}}{kT} \quad (2.10)$$

Where a is the characteristic size of the particle, k is the Boltzmann's constant, and T is the temperature.

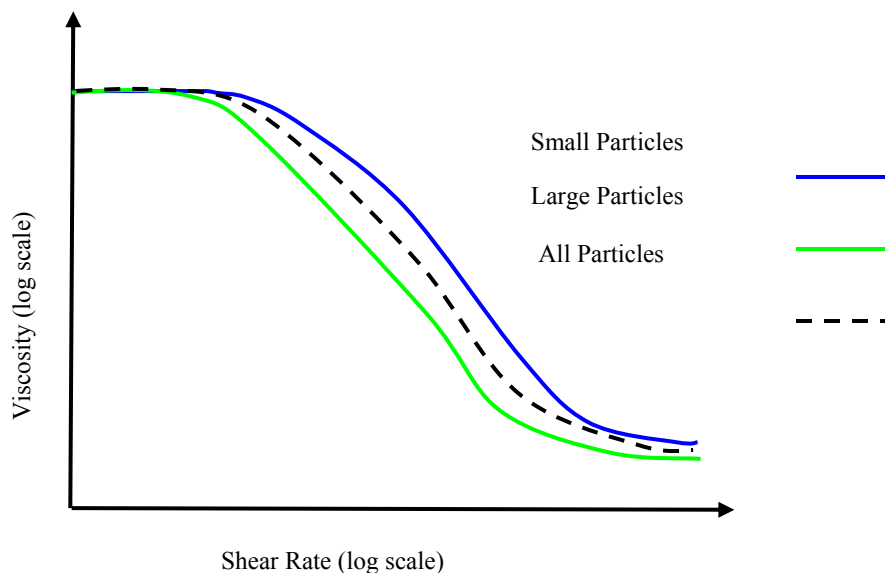


Figure 2.11 A Schematic Diagram of Viscosity as a Function of Shear Rate for Suspensions with Different Particle Sizes¹⁰

Figure 2.13 shows the qualitative variation of viscosity for mono-disperse systems with different particle size in a concentrated suspension. If the suspension is dilute (i.e. $\phi \leq 0.20$), a bi-modal suspension with size ratio of 4 showed less than 6% decrease in relative viscosity.²⁹ In dilute systems, it is expected that change in particle sizes will not represent a large change in viscosity.

Pigments with narrow PSD will show higher viscosity than pigments with a broad PSD due to better packing between particles in pigments with broad PSD. In suspensions with broad PSDs, small particles tend to fill the small voids between big particles, so that higher solids loadings can be obtained with a small increase in viscosity. To achieve higher solids content with relatively low viscosity, the size ratio between the small and large particles is important. The larger this ratio is, the higher the solids concentration

that can be achieved. Figure 2.13 shows an example on how the packing fraction increases with broader PSDs.

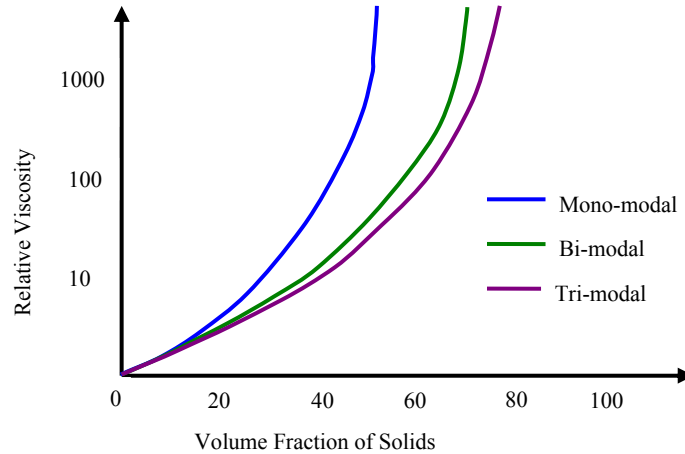


Figure 2.12 Relative Viscosity for Volume Fractions of Uni-modal, Bi-modal, and Tri-modal Systems³⁰

From previous observations of the behavior of bi-modal suspensions, three parameters have been found to be most relevant for the viscosity of bi-disperse suspensions: total particle concentration ϕ_V , size ratio λ , and fraction of small particles ζ .³¹ If the total particle concentration and size ratio are kept constant, a minimum in the viscosity occurs when the small particle fraction is approximately between 0.25 and 0.35^{9,32} (see figure 2.14). If the total particle concentration and small particles fraction are kept constant, the rheology can be optimized by increasing the particle size ratio.³³

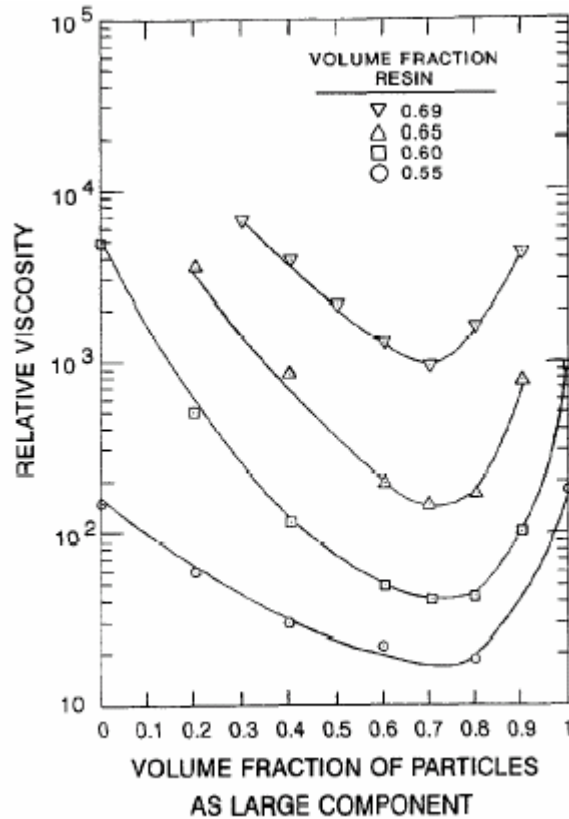


Figure 2.13 Effect of the Relative Amount of Large Particles in a Bimodal Suspension Containing 0.68 and 0.21 μm Particles, on the Viscosity at a Shear Stress Level of 1.0 dyn/cm. The data was taken at 24°C.⁴⁰

In summary, both particle size and size distribution are important for coating rheology. An appropriate combination of sizes can potentially be used to optimize the system's fluidity and enable the use of formulations with higher solids volume fractions.

2.4.1.2 Particle Shape

The viscosity of a suspension depends on particle shape (see Figure 2.15) since particle movements are influenced by their ability to rotate and translate. In the presence of neighboring particles with the same shape, sphere-like particles can rotate more easily

about their axis than plate-like or rod-like particles, which require a space equivalent to the length of their longest axis to perform this action. When plate- or rod-like particles do not have this minimum space, the interaction due to particle-to-particle contacts will increase viscosity. Figure 2.15 shows the qualitative impact on relative viscosity of particle geometry.

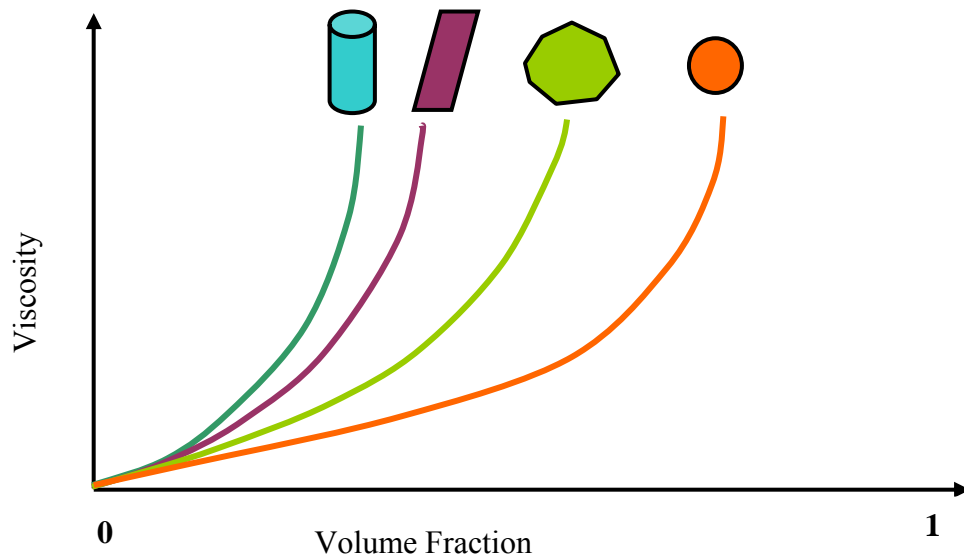


Figure 2.14 Viscosity as a Function of Volume Fraction for Different Particles Geometries²

Aspect ratio is a key parameter for characterizing basic particle shape:

$$\text{Aspect Ratio} = \frac{\text{Length of longest axis}}{\text{Length of shortest axis}} \quad (2.11)$$

According to equation (11), sphere-like particles have aspect ratios close to one. As the aspect ratio increases, so does viscosity. This effect happens because of the less likelihood of large aspect ratio particles to rotate due to interaction with neighbor particles.

As previously mentioned, viscosity is affected by the particle volume fraction. Particles with high maximum packing fractions have lower viscosity at high solids loadings than particles with low packing fraction values. This is the result of better ordering of the particles to enable fluidization of the suspension.²⁸

Theoretically, cubic particles could have the highest packing fraction of all different geometries because if they are arranged together in a perfect packing there will not be spaces or void volumes between them, the maximum packing fraction being almost 1. For spheres, the well-known random packing fraction is approximately 0.64. Ellipsoids (i.e. M&M candies) when randomly packed showed a packing fraction of approximately 0.72.³⁴ The explanation is that for an extremely isometric object (i.e. a sphere) the forces exerted by neighbors can only cause translation, not rotation. Forces exerted in an ellipsoid can cause both: translation and rotation. To ensure that the net force exerted adds up to zero to reach static equilibrium, ellipsoids require more direct contacts with neighbors than spheres, which results in a higher volume fraction.³⁵

In the paper coating industry, improvement of pigment packing leads to favorable rheology (i.e. lower viscosity) at high solids content. Calcite PCC has a sphere-like particle shape with low aspect ratio. Its low aspect ratio produces coatings with lower viscosity than aragonite PCC which has a larger aspect ratio.

2.4.2 Interactions between Coating Components

The surface chemistry of pigments determines the inter-particle interactions that play an important role in the coatings rheology, i.e. surface charge, adsorption of additives, and

ion exchange equilibrium. Coating formulations have a liquid phase that has a major impact on the coating rheology. The viscosity of the liquid phase depends on the amounts of soluble material and the interaction between the components. Absorption of the binder and additives on the pigments can lead to a lower suspension viscosity.

CHAPTER 3

OBJECTIVE

Coating formulations need to be higher in solids content to improve the properties of the coated paper, increase production rates, and reduce energy cost. An increase in solids content can be achieved by optimizing the packing fraction of the pigment. Optimum packing fraction can be reached by selecting pigments with appropriate particle size, particle size distribution, and shape. Researchers have found that by using a non-narrow PSD or a combination of uni-modal particle sizes, the viscosity of coatings remain the same or decreases even when the percent of solids in the suspension is increased.^{28, 33, 36} Shapiro and Probst¹ performed experimentation on bi-modal suspensions with size ratio of 4:1 and 2:1. They found that the small particles fraction that optimizes rheology through better particle packing is in the range of 0.25 to 0.45. Viscosity measurements were performed on suspension containing glass beads of 40 to 160 μm in glycerin (5 % water) at a temperature of 11.5 °C. Toivakka and Eklund³¹ performed particle motion simulation to predict the rheology of bi-disperse suspensions showing that for a suspension with particle concentration of 0.65 and size ratio of 2.5, viscosity reaches a minimum when the small particles fraction is 0.2. The paper coatings industry has not been able to implement these concepts since its raw material is not as controlled and well-defined as, for example glass beads.

By performing a systematic rheological study of the interactions between different pigment sizes, particle size distributions, and shapes in coating formulation, this study aims to answer questions that will help the paper coatings industry to optimize their processes. Questions that have not been addressed by previous researches include: What happens when we use different particles sizes and shapes with narrow PSD and which are currently available in the industry? Would this produce a large change in coated paper properties? How does the geometry (shape) of the pigments and their packing fractions impact on rheology? And which geometrical combinations optimize the rheology?

Our study correlates more closely to actual results that would be obtained by implementing coating pigments available in the market. Raw material includes calcite and aragonite precipitated calcium carbonate (PCC). Aragonite PCC has a rhombohedra shape with aspect ratio of 3 while calcite PCC has an ovoid shape with low aspect ratio ~ 1.5 . Calcite PCC has a size of ($D_{50}=0.4 \mu\text{m}$) and Aragonite has three sizes: $D_{50}=0.6 \mu\text{m}$, $D_{50}=1 \mu\text{m}$, and $D_{50}=2.0 \mu\text{m}$ respectively. Most notably most of the used materials (pigments) are available, thus allowing for immediate implementation of this technology in the coatings industry.

The relevancy of our project relays in that the suggested concepts could be immediately implemented into the paper coatings operations. Our proposal aims to improve the efficiency and profitability of the paper coatings industry at almost negligible or inexistent investment cost.

CHAPTER 4

MATERIALS AND METHODS

This chapter provides a detailed description of the materials, techniques, and equipment used to perform the study of the rheological properties of paper coatings. Materials and methods are divided in four parts:

- Coating formulation used for experiments
- Experimental design
- Rheometry
- Coated paper testing

4.1 Coating Formulation Used for Experiments

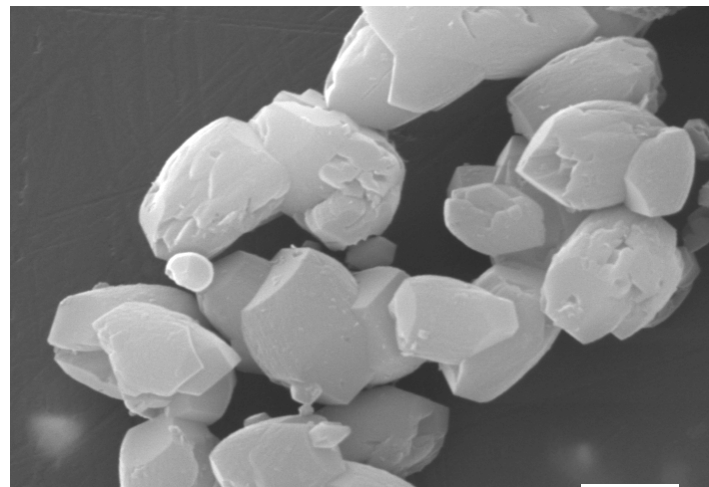
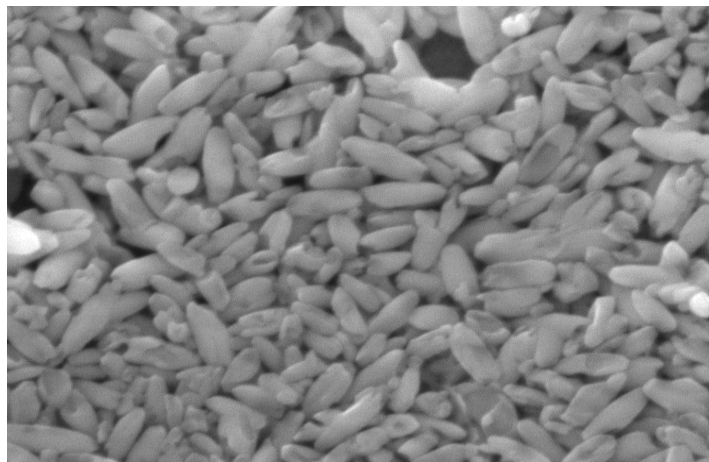
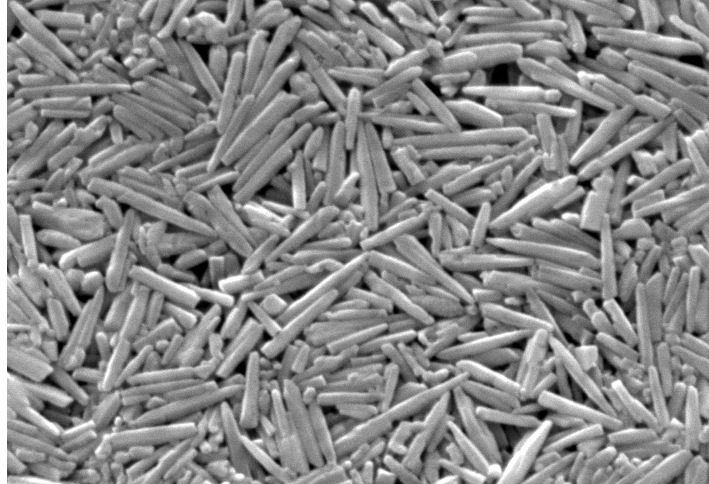
Chapter 2 discussed the components of a typical coating formulation. The objective of this study was to focus on the influence of size and shape of pigment on coating viscosity. Therefore, the coating formulations studied were limited to three basic components, pigment, starch and latex. The proportions of the components were the same for all of the coatings tested, by dry weight 100 parts pigment, 13 parts binder, and 3 parts flow modifier (cationic starch). In this study, only the pigment portion of the coating formulation was changed. Four different pigments were used, both alone and in pairs.

The target solids content for the coatings was 65 wt % of solids. The standard formulation was selected because of its simplicity, similar studies in the literature^{2,37} and consultation with industry.³⁸

The pigments used were precipitated calcium carbonate (PCC) provided by Specialty Minerals Inc. The properties of the four pigments are shown in Table 4.1. SEM images of three of the pigments are presented in Figure 4.1. The SEM image for Albagloss M is not shown, but this pigment is a calcite as well, with a shape that is intermediate to Albagloss S or XL. The pigments were supplied as aqueous suspensions at 70 wt % of solids. A small amount of proprietary dispersant was present in the suspensions. All of the pigments are commercially available and represent the state-of-art in PCC pigments. The materials were selected because of their commercial relevance and well-defined particle size and shape.

Table 4.1 Pigments Used in tested Coating Formulations

		Size (µm)			Aspect ratio	Density (g/cc)	pH
		D ₂₀	D ₅₀	D ₉₀			
		Calcite	Albagloss S,	0.4			
Albagloss M,			1.0		~1.0 to 1.5	2.71	7-9
Albagloss XL,	1.4		2.0	3.5	~1.0 to 1.5	2.71	7-9
		Size (µm)			Aspect ratio	Density (g/cc)	pH
		D ₂₀	D ₅₀	D ₉₀			
Aragonite	Opacarb,	0.2	0.4	0.8			



10,000

2 μ m

Figure 4.1 (Top) Opacarb A40 PCC (Aragonite), (Middle) Albagloss S PCC (Calcite), and (Bottom) Albagloss XL PCC (Calcite)

A styrene-butadiene latex was selected as binder since it is the prevalent binder in the paper coatings industry. CP 620 NA Latex from The Dow Chemical Company was used. The latex was supplied at 50 wt % of solids, had a density of approximately 1 g/cc, a pH of 6.0, and a median particle size of 1780 angstroms. The flow modifier used was a liquid cationic starch, Structurecote 1887, provided by Vynamul Polymers as a solution that contains 25 wt% of starch solids. The liquid starch had a density of approximately 1 g/cc, and pH of 6.5. Hydroxyl-ethylated starch could have also been used; however, it was available only in powder form and would have required that a new batch be made for each coating formulation due to aging spoilage.

The mixing order of the coating formulation components was based on the concept of maintaining the lowest possible mixture viscosity at each step in the process. This results in optimum mixing of the components, complete surface coverage of solid materials and minimum energy expenditure. Thus, the order of addition was obtained by analyzing the flow-curves for the different coating components. Figure 4.2 shows the viscosity as function of shear rate for the individual coating components and combinations of the coating components. The pigment used in this experiment was Albagloss M since its particle size is in between Albagloss S and XL. Each pure component was analyzed at its original solids weight percent except for pure Albagloss M, which was diluted with water to 65 wt % of solids. It can be observed that starch at 25 wt% of solids and mixtures containing it are the most viscous fluids in the shear rate range relevant to mixing. The latex-pigment mixture and pure latex are the fluids with the lowest viscosity. Therefore, our mixing order was chosen as: pigment, water, latex, starch. The first component to be

mixed with the PCC pigment would be water followed by latex, thus keeping the viscosity as low as possible. This order will guarantee an optimum mixing and surface coverage of pigment with binder while ensuring an efficient use of mixing energy.

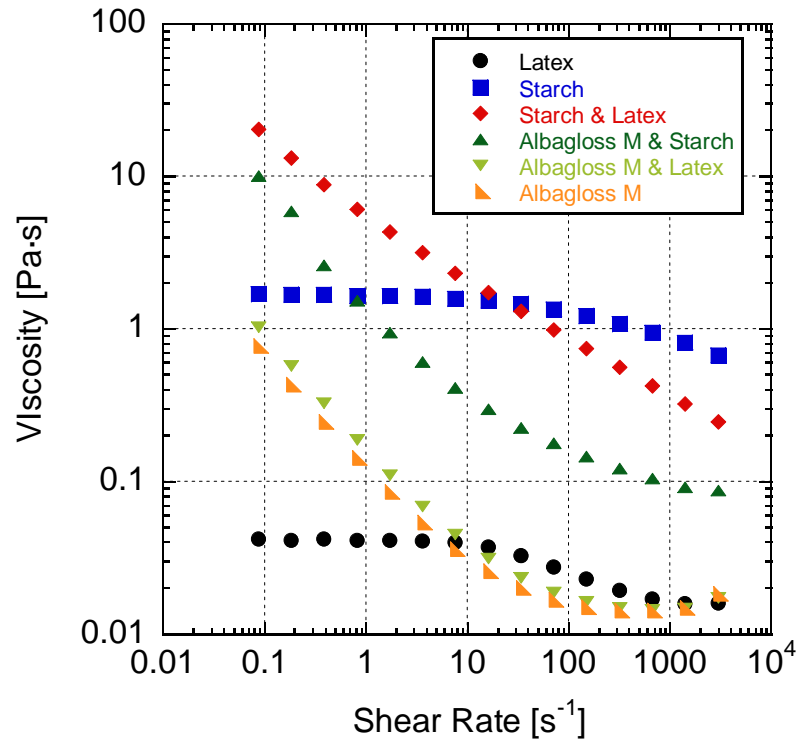


Figure 4.2 Base Fluid of Experimental Coating Formulation at 20 °C

The details of the mixing are as follows:

1. Add pigment to 200 ml beaker
2. Add the amount of water calculated
3. Add latex and mix at 1500 rpm during 1 minute using a helix propeller (1.5 in diameter)
4. Add liquid starch

5. Mix for 10 minutes at 1500 rpm

Batches of single pigment coating formulations were prepared with the composition listed in table 4.2.

Table 4.2 Single Pigment Coatings Preparation

Compound	Parts	Solid (gr)	Raw Material (gr)	Water (gr)
Albagloss S	100	60.02	83.83	23.81
Latex	13	7.82	15.65	7.83
Starch	3	1.81	7.23	5.42
		69.66	106.71	37.06

PCC Conc. = 0.716

Total Solids wt% = 65.28

Note: Amount of water added (gr) =

0.45

SOLIDS% =

65.0

Compound	Parts	Solid (gr)	Raw Material (gr)	Water (gr)
Albagloss M	100	59.39	82.95	23.56
Latex	13	7.87	15.73	7.87
Starch	3	1.81	7.23	5.42
		69.06	105.91	36.84

PCC Conc. = 0.724

Total Solids wt% = 65.21

Note: Amount of water added (gr) =

1.35

SOLIDS% =

64.4

Mini-Vortexer at 70% of the maximum speed to avoid the formation of micro-bubbles in the coating. After mixing, the sample was sonicated for 1 min to break-up particle aggregates and extract remaining micro-bubbles from the fluid. The sonicator used was SF20H from Fisher Scientific.

4.2 Experimental Program

The objective of this study was to examine the influence of pigment size and shape on the viscosity of mixed pigment pairs. Pigments were combined to study different size and shape combinations at different pigment ratios. The experimental program consisted of two parts,

1. Coatings with pigments of same shape but different sizes,
2. Coatings with pigments of different shape and size

Figure 4.3 shows the combinations of pigments with the same shape that were investigated and the pigment ratios (by weight). The combination of Albagloss M with Albagloss XL was omitted from the experimental matrix because it was assumed the results would fall between those for the combinations shown in the Figure.

Figure 4.4 shows the combinations utilizing pigments with different shapes and sizes. As with the previous groupings, the mixtures of Opacarb and Albagloss M were omitted.

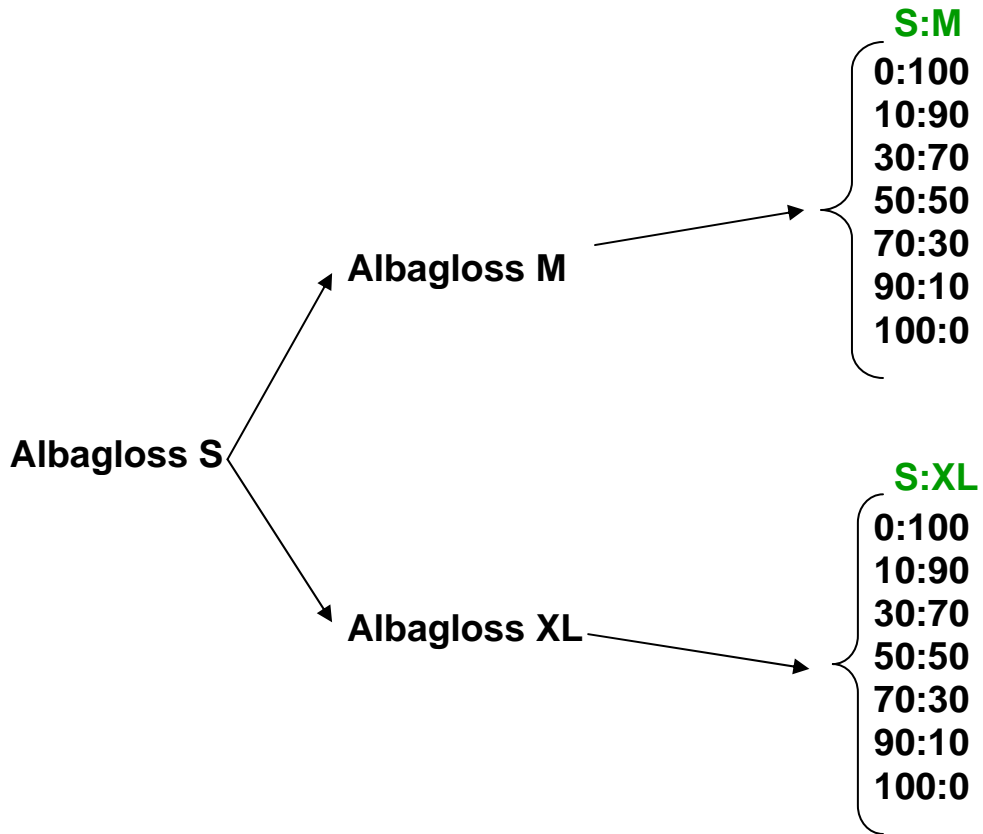


Figure 4.3 Scheme for the Combination of Coatings Based on Pigments with Same Shape but Different Particle Size

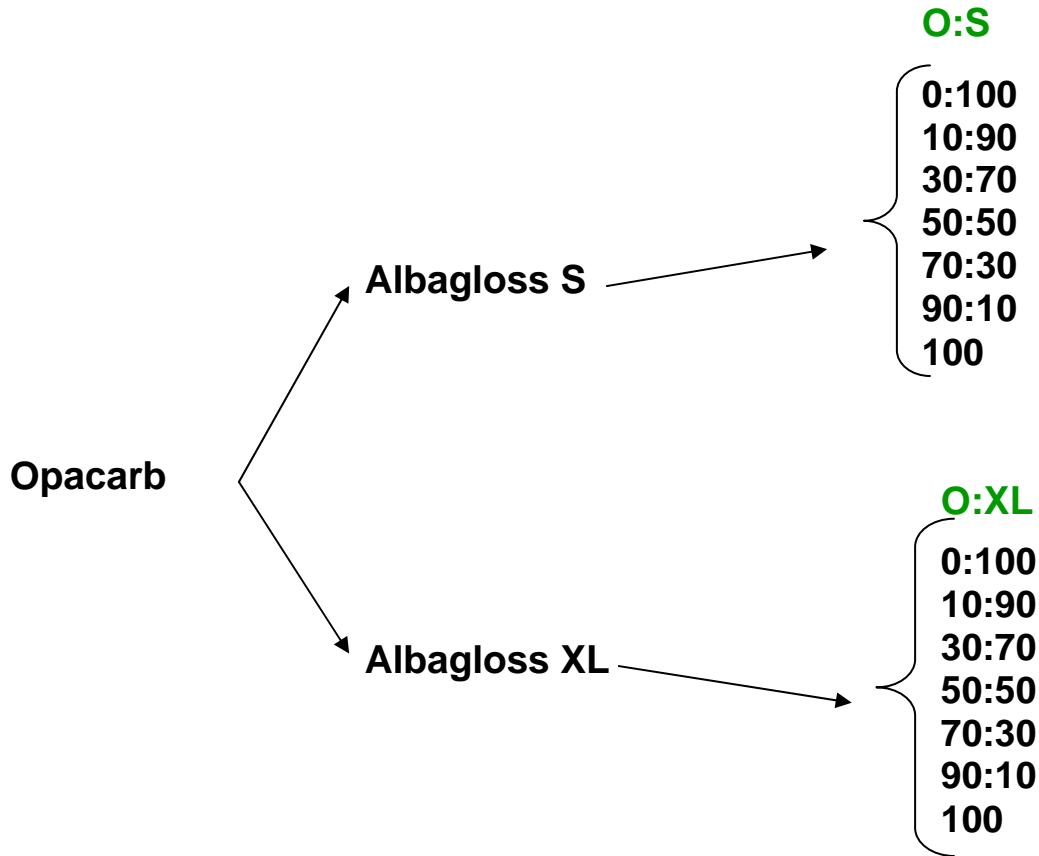


Figure 4.4 Scheme for the Combination of Coatings Based on Pigments with Different Shape and Particle Size

4.3 Rheometry

To perform measurements in the rheometer, a measuring geometry has to be chosen. The two geometries available in the laboratory are cone and plate (CP) and Couette cylinders (CC), which are both part of the Compact Rheometer MCR 300 from Paar-Physica. The main differences between these geometries are the available surface performing the measurement and the amount of sample volume that they require.

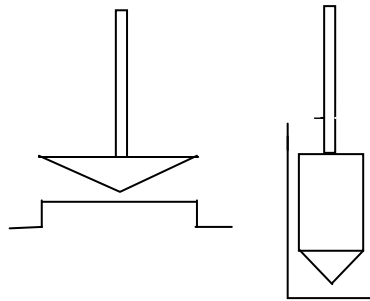


Figure 4.5 Cone and Plate (Left) and Couette Cylinders (Right)

In theory, both geometries should give the same results. During experimentation, it was observed that there are slight variations. The key factor was sedimentation of pigment particles, because coating pigments such as PCC or Kaolin are significantly denser than the suspending fluid. Sedimentation produces a variation in the concentration of the suspension being measured, this variation in concentration affects in a larger scale the cone and plate configuration since pigments sediment faster due to the shorter distance they have to travel before touching the plate. To choose an adequate measuring geometry and experimental set-up, two preliminary experiments were performed. The first was used to determine time required for the mixture to reach steady-state at a selected shear rate conditions. The results were used to determine the time settings of the flow-curves. The second was a hysteresis experiment used to determine the effect of repeated exposure to a range of shear rate conditions. The coating formulation used was as follows:

- Kaolin Clay³⁹ 100 parts
- Latex⁴⁰ 13 parts
- Starch⁴¹ 3 parts

Kaolin was used, because at the time of these experiments PCC pigments were unavailable.

4.3.1 Time Setting Experiment

The first step before performing any rheological measurement is to make sure that the sample is in rheological steady-state. After sample loading, particles are initially random distributed in the base fluid causing artifacts in the measurements at very low shear rates if the measuring time does not allow the sample to reach steady state before data collection.

The time necessary to allow the system to reach steady state can be estimated by performing flow-curves with different time settings. Three different flow-curves with 25, 50, and 100 seconds of separation between data points were performed. Figure 4.6 shows the results for cone and plate geometry, the effects caused by sedimentation can be seen by comparing the curve at 25 s with any other of the curves. The curves for 50 and 100 s present lower viscosity because the cone is measuring a more water-like fluid caused by pigment sedimentation on the plate, thus, sedimentation can also compromise reproducibility. Figure 4.7 shows the results for the Couette cylinders geometry for time settings of 25, 50, and 100 seconds.

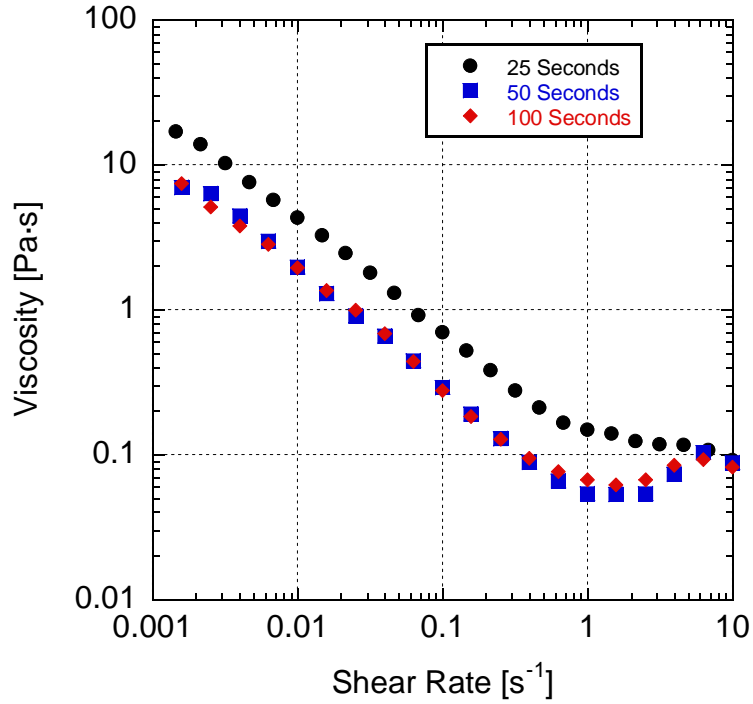


Figure 4.6 Cone and Plate: Flow-curves for Different Time Settings at 23.5 °C

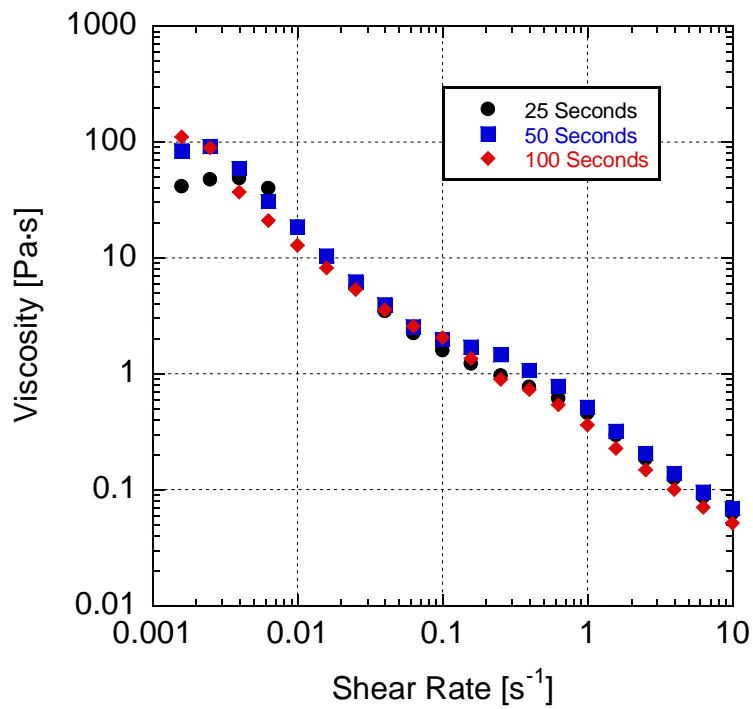


Figure 4.7 Couette Cylinders: Flow-curves for Different Time Settings at 23.5 °C

Both geometries presented an artifact at shear rates (0.001 to 0.005 s⁻¹) not relevant to the paper coatings industry. The artifact is present as a sudden increase of viscosity at low shear rates. This phenomena is caused by the short period of time waited before taking a data point, thus, data is taken before particles are pushed into contact. The increase in viscosity is caused by the first interactions between particles. This artifact disappears once the shear rate is approximately 0.005 s⁻¹ because most of the pigments are now in contact with neighboring particles and a steady-state structure has been formed. This type of artifact can be avoided by increasing the time between measuring points, but the cost of doing this is a long measuring time. Since the shear rates at which it is present is not relevant for the paper coatings industry, 25 seconds between data points was used to optimize experimentation time and this setting gave reliable results at shear rates relevant to the industry (shear rates above 0.01 s⁻¹).

4.3.2 Hysteresis Experiment

A hysteresis experiment is used to determine how a suspension behaves as it transitions from rheological non-steady-state to rheological steady-state phase and vice versa. A kaolin coating sample was run in both geometries from low-to-high shear rates followed immediately after by a high-to-low run. In this experiment, the range of shear rate was from 0.001 to 3800 s⁻¹, which were the limits of the rheometer. Figure 4.8 shows the hysteresis comparison for the two rheometer geometries.

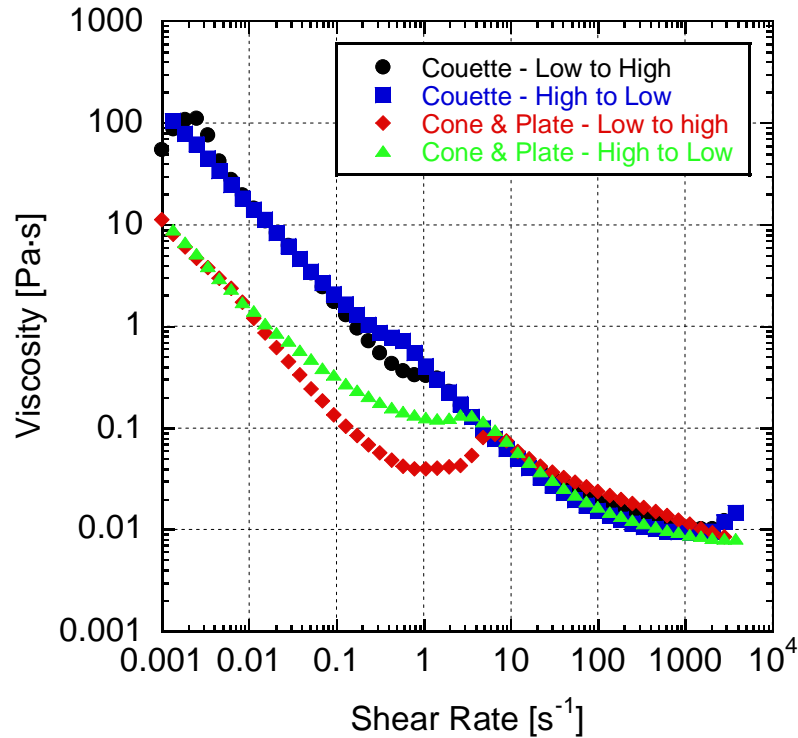


Figure 4.8 Hysteresis of Cone and plate vs Couette Cylinders

It is observed that Couette cylinders geometry showed less hysteresis than cone and plate. Potential sedimentation played an important role in the geometry selection. Sedimentation promotes measurements in a more water-like fluid layer at the top of the suspension as previously mentioned for cone and plate. In Couette cylinders, the particles have to travel a longer distance before settle down. The walls of the geometry are along the vertical axis, so that the thin fluid layer at the top has negligible effect on the measured stress. Another key factor is evaporation, in Couette cylinders this is not an issue because the sample volume is large enough so that the evaporated water amount is small in comparison to total loaded sample volume and the measuring surface is not affected since it is well immersed in the fluid. For cone and plate even evaporation of small amounts of water represents an issue comprising reproducibility since the

boundaries of the cone is the section being immediately affected by evaporation and because of the small sample volume that is loaded.

Based on these results, the Couette cylinder geometry was selected as the measuring system. Another advantage is sample loading, which is easier to perform in Couette cylinders due to the larger sample volume required (3.7 ml vs. 0.6 ml for cone and plate).

4.4 Procedure for Rheological Data Collection

Experimental data for rheological analysis was extracted from the coatings flow-curves using a time setting of 25 seconds between data points. All the runs were performed at 20 °C to prevent evaporation. Three experimental runs were performed on each coating sample.

The first experimental immediately after loading the samples into the Couette geometry of the rheometer was a shear rate sweep from low to high shear rates (0.001 to 3000 s⁻¹). After the first run, a second experimental run was performed, varying the shear rate from high to low (3000 to 0.001 s⁻¹). Finally, the third experimental run consisted of consecutive low-to-high and high-to-low shear rate sweeps (0.001 – 3000 – 0.001 s⁻¹). In figure 4.9, rheological data from the entire test sequence are presented for a typical coating formulation, which contains a mixture of two pigment types (Opacarb and Albagloss XL). The reason behind performing sequential experimentation on the same sample is to check the presence of hysteresis in the system due to flow history in the

coating. Opacarb and Albagloss XL were chosen as example because their combination presents significant hysteresis effects. The first experimental run showed all the time the highest viscosity. The explanation is that the pigment particles are initially randomly oriented after sample loading. Once shear is applied, particles tend to align in the flow direction, which results in shear-thinning behavior. After the first run, the suspension has flow history and if it is exposed again to a shear rate, sample deformation will require less energy, so that a slightly lower viscosity is observed. In the third run there is little hysteresis due to the flow history of the coating formulation.

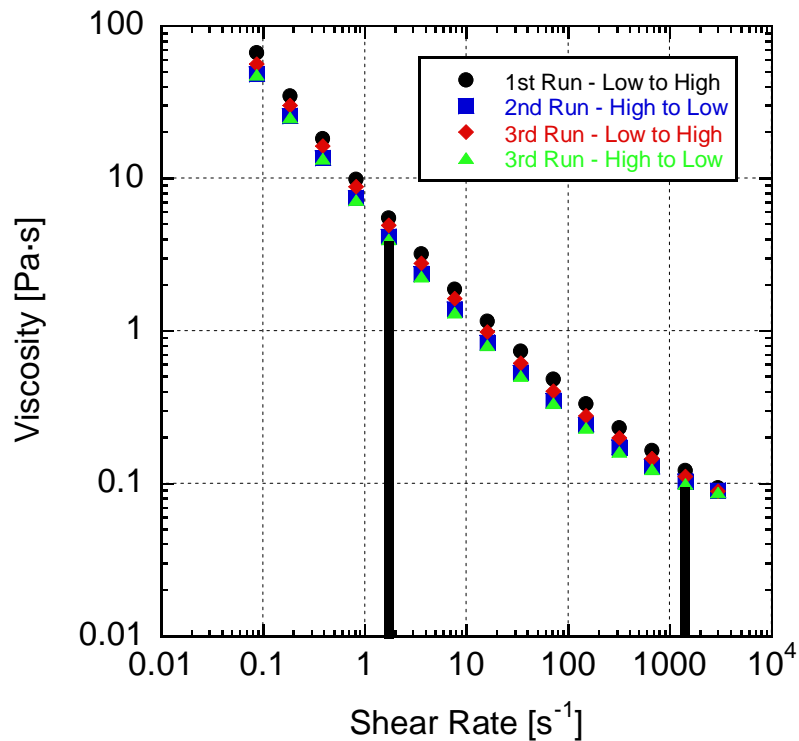


Figure 4.9 Three Experimental Runs for the Opacarb:Albagloss XL 90:10 Coating and Data Points Selection at Two Different Shear Rates Relevant to the Industry

From flow-curves, data at two shear rates (1.73 and 1420 s^{-1}) relevant to the coatings industry was selected. Operations in the coatings industry such as storage, pumping, mixing, and application occur in this range. Also 1420 s^{-1} is the highest reliable shear rate that can be achieved with the available compact rheometer; however, higher shear rates ($100\,000 \text{ s}^{-1}$) can be achieved by using either a Hercules High Shear Viscometer. Figure 4.9 shows the selection of the two points in the flow-curve which will be analyzed in the results section.

4.5 Coated Paper Testing

To analyze the properties of the paper coated with the experimental formulations, four standardized tests were performed: glossiness, roughness, and brightness. The coating was applied to the base-stock (copy-grade paper) using a laboratory rod coater (RD S 55) from R.D. Specialties Inc. Once the coating is prepared, a small amount is poured on the paper and it is spread by applying gentle pressure to the rod and driving it through the paper from the top to the bottom. After coating the paper-sheet, it was stretched utilizing metal frames and was air-dried for 48 hours.

Once the coated paper was air-dried, a three roll super-calender was used to achieve a more glossy and smooth surface. The three roll calendar was manufactured by Hertel Machine. It is hydraulically loaded with the top and bottom rolls being steam heated. At 20 psi steam pressure, the rolls are typical heated to approximately 212 to 220 degrees F. The top and bottom rolls have chrome surfaces with 16" face widths and 10"

diameters. The middle soft roll has a face width of 15" and a diameter of 14 inches. The operating speed range is 100 to 800 fpm but is typically operated at 100 fpm. The machine average operating pressure range of approximately 900 to 1500 psi for a 12" web.⁴² The samples were super-calenderized at approximately 900 psi, a speed of 100 fpm, and approximately 212 °F in pilot plant super-calender.



Figure 4.10 Three Roll Super-Calender Used for the Experiments

The coated paper was placed into a 20 % humidity-controlled room for 48 hr, and then it was passed to the 50 % humidity-controlled room for 24 hr before performing any test. The reason behind this is that remaining moisture in our paper can affect tests results due

to the sensibility of paper samples to water. Testing methods were performed according to TAPPI Standards:

- Glossiness: Gloss 75° (only in machine direction), T 480
- Roughness: Parker Print-Surf, T 538 om-01
- Brightness: ISO-Brightness, T 452 om-02
- Porosity: Gurley LP (25 cc) T 460

Gloss of paper, T 480 om-99, is for measuring the gloss of paper at 75° (15° from the paper) through specular reflection. The light intensity is measured over a small range of reflection angle. The test was performed 10 times for each coated sample in the machine direction since this is presenting the highest value of glossiness.⁴³

Roughness using Parker Print-Surf, T 538 om-01, test performs a measurement of the air-flow between the specimen and two pressurized, concentric annular lands that are impressed into the sample from the top side. The rate of air-flow is related to the surface roughness of paper.⁴⁴

ISO-brightness, T 452 om-02, determines the brightness of white, near white, and naturally colored paper. It is a numerical value of the reflectance factor of a sample with respect to blue light of specific spectral and geometric characteristics. The instruments employs 45° illumination and 0° viewing geometry with the illuminating and viewing

beams adjusted so that translucent materials are evaluated on an arbitrary but specific scale.⁴⁵

Gurley LP test, T 460, determines the porosity of paper and board by passing an air-flow through the paper. Porosity is estimated by taking the time that a determined air volume takes to pass through the paper. The equipment used is called densitometer. The results are given in seconds and can be converted into cc/s.

CHAPTER 5

RESULTS AND DISCUSSION

In this chapter, experimental result will be presented and discussed in five parts:

- Flow-curves of individual pigments and some pigment mixtures
- Viscosity of bi-modal coatings produced by mixing uni-modal coating pigments of equal shapes
- Viscosity for mixtures of particles with different shapes and size
- Properties of coated paper surfaces to correlate coating performance with rheological results

5.1 Coating Flow-Curves

Experimental data for rheological analysis was extracted from the coating flow-curves. These flow-curves were obtained during three different experimental runs on each sample, as explained in Materials and Methods (section 4.4).

Once the experimental protocol was established, rheological characterization of the individual pigments was carried out. To this purpose, coating formulations were prepared aiming 65 wt.% of solids (46 % by volume). In figure 5.1, the resulting flow-curves are presented. The data points were taken from low to high shear rate (0.001 to

3000 s⁻¹) immediately after loading the sample in the Couette cylinders system. As a result, the samples do not have significant shear history at the time of the measurement. This choice was made, because it can be assumed that in the coating application the pigment particles do not have significant flow history before being pumped.

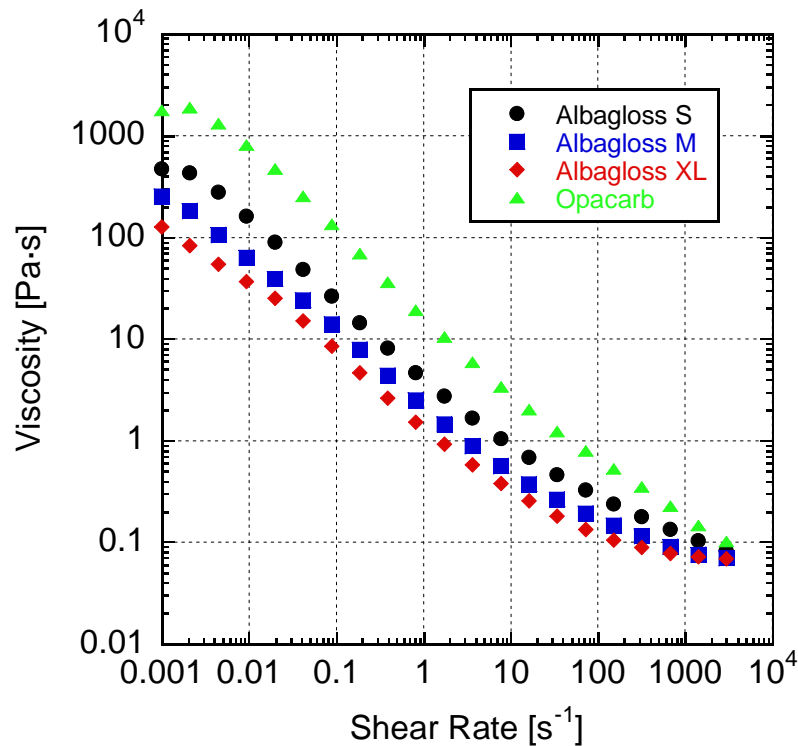


Figure 5.1 Flow-Curves for each Single Pigment Coating from Low to High Shear Rates (0.001 to 3000 s⁻¹)

Figure 5.1 shows the impact of particle size and shape on suspension viscosity as expected according to background information provided in section 2.4.1. The coating formulation containing Opacarb, which is the smallest pigment with the most anisotropic shape, has the highest viscosity at all shear rates. The high viscosity of the coating containing Opacarb is caused by particle-to-particle interactions favored by the acicular

shape of the pigment. At very low shear rates, the suspension shows higher viscosity, because the amount of energy necessary to move the Opacarb particles while maintaining a random overall random distribution is larger. In small-particles suspensions, the effect of Brownian motion which randomizes particle configurations, extends to higher shear rates (see discussion of Péclet number in section 2.4.1, figure 2.12). Therefore, when a suspension is being sheared, higher values of shear rate are required to achieved the same shear-thinning behavior as for larger particles. The aspect ratio of Opacarb is approximately 3, which is higher than for any of the other pigments, and as aspect ratio increases, so does viscosity. The acicular or needle-like shape of Opacarb promotes particle rotation, which will induce additional interactions with neighboring particles, thus raising the viscosity. Shear-thinning for Albagloss XL is achieved at lower shear rates because the hydrodynamic forces of the shear flow are larger at the same shear rate (see 2.4.1: equation 10). Therefore, the largest particles, Albagloss XL ($D_{50} = 2 \mu\text{m}$), have the lowest viscosity. In addition, Albagloss XL has a low aspect ratio of approximately 1.5, which also lowers suspension viscosity at low shear rates. Therefore, the combination of particle size and shape explains the results obtained in figure 5.1. All the coatings combinations had shear-thinning characteristics in the flow-curves.

After measuring the flow curves of individual pigments, the rheology of pigment mixtures was investigated. Coating flow-curves for the majority of possible coating combinations were performed. For example, Figure 5.2 shows the flow-curves for two uni-modal and three bi-modal coatings of Albagloss S and Albagloss XL at 65 wt. % of solids. Again, data are presented for the first flow curve after sample loading. The upper

and lower curves are the uni-modal coatings formulations and the curves in between follow a monotonically decreasing viscosity as the fraction of Albagloss S (small particles) in the mixture decreases. The different weight ratios for the Albagloss S/Albagloss XL mixtures are: 0/100, 30/70, 50/50, 70/30, 100/0.

Figure 5.2 shows that flow-curves of bi-modal coatings with different mixing ratios fall in between the flow-curves of the uni-modal coatings. This happens because a different balance between Brownian motion and hydrodynamic forces is introduced when small and large particles are combined. As the fraction of small particles decreases, the effective Péclet number of the suspension increases. The larger particle size increases the hydrodynamic forces and promotes shear-thinning behavior at high shear rates.

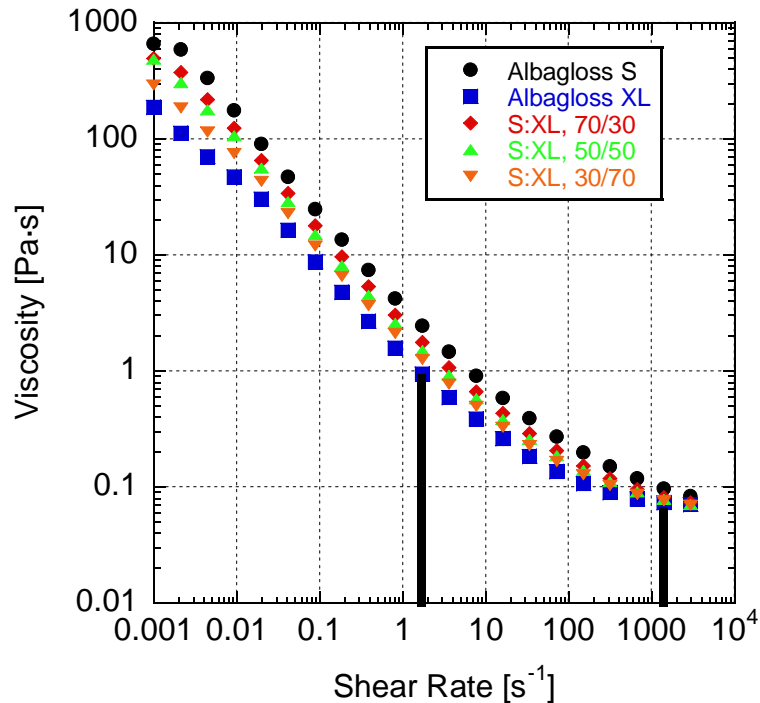


Figure 5.2 Flow-Curves for Albagloss S (0.6 μm) and Albagloss XL (2.4 μm) Coatings and Combinations of Different Ratios of them in the Mixture

5.2 Viscosity of Coating Mixtures with Pigments of Same Shape

In the remainder of this chapter, viscosity data will be analyzed predominantly at two shear rates relevant for the industry, 1.73 and 1420 s^{-1} , to facilitate discussion. Shear rates of 1.73 s^{-1} and 1420 s^{-1} (see section 4.4) were chosen, because operations in the coatings industry such as storage, pumping, mixing, and application occur in this range. Also 1420 s^{-1} is the highest reliable shear rate that can be achieved with the available compact rheometer.

The viscosity was analyzed for bi-modal coatings produced by mixing uni-modal PCC coatings with pigments of the same shape but different size and narrow PSD, with the fraction of small particles ranging from 0 to 1. The flow-curves were measured according to the protocol described in section 4.4.

Albagloss XL ($D_{50}= 2 \mu\text{m}$), Albagloss M ($D_{50}= 1 \mu\text{m}$), and Albagloss S ($D_{50}= 0.6 \mu\text{m}$) are all calcite (sphere-like) PCC with low aspect ratio in the range of approximately 1 to 1.5 for Albagloss XL, and 1.5 to 2 for Albagloss S. SEM images of both pigments are shown in Section 4.1. Figure 5.3 to 5.10 present the results obtained from the rheological analysis of the coatings combinations and the reproducibility of the data. Viscosity data are presented for the three experimental runs at the two selected shear rates as a function of the weight fraction of smallest particles in the mixture. Viscosity data are presented as relative viscosities by normalizing the data of the mixtures with the viscosity of the coating with only large pigment particles (i.e. the intercept with the vertical axis is normalized to 1 for all curves).

Experimental reproducibility is presented in Figures 5.5, 5.6, 5.9, and 5.10 for the first experimental run after sample loading since it has the higher error due to the absence of flow history. All experiments were performed twice to check reproducibility. The error bars resulted from obtaining the absolute error of the two performed experiments. To obtain the absolute error, the difference between the two experiments was determined and divided by two.

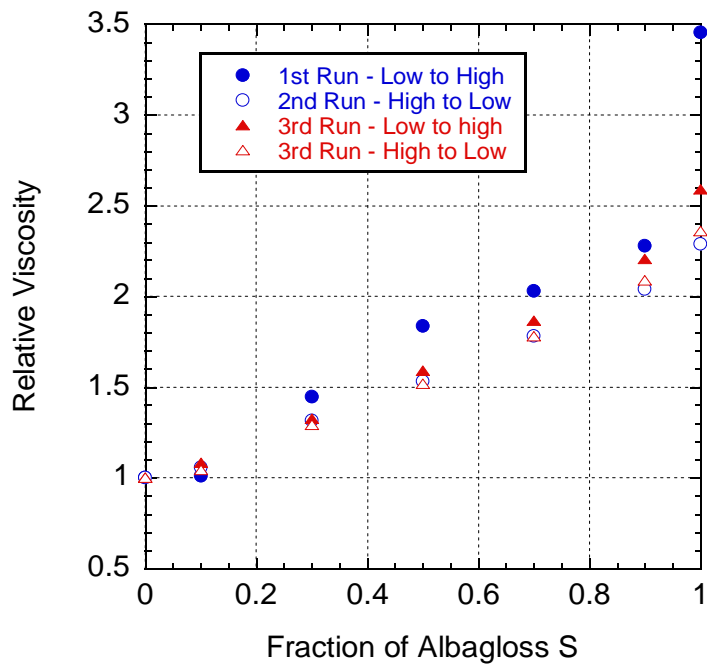


Figure 5.3 Relative Viscosity for Albagloss S: Albagloss XL combination at 1.73 s^{-1} for the Three Experimental Runs

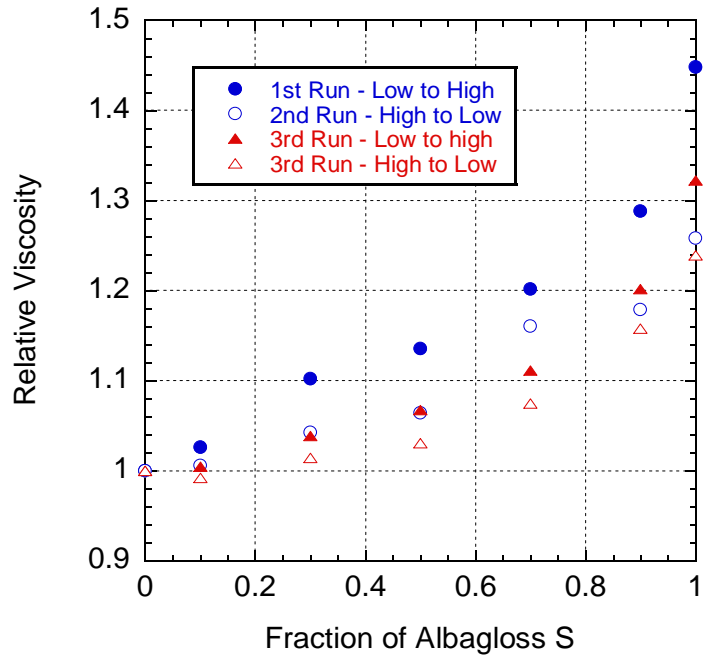


Figure 5.4 Relative Viscosity for Albagloss S: Albagloss XL combination at 1420 s^{-1} for the Three Experimental Runs

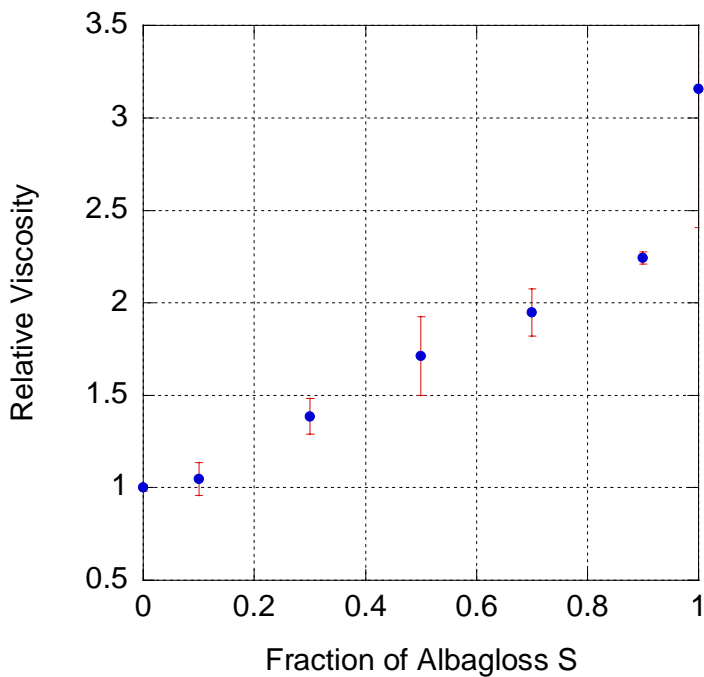


Figure 5.5 Reproducibility of the First Experimental Run for Albagloss S: Albagloss XL at 1.73 s^{-1}

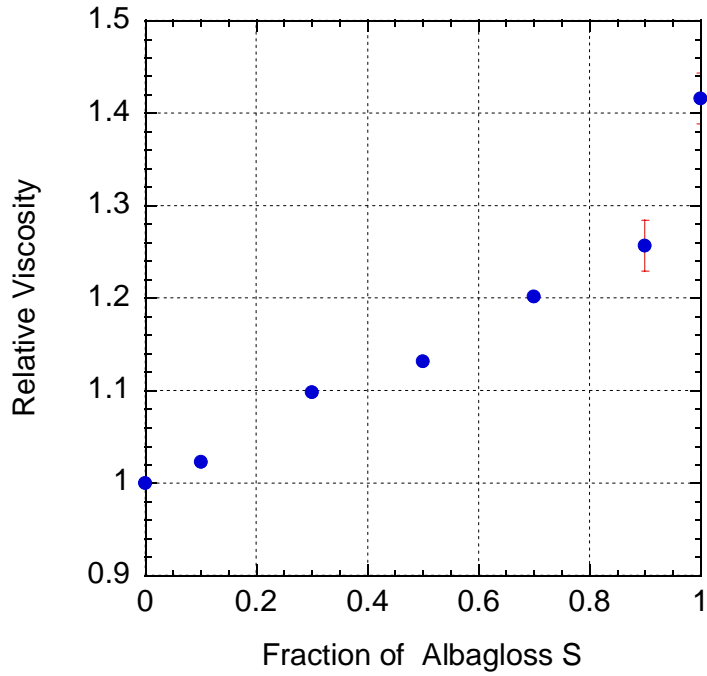


Figure 5.6 Reproducibility of the First Experimental Run for Albagloss S: Albagloss XL at 1420 s^{-1}

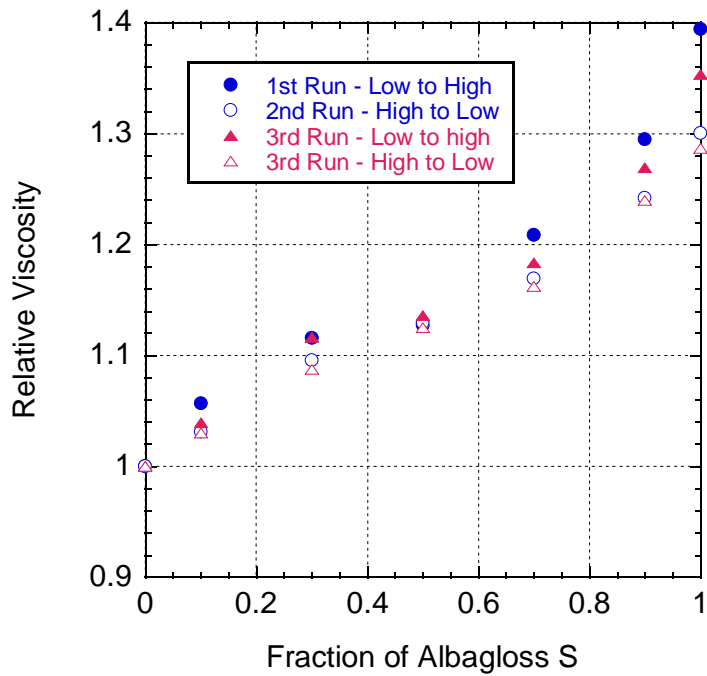


Figure 5.7 Relative Viscosity for Albagloss S: Albagloss M combination at 1.73 s^{-1} for the Three Experimental Runs

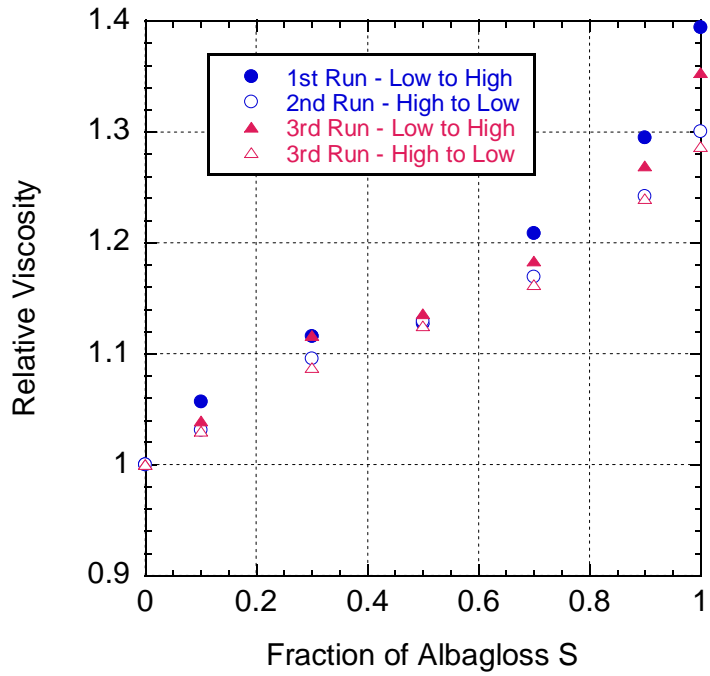


Figure 5.8 Relative Viscosity for Albagloss S: Albagloss M combination at 1420 s⁻¹ for the Three Experimental Runs

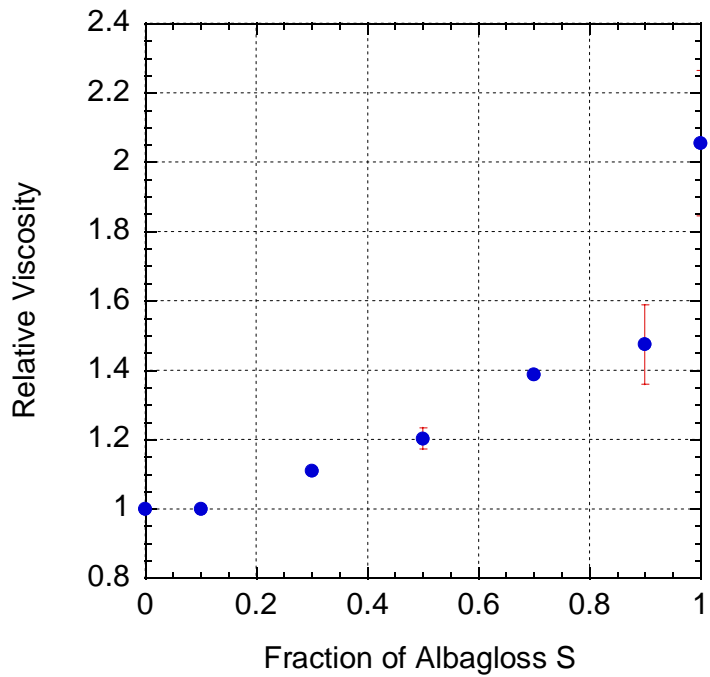


Figure 5.9 Reproducibility of the First Experimental Run for Albagloss S: Albagloss M at 1.73 s⁻¹

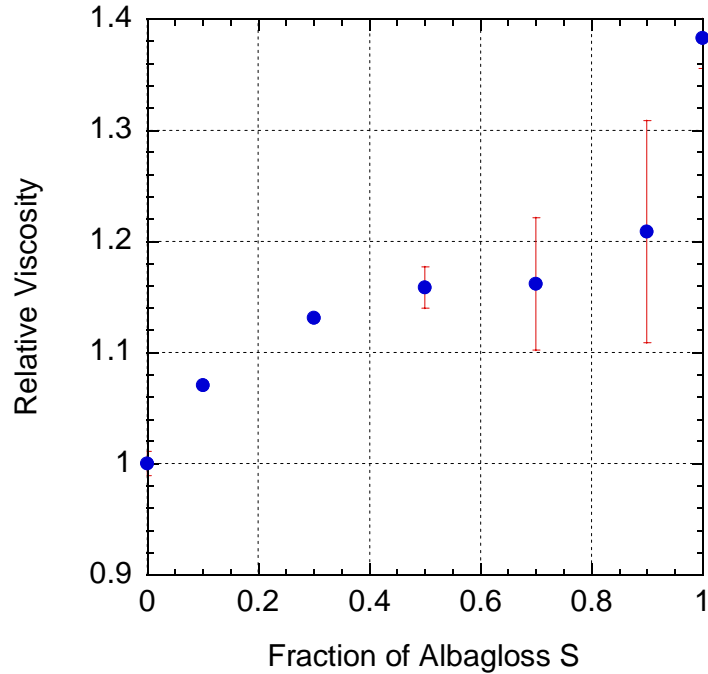


Figure 5.10 Reproducibility of the First Experimental Run for Albagloss S: Albagloss M at 1420 s^{-1}

According to Shapiro and Probstein⁴¹, in a bi-modal suspension with a size ratio of 4 and solids weight fraction below 0.45, the viscosity will exhibit a minimum when the fraction of small particles is in the range of 0.3 to 0.4. Their explanation is that such a bi-modal mixture has a maximum packing fraction of 0.71, as compared to 0.63 ± 0.01 for the uni-modal suspensions. Shapiro and Probstein used glass beads of 40 and 160 μm in a glycerine/water solution (ratio 95/5 by weight). In their experimentation, the particles are above colloidal size ($>10\mu\text{m}$), so that Brownian motion does not play an important role in comparison to hydrodynamic forces. However, their observations regarding the combination ratios at which there is a minimum in viscosity, are in agreement with previous experimentation by Farris.⁴⁶ Farris proposed a model to estimate the viscosity of bi-disperse suspensions; this model is inadequate for suspensions of colloidal size

particles, since it does not account for Brownian motion. Most of the modeling work performed by researchers has not been of industrial relevance since coating pigments are in the colloidal size range, have not a perfect spherical shape, and the models lack accounting of Brownian motion due computational cost. For example, Toivakka and Eklund³⁷ concluded that due to the complexity of particle interactions in concentrated suspensions, the prediction of viscosity for systems more complex than a bi-modal spherical particles suspension has not been accurate enough.

An interesting point of reference is the work performed by Zaman and Moudgil⁴⁷ on bi-disperse suspensions of colloidal size: 0.6 ± 0.05 , 0.85 ± 0.05 , and $1.5 \pm 0.1 \mu\text{m}$. An aqueous solution of 0.01 mole/liter of NaNO_3 at a pH of 9.5 was used as base fluid at 25 °C. The rheological measurements were performed on mixtures with a total particle volume fraction of 0.5 at a shear rate of 1000 s^{-1} . Figure 5.11 presents a comparison of the results obtained by Zaman (solid triangles) utilizing SiO_2 spherical particles, and the results obtained by using Albagloss S and Albagloss M coating mixture (solid squares). The average particle size used by Zaman was 0.6 and 0.85 μm . For this comparison, Albagloss S and M were used since their size ratio is the most comparable to the literature data. The comparison was performed at 1000 s^{-1} , since this is the shear rate at which Zaman and Moudgil results are reported. The solids volume fraction is 0.5 for the suspension used by Zaman and 0.46 for our PCC coatings.

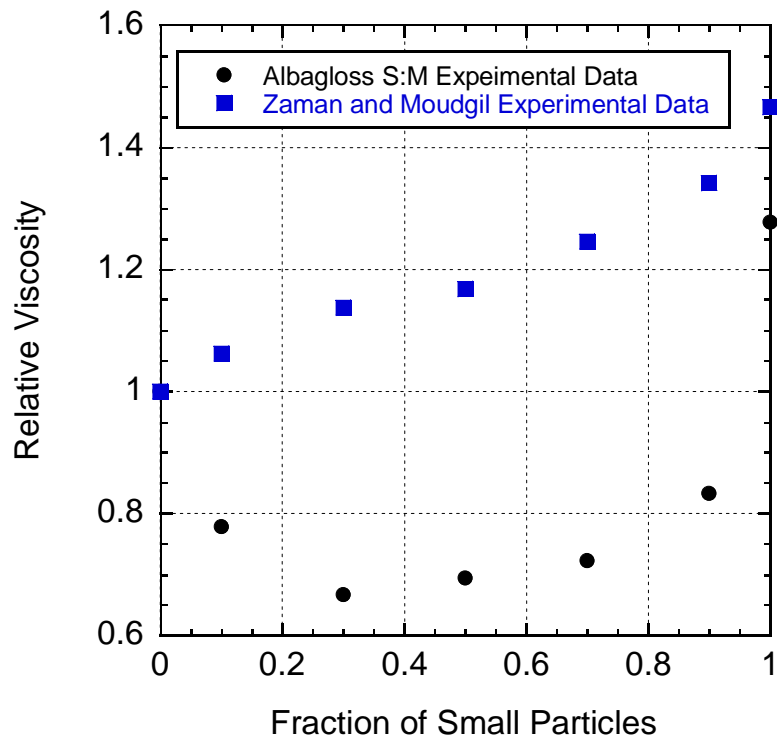


Figure 5.11 Comparison of Relative Viscosity of Silica Particles Suspension at 50 vol.% with Average Sizes 0.6 and 0.85 μm and PCC Albagloss S and M Suspension at 48 vol.% with Average Sizes 0.6 and 1.0 μm at 1000s⁻¹.

A minimum in viscosity at a fraction of 0.4 of small particles, as in Zaman’s data, was not observed for the coating based on Albagloss S and M. Although the size ratio of both suspensions is comparable, the PCC pigments are not as spherical as silica particles and the silica particle size distribution is narrower than PCC. The silica particles have a more efficient packing; this can be easily observed if the viscosity of both single small particle suspensions are compared. Silica (size 0.6 μm) has a higher maximum packing fraction, thus, the viscosity of the silica suspension is lower than the PCC Albagloss S coating at approximately 50 vol %. The concept showed by Zaman et al is of limited applicability to the paper coating industry, since most of the particles encountered in industrial suspensions are not well-defined hard-spheres like silica.

In the first experimental run of both bi-modal coatings, interesting changes in viscosity occurred when 10 % by weight of large particles were added to 90% by weight of Albagloss S. At 1.73 s^{-1} , the relative viscosity decreased by $43 \pm 6 \%$ for the mixture of Albagloss XL : Albagloss S (see Figure 5.3 blue solid diamond) , and $29 \pm 9 \%$ for the Albagloss M : Albagloss S (Figure 5.7 blue solid diamond). At 1420 s^{-1} , the relative viscosity of Albagloss XL : Albagloss S decreased by $18 \pm 3 \%$ (see Figure 5.4 blue solid triangles), and for the Albagloss M : Albagloss S mixture it decreased $7 \pm 8 \%$ when 10% large particle were added (see Figure 5.8 blue solid triangles).

The hypothesis is that the viscosity change is due to an increase on the coating packing fraction because of the 90:10 combination of small and large particles. The higher degree of packing facilitates the mobility of particles in the two bi-modal coatings in comparison the mobility of the uni-modal coatings; this would produce higher fluidity and, thus, lower viscosity (see figure 5.11). The coating mixture of Albagloss XL : Albagloss S has a larger decrease in viscosity than the Albagloss M : Albagloss S mixture because the size ratio of the XL:S is approximately twice that for M:S (see Figure 5.11 and 5.12). In literature, it has been reported that, the larger the size ratio, the lower the viscosity.⁴¹ The large size ratio of the XL : S coating allows the small particles to efficiently fill in the voids between large particles, which creates a higher packing fraction and also serve as “ball bearing” to decrease the hydrodynamic forces created by the particle-to-particle interaction.⁸

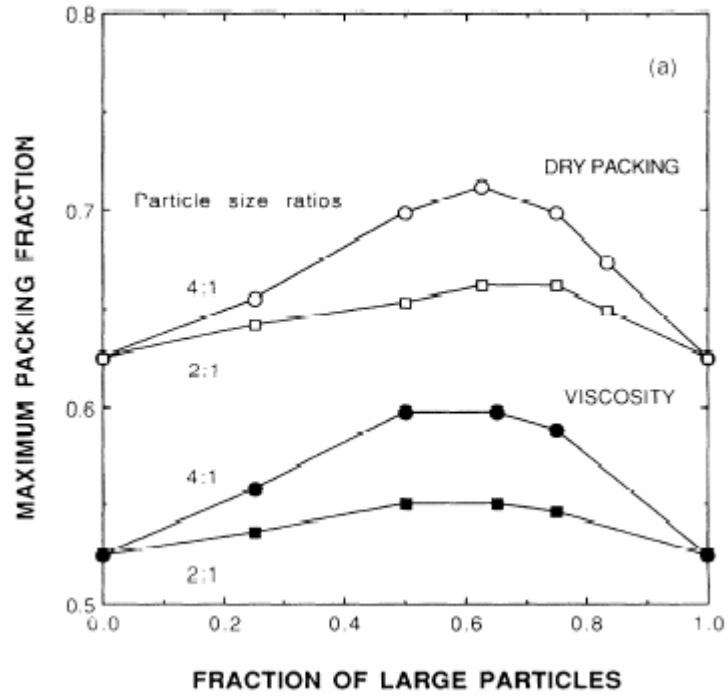


Figure 5.12 Comparison of Fluidity limit and Dry Random-Close-Packing Fraction for Bidisperse Suspensions with Particle Size Ratios of 2:1 and 4:1. Open symbols are dry packing measurements and Solid Symbols are Viscosity Measurements.

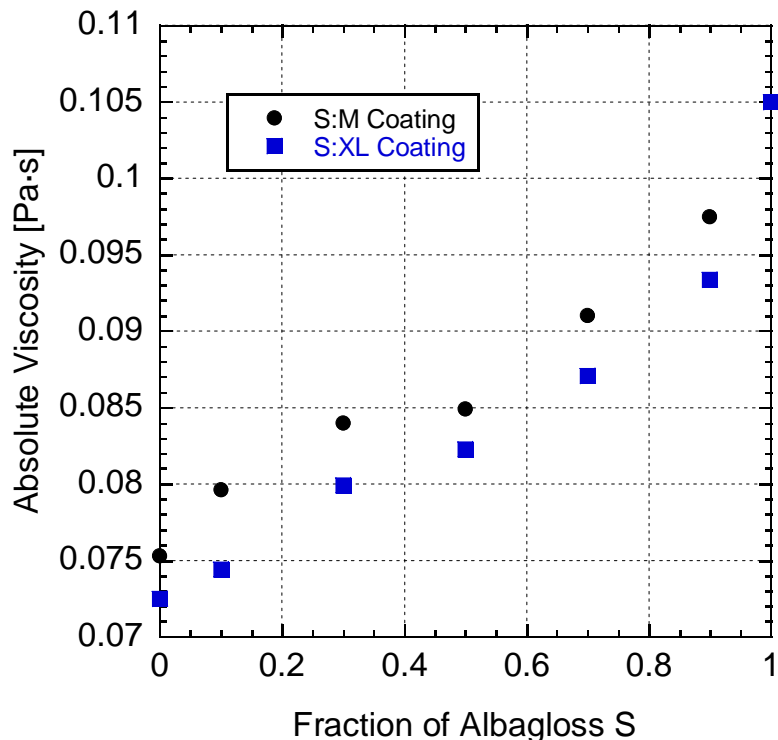


Figure 5.13 Absolute Viscosity of Albagloss S: Albagloss M Coating (blue triangles) and Albagloss S: Albagloss XL Coating (red squares) at 1420 s^{-1} for the First Experimental Run

For the third experimental run, the presence of hysteresis can be observed at both shear rates for both pigment combinations (see Figures 5.3, 5.4, 5.7, and 5.8). At low shear rates (1.73 s^{-1}), hysteresis will be greater because of the effects of Brownian motion. At high shear rates (1420 s^{-1}), hysteresis is smaller since the high shear aligns the particles. Hysteresis arises from the flow history that the suspension acquires with the alignment of the pigments after the first experimental run. In the majority of the cases (except for Figure 5.7), the second and third experimental run present lower viscosities than the first experimental run. This occurs because the particles have been aligned in the first run and thus the energy necessary to make the coating flow will be less than when the particles were randomly oriented. From Figure 5.14 it can be observed that hysteresis is greater

for larger size ratios. In this case, the coating of Albagloss S and Albagloss XL presents a slightly larger hysteresis because its larger size ratio produces a higher maximum packing fraction. Due to resulting higher fluidity at the same solids load, particles will be able to move more easily, thus, preventing particles from forming an organized solid-like structure.

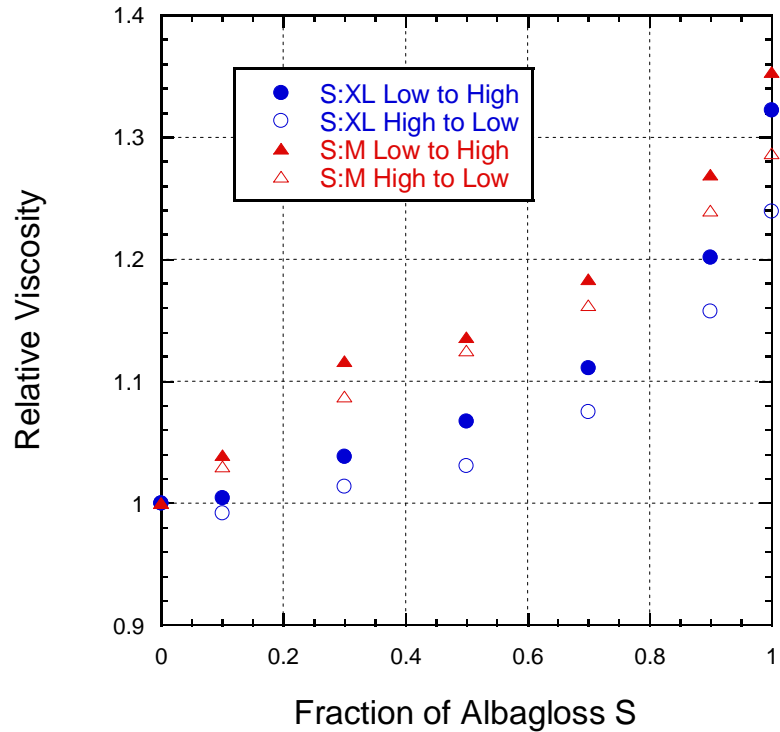


Figure 5.14 Hysteresis in the Third Experimental Run for the Two Pigment Combinations of Different Size at 1420 s^{-1}

From the results for PCC particles with the same shape it can be inferred that pigment packing is not efficient enough to produce a minimum in the viscosity as suggested by Zaman and Moudgil. However, a positive impact in coating viscosity is observed when 10 % of large PCC particles are added to a system containing small PCC particles.

5.3 Viscosity of Coating Mixtures with Pigments of Different Shape

A viscosity analysis for two combinations of coatings with different particle shape was carried on at the selected shear rates. Opacarb ($D_{50}= 0.4 \mu\text{m}$), Albagloss S ($D_{50}= 0.6 \mu\text{m}$), and Albagloss XL ($D_{50}= 2 \mu\text{m}$) have different sizes and shapes. Opacarb has an aragonite (needle-like) shape with aspect ratios of approximately 3 to 4 while Albagloss XL and S (calcite) have aspect ratios in the range between 1 and 2 (see section 4.1). Figure 5.15 to 5.22 present the results obtained from the rheological analysis of the coatings combinations and the reproducibility of the data, analogous to the data in the previous section for bimodal mixtures of same-shape particles.

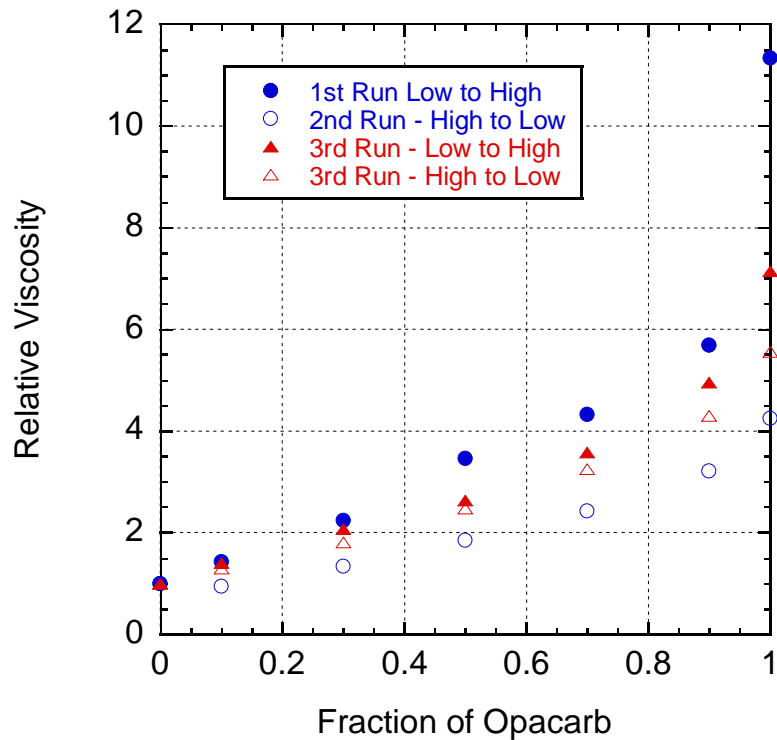


Figure 5.15 Relative Viscosity for Opacarb : Albagloss XL combination at 1.73 s^{-1} for the Three Experimental Runs

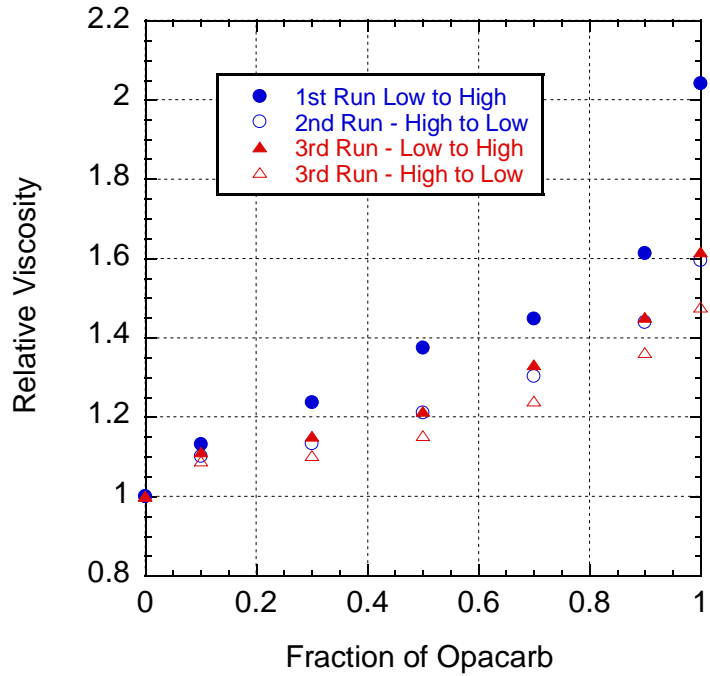


Figure 5.16 Relative Viscosity for Opacarb : Albagloss XL combination at 1420 s^{-1} for the Three Experimental Runs

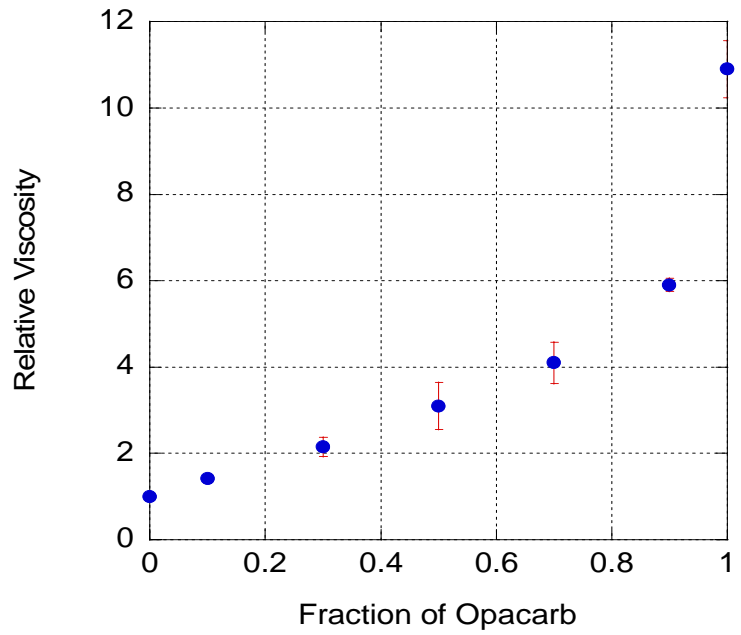


Figure 5.17 Reproducibility of the First Experimental Run for Opacarb : Albagloss XL at 1.73 s^{-1}

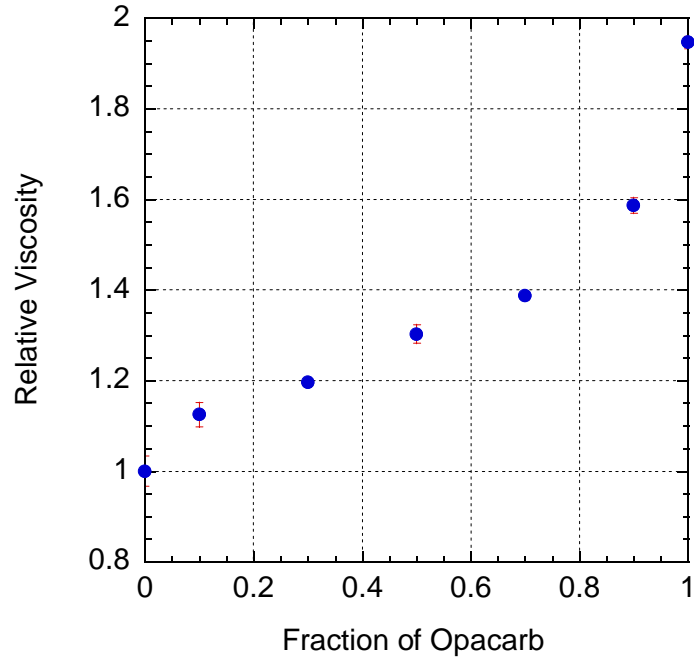


Figure 5.18 Reproducibility of the First Experimental Run for Opacarb : Albagloss XL at 1420 s^{-1}

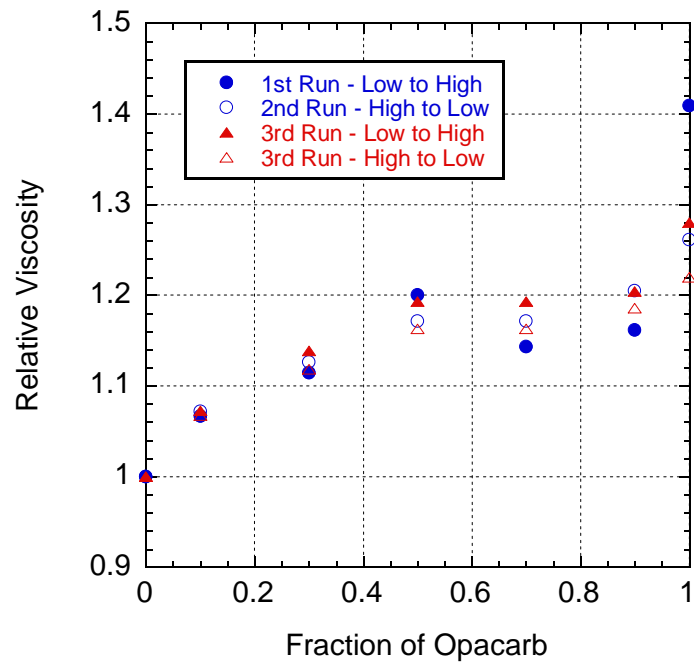


Figure 5.19 Relative Viscosity for Opacarb : Albagloss S combination at 1.73 s^{-1} for the Three Experimental Runs

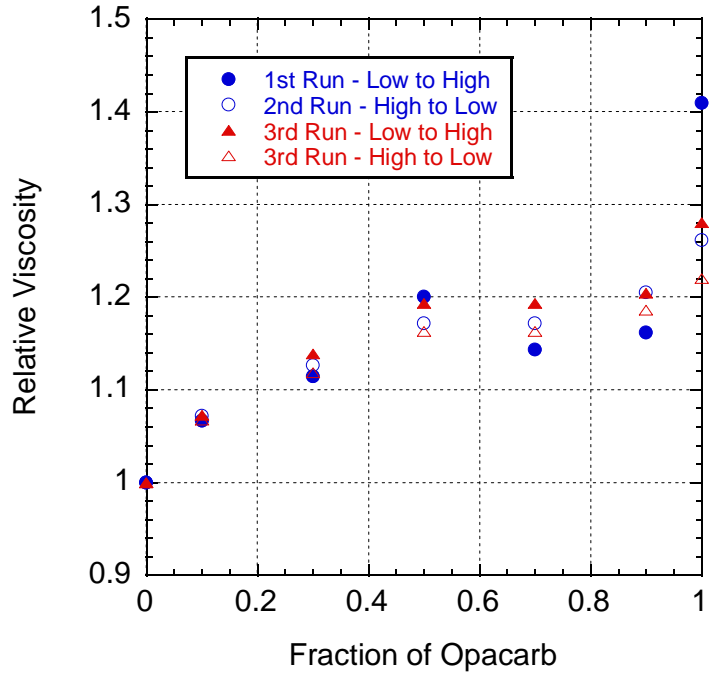


Figure 5.20 Relative Viscosity for Opacarb : Albagloss S combination at 1420 s⁻¹ for the Three Experimental Runs

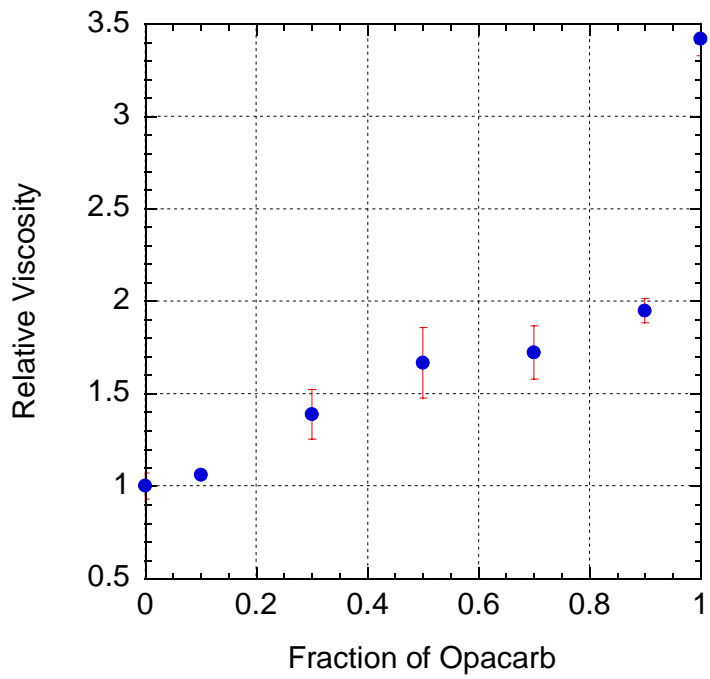


Figure 5.21 Reproducibility of the First Experimental Run for Opacarb : Albagloss S at 1.73 s⁻¹

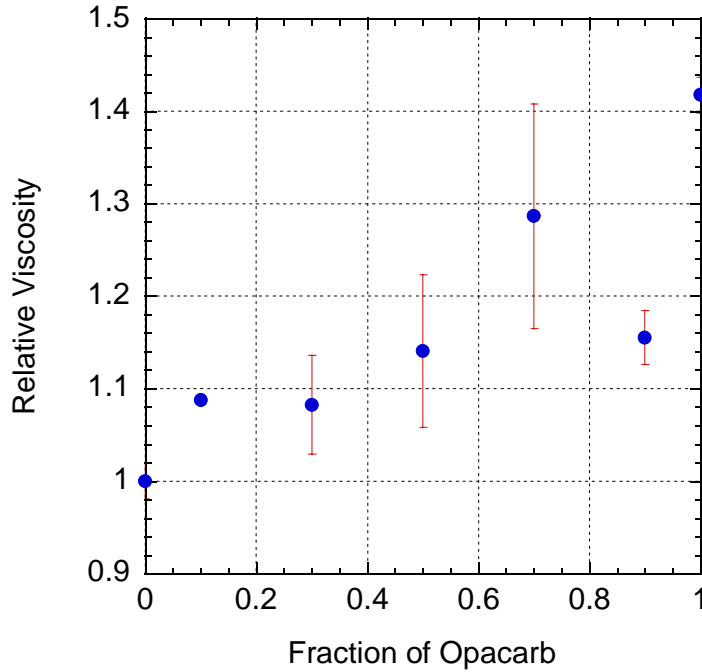


Figure 5.22 Reproducibility of the First Experimental Run for Opacarb : Albagloss S at 1420 s^{-1}

The combination of different shapes of PCC makes this study innovative. Shapiro and Probstein⁴¹, Toivakka and Eklund⁴⁵, Zaman and Mougil⁵⁵, and Tsai et al⁵⁶ all used well-defined spherical particles (i.e., glass beads) to perform their studies and noticed a minimum in viscosity when the fraction of small particles is approximately between 0.20 and 0.40 which does not agree with our results. Most of the mentioned authors used similar particles, and their results agree with each other. However, PCC as observed in section 4.1, has slightly irregular shapes producing a lower packing efficiency than the glass beads used by other researchers. Even though a viscosity minimum is not present when using different PCC particle shapes, such mixtures can potentially increase the packing fraction due to a more organized particles structure. Spheres are not the geometrical bodies with the highest possible maximum packing fraction. In the study of

Donev⁴⁹, it was observed that ellipsoids have a higher random close packing than spheres, suggesting that combinations of different geometries could have a positive impact on rheology. There has not been a relevant systematic study to account for geometrical combinations other than spherical. In this study, the availability of PCC with different shapes makes it possible to use pigment combinations of different sizes and shapes. The combination of different PCC shapes provides an opportunity for innovation.

Albagloss XL has $D_{50}=2\ \mu\text{m}$, and Opacarb has $D_{50}=0.4\ \mu\text{m}$. At a shear rate of $1.73\ \text{s}^{-1}$, when Albagloss XL particles are added so that the Opacarb fraction in the mixture is 0.9, the viscosity drops $50 \pm 4\ \%$ in comparison to the viscosity of a pure Opacarb coating. The effect is diminished in the second and third experimental run because of the particle alignment but there are still significant decreases of viscosity at the same small particles fraction of 0.9. Good reproducibility was obtained at this shear rate, see Figure 5.17.

The effects of mixture composition on viscosity were also measured at a shear rate commonly found in the industry during pumping, mixing, and coating application operations; results for a shear rate of $1420\ \text{s}^{-1}$ are provided in Figure 5.16. For the first run, the change in viscosity when the fraction of Opacarb is 0.9 is $21 \pm 3\ \%$ in comparison to the viscosity of pure Opacarb coating.

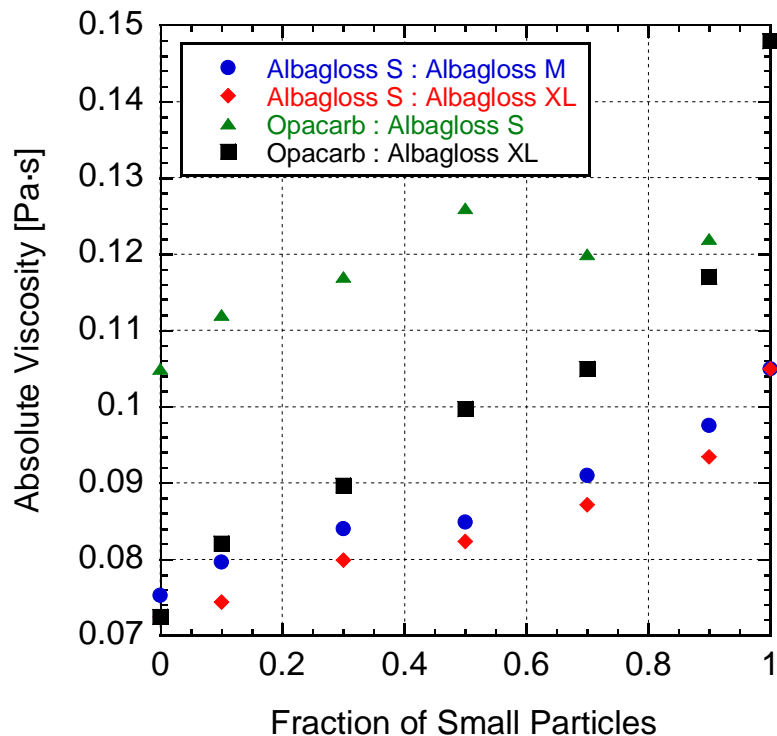


Figure 5.23 Absolute Viscosity of the Four Pigments Coatings Combinations in the First Experimental Run at 1420 s⁻¹

Due to its large size ratio in comparison to the other three coating combinations, an interesting combination of size and shape resulted from the mixing of Albagloss XL and Opacarb. The summarized results in Figure 5.23 show that this pigment combination has the most dramatic reduction of viscosity upon the addition of a small fraction of large particles. This suggests the system has the highest maximum packing fraction among the four coatings. The key factors making it the most relevant result are:

1. The large size ratio of Albagloss XL to Opacarb
2. The pigment shape combination that potentially causes Opacarb to fill in the void spaces between Albagloss XL particles better than Albagloss S

- The better fluidity due to higher achievable packing fraction obtained with the 90/10 Opacarb to Albagloss XL ratio

Hysteresis is encountered more significantly for mixtures of different shapes than for different sizes mixtures, provided that the size ratio for both mixtures is approximately the same. This is potentially related to increases in the maximum packing fraction. The size ratio of Albagloss XL to Opacarb in conjunction with the shape combination makes this the coating combination with highest hysteresis as observed in Figure 5.24 (compare with fig. 5.14).

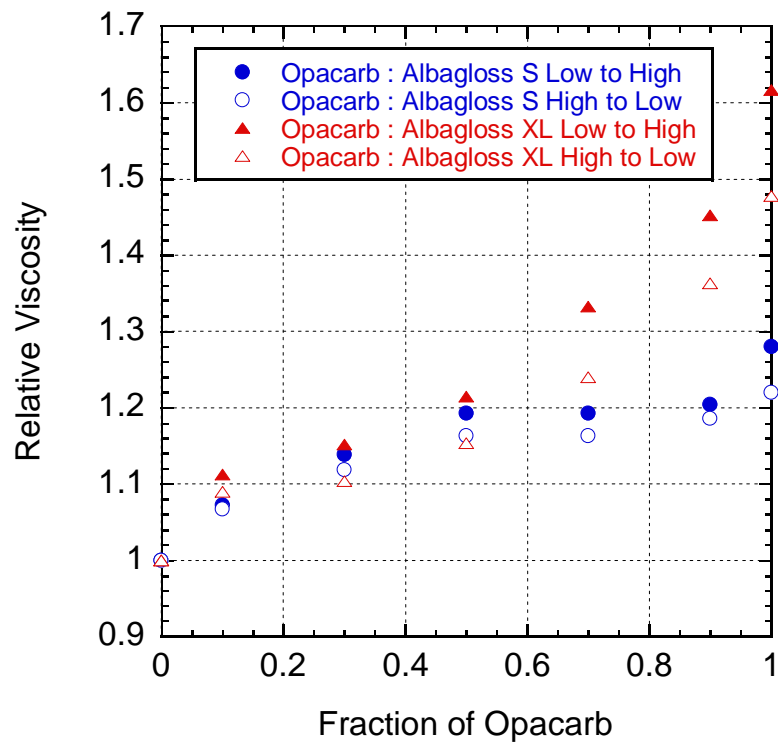


Figure 5.24 Hysteresis for the Third Experimental of Two Pigment Coating Combinations of Different Shape and Size at 1420 s^{-1}

As previously mentioned, a key factor regarding the large viscosity decrease of Opacarb:Albagloss XL (90/10) coating, is the more efficient packing in comparison to the other coatings in this research. The combination of the rhombohedra shape and small size of Opacarb can produce a more efficient packing in the voids of Albagloss XL, thus allowing a higher fluidity of the paper coating.

For a systematic comparison of the rheology of the different pigment size and shape combinations, the absolute viscosity and percent of decrease in viscosity by utilizing different combinations are provided in Figures 5.26 to 5.29.

As previously mentioned, Opacarb has the highest viscosity among all the coatings, when larger particles are added; it presents the most dramatic decrease in viscosity for both shear rates reported. The objective of figures 5.26 and 5.27 is to show a clearer comparison of the viscosities of the different coatings. The percent decrease in viscosity of the two more relevant results from the section 2 and 3 of the results, the addition of Albagloss XL to Albagloss S and Opacarb, are presented in figures 5.28 and 5.29.

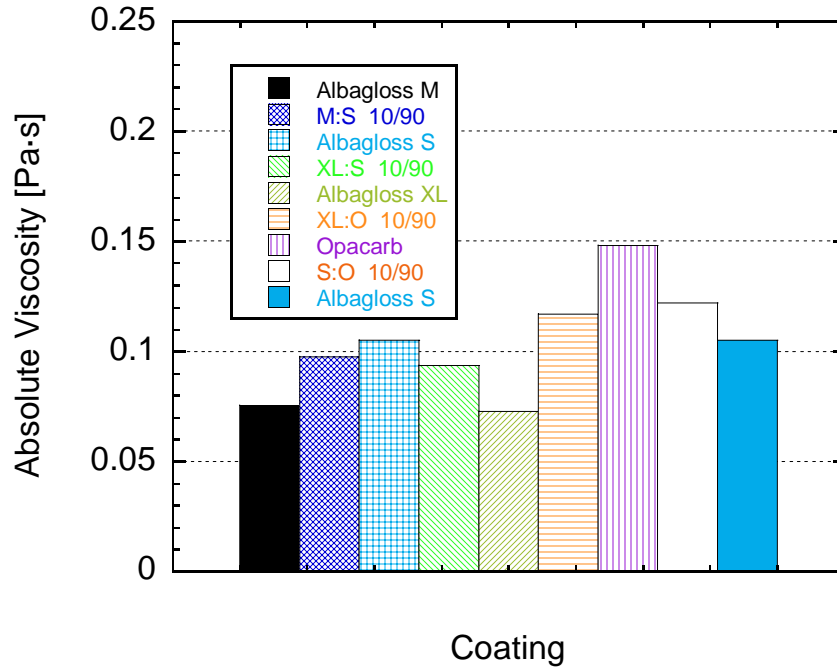


Figure 5.25 Absolute Viscosity of the Coatings at 1.73 s^{-1}

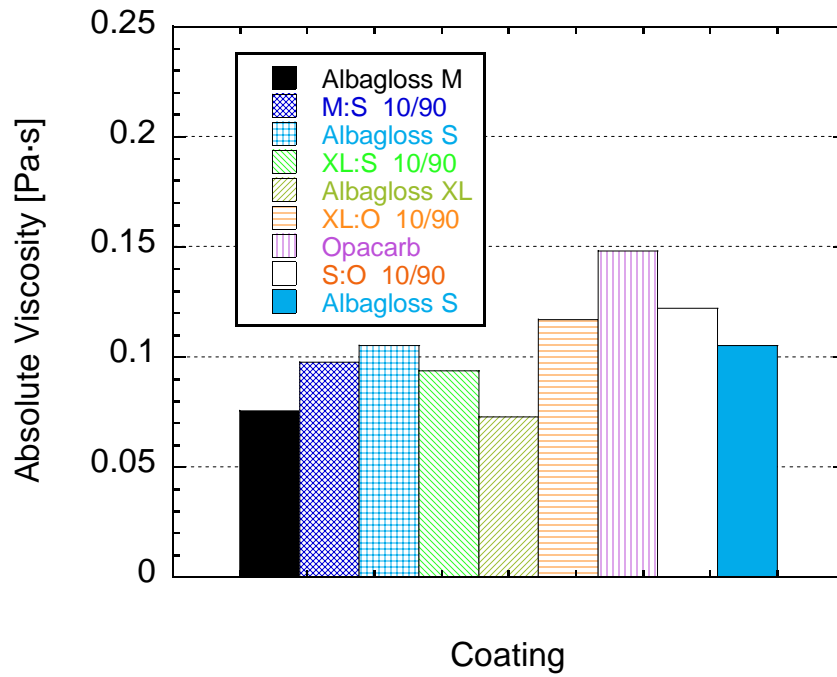


Figure 5.26 Absolute Viscosity of the Coatings at 1420 s^{-1}

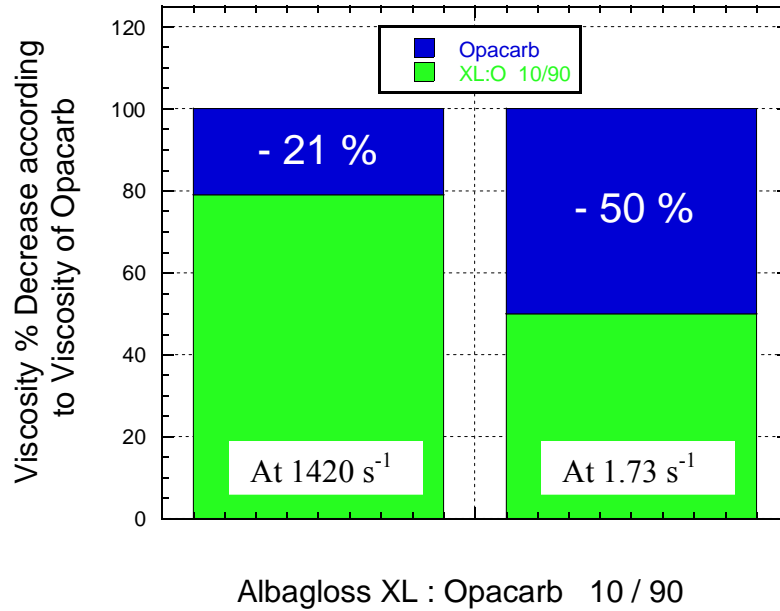


Figure 5.27 Decrease in Viscosity by Using Opacarb / Albagloss XL (90/10) Combination. Each entire bar represents the viscosity of pure Opacarb coating.

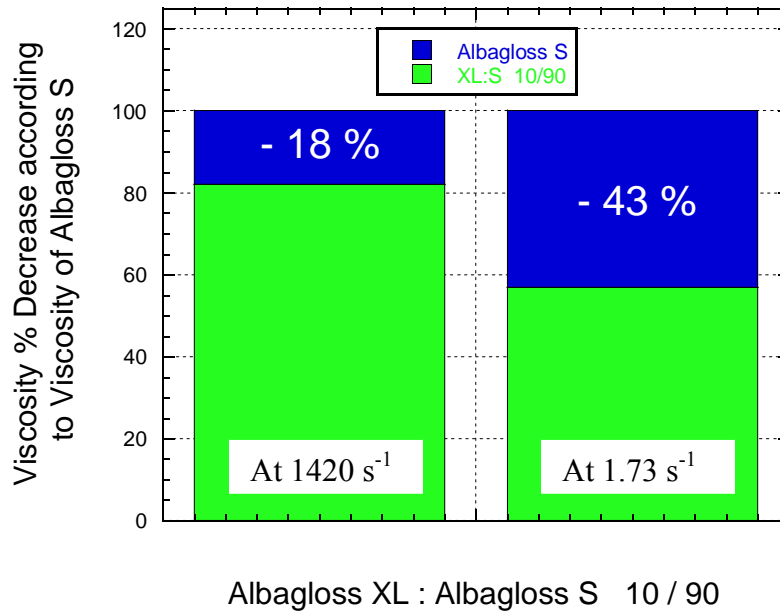


Figure 5.28 Decrease in Viscosity by Using Albagloss S / Albagloss XL (90/10) Combination. Each entire bar represents the viscosity of pure Albagloss S coating.

5.4 Paper Testing Results

To support the theory of a higher packing fraction when a combination of Opacarb and Albagloss is used, an analysis of the properties of coated paper was performed. It is expected that the particle packing efficiency will have an effect on brightness, gloss and surface roughness. Therefore, coated paper substrates were generated for four coating formulations: pure Albagloss XL, pure Albagloss S, pure Opacarb, and Opacarb:Albagloss XL mixture at ratio 90:10. Glossiness, roughness, porosity, brightness and a wax picking tests were performed according to TAPPI standards, as described in section 4.5. For each test, ten measurements were performed on each coated paper sample. Out of the ten measurements, three were performed on three different sheets, the tenth measurement was performed on one of the previous sheets (randomly selected). For porosity, only three measurements per coated sample were performed.

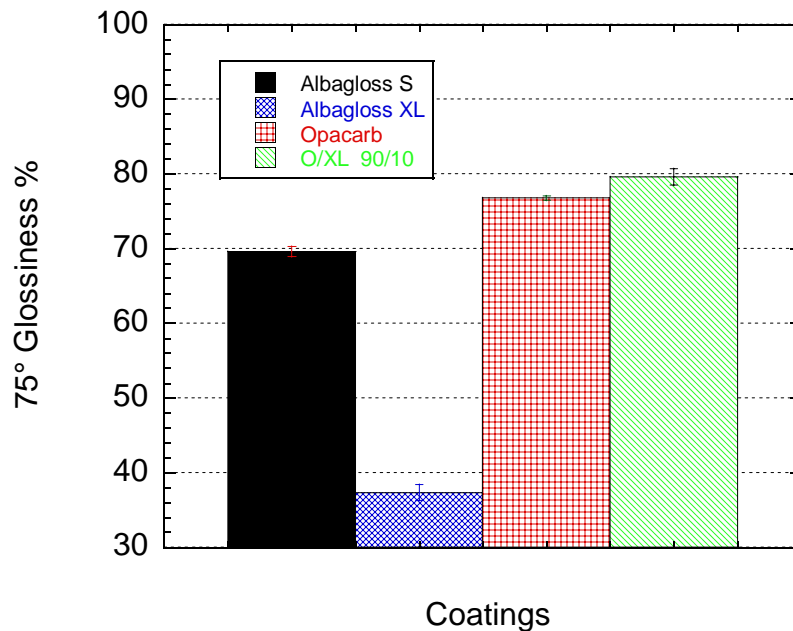


Figure 5.29 Glossiness test

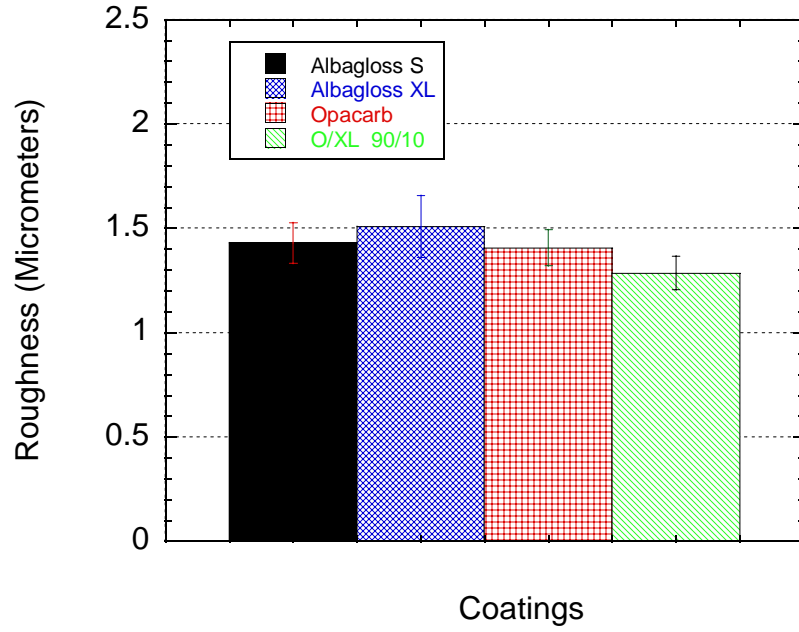


Figure 5.30 Roughness Test

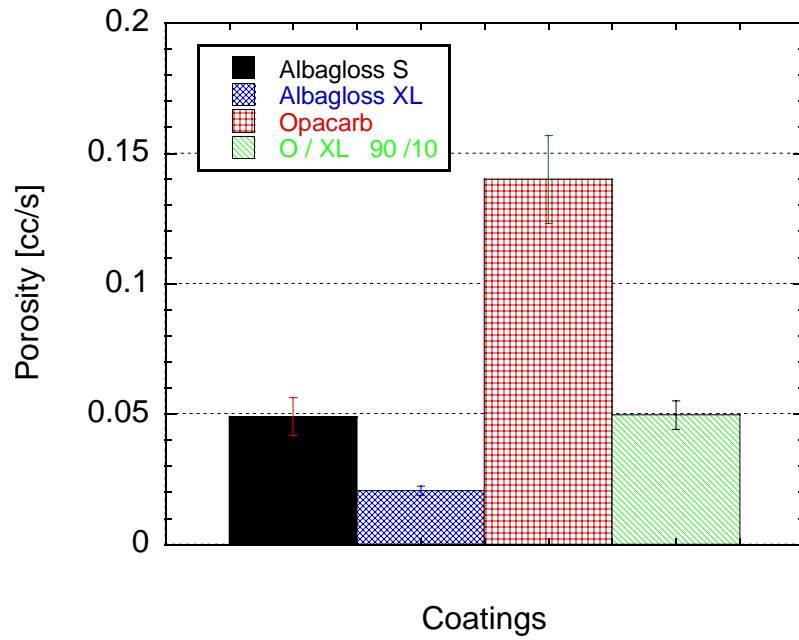


Figure 5.31 Porosity Test

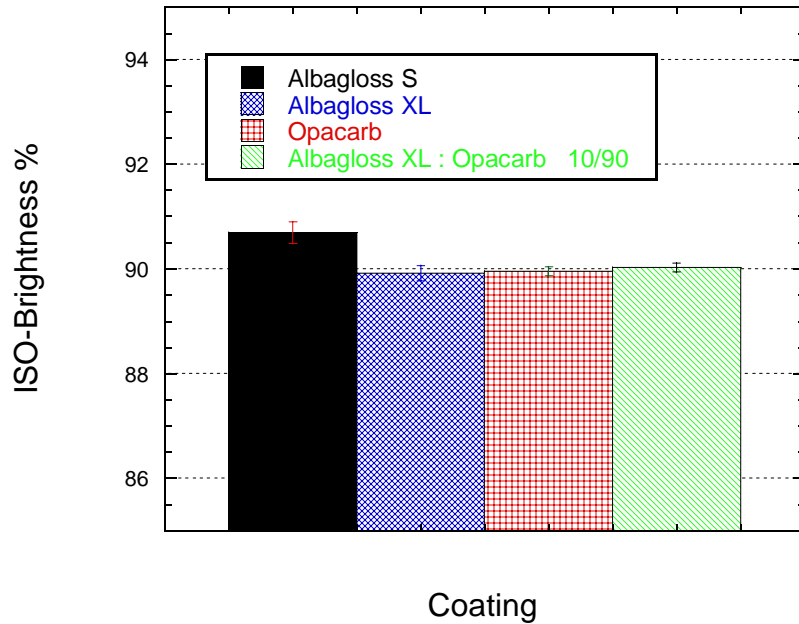


Figure 5.32 ISO-Brightness

Results show that the glossiness for the bi-modal coating is higher than all pure coatings, suggesting a better packing with the absence of pores due to the presence of small pigments that fill the voids. Glossiness of Opacarb:Albagloss XL (90/10) was 80 ± 1 % in comparison to pure Opacarb coating of 77 ± 0.3 %.

Roughness characterizes about the surface morphology of coated paper by indicating the average height between the valleys and the peaks of the surface. The mixture Opacarb:Albagloss XL (90/10) presented the lowest roughness, 9 ± 0.5 % lower than the Opacarb coated paper. Once again, this can directly be explained by a denser pigment packing.

Porosity is the clearest indicator of packing. The test is based on the volumetric flow rate of air through the coated paper, measuring the time that it takes for 25 cc of air to pass through the sheet at standardized pressure. From the porosity results it can be observed that the mixture of Opacarb and Albagloss XL presents less porosity than Opacarb. Apparently, when 10% of large particles are added to the Opacarb particles, the maximum packing fraction of the mixture is increased. Packing fraction can be inferred from dry packing according to Shapiro and Probstein (see Figure 5.12), therefore supporting the hypothesis that the decrease in viscosity when adding 10% of large particles is caused by a superior particle packing since the porosity and glossiness tests suggest it.

Brightness is not a clear indicator of packing but it is also slightly enhanced by the bi-modal nature of the coating. ISO-Brightness was about the same for the bi-modal coating ($90 \pm 0.07\%$) as for pure Opacarb ($89.95 \pm 0.06\%$).

The pigment size and shape combination of Opacarb and Albagloss XL in a ratio of 90/10 have a positive impact in the coated paper properties due to a significant change in properties, increase in glossiness and decrease in porosity. Higher glossiness leads to higher ink gloss and a better looking surface, lower porosity leads to higher blister resistance when the coated paper is being dried. Therefore, we can conclude that it is possible to achieve a decrease of coating viscosity without compromising the coated paper quality, which makes this an attractive idea.

5.5 Results Modeling

For concentrated suspensions ($\phi > 0.4$), modeling of uni-modal suspensions can be performed by using the Krieger-Dougherty equation (section 2.2.5) or a slight modification of it by varying the power at which the term that includes the volume fractions is raised. By modifying this term, using values usually between 2 and 3, the equation can perform a better fit to account for colloidal interactions (Dames et al., Quemada⁴⁸). As for bi-disperse suspension there is no exact model that could fit all data for colloidal size particles or different size ratios (see Figure 5.34 by Zaman et al.³). In Farris⁴⁶ model colloidal forces are neglected, this is the reason why the agreement between data observed by Zaman (colloidal particles) can not be predicted by Farris model.

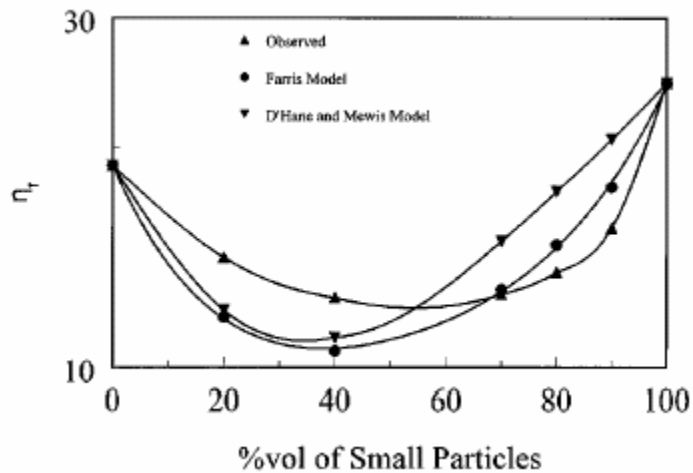


Figure 5.33 Comparison between the observed relative viscosity and predicted values from the Farris and D'Haene and Mewis model for 50 vol% bidisperse silica suspensions containing 0.6 and 0.85 μm silica particles at a shear rate level of 1000 s^{-1} at $25 \text{ }^\circ\text{C}$.³

Since there is no direct rational procedure to account for all the potential variables, an empirical method was proposed by Zaman and Moudgil to calculate the viscosity of bi-modal suspensions based on the viscosity of bi-modal suspensions as a function of volume fraction of small particles in the mixture and the viscosity of related mono-sized suspensions. There the empirical model would once again express the relative viscosity in terms of volume fractions but since it is based on observations it accounts for the hydrodynamic forces and particle-to-particle interactions. Once the data is represented in the requested form, the experimental data is adjusted with a third order polynomial. According to Zaman and Moudgil, the resulting equation can predict the behavior of the same suspension at different volume fractions.

D'Haene and Mewis considered the bi-modal dispersion as a suspension of coarse spheres in a “quasi-continuum” suspension formed by small particles in a Newtonian fluid.⁴⁹ The model proposed by D'Haene and Mewis performs a good fit for bi-modal colloidal suspension of large size ratios (size ratios approximately above 6) and it has some of its fundamentals on the Krieger-Dougherty equation. The size ratio of the PCC used in this research is approximately 5 for Albagloss XL:Opacarb and 3.3 for Albagloss XL:Albagloss S and the suspending fluid is non-Newtonian (latex, starch, and water). Also in some mixtures the shapes of PCC is different. All these factors that differ from the experimental conditions of D'Haene and Mewis lead to the conclusion that a modified D'Haene and Mewis model could potentially provide us with the capability of predicting results when PCC is used. To come up with a model backed-up by data, further rheological experimentation should have been done with PCC-Based coatings at

different volume fractions. With the available data, an idea of parameters that would impact our model if there were enough experimental information can be obtained.

According to a modified Krieger-Dougherty model the viscosity of a mono-disperse suspension of small particle could be obtained with,

$$\eta_{small} = \eta_{BaseFluid} \cdot \left(1 - \frac{\varphi_{Small}}{\varphi_{max,Small}} \right)^{-\beta\varphi_{max,Small}} \quad (5.1)$$

where β is derived from the size ratio, and shape of the particles to perform a better fit of the experimental data. Then for a bi-disperse suspension if the assumption of D’Haene and Mewis is considered regarding the consideration of the suspension of small particles as the base fluid for a “mono-disperse” suspension of large particles, the equation 7.1 would be as follows,

$$\eta_{Bi-disperse} = \eta_{small} \cdot \left(1 - \frac{\varphi_{XL}}{\varphi_{max,XL}} \right)^{-\alpha\varphi_{max,XL}} \quad (5.2)$$

where α is a parameter that accounts for colloidal interactions, shape, and size ratio effects. Now combining equations 7.1 and 7.2 the full equation for the bi-disperse suspension can be obtained,

$$\eta_{Bi-disperse} = \eta_{BaseFluid} \cdot \left(1 - \frac{\varphi_{Small}}{\varphi_{max,Small}} \right)^{-\beta\varphi_{max,Small}} \cdot \left(1 - \frac{\varphi_{XL}}{\varphi_{max,XL}} \right)^{-\alpha\varphi_{max,XL}} \quad (5.3)$$

With the equation for bi-disperse suspensions and the available experimental data, a relation to estimate the effect of particle shape that has to be accounted for in future models can be performed by obtaining the viscosity ratio between two coating mixtures.

Both coating have in common the same large particle, Albagloss XL. The difference relies in the small particles with different shape in the mixture. The ratio of Opacarb:Albagloss XL to Albagloss S:Albagloss XL is obtained by the following equation,

$$\frac{\eta_{Opacarb:XL}}{\eta_{Small:XL}} = \frac{\eta_{BaseFluid} \cdot \left(1 - \frac{\varphi_{Opacarb}}{\varphi_{max,Opacarb}}\right)^{-\beta_{Opacarb}\varphi_{max,Opacarb}} \cdot \left(1 - \frac{\varphi_{XL}}{\varphi_{max,XL}}\right)^{-\alpha\varphi_{max,XL}}}{\eta_{BaseFluid} \cdot \left(1 - \frac{\varphi_{Small}}{\varphi_{max,Small}}\right)^{-\beta_{Small}\varphi_{max,Small}} \cdot \left(1 - \frac{\varphi_{XL}}{\varphi_{max,XL}}\right)^{-\alpha\varphi_{max,XL}}} \quad (5.4)$$

then, equation 7.4 simplifies to,

$$\frac{\eta_{Opacarb:XL}}{\eta_{Small:XL}} = \frac{\left(1 - \frac{\varphi_{Opacarb}}{\varphi_{max,Opacarb}}\right)^{-\beta_{Opacarb}\varphi_{max,Opacarb}}}{\left(1 - \frac{\varphi_{Small}}{\varphi_{max,Small}}\right)^{-\beta_{Small}\varphi_{max,Small}}} \quad (5.5)$$

The ratio of the viscosities can provide us with some insight regarding the effect of shape (see Figure 5.35) and how it should be taken into consideration when modifying the Krieger-Dougherty equation. From figure 5.35 it can be observed that at high shear rates the effect of shape on viscosity will be small since the experimental data shows to be close to constant at 1420 s^{-1} . This result means that when modeling coatings assuming high shear rates, shape can be a negligible factor for the modeling. If results are being modeled at low shear rates, from Figure 5.35 it can be observe that a shape factor has to be included into the formula.

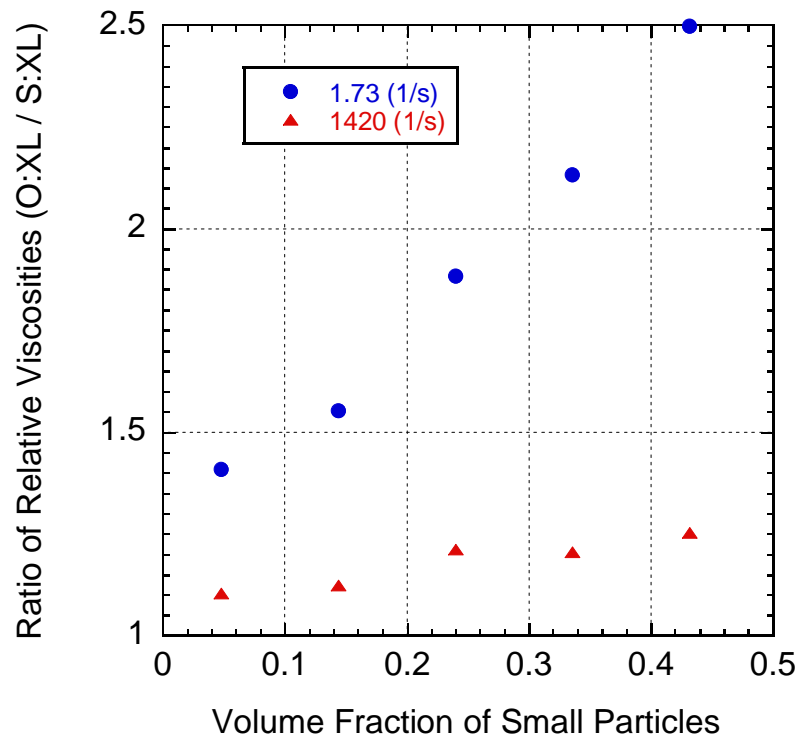


Figure 5.34 Ratio of Absolute Viscosities of Opcarb:AlbaglossXL and Albagloss S and Albagloss XL at Two Different Shear Rates

Since there is no direct rational procedure to account for all the potential variables, an empirical method was proposed by Zaman and Moudgil to calculate the viscosity of bi-modal suspensions based on the viscosity of bi-modal suspensions as a function of volume fraction of small particles in the mixture and the viscosity of related mono-sized suspensions. There the empirical model would once again express the relative viscosity in terms of volume fractions but since it is based on observations it accounts for the hydrodynamic forces and particle-to-particle interactions. Once the data is represented in the requested form, the experimental data is adjusted with a third order polynomial. According to Zaman and Moudgil, the resulting equation can predict the behavior of the

same suspension at different volume fractions. The model of Zaman and Moudgil is derived as follows,

$$\eta_{rel} = H(\varphi_f) \cdot G(\varphi_c) \quad (5.6)$$

where $H(\varphi_f)$ is the viscosity of the suspension with small particles and $G(\varphi_c)$ is an unknown function which is being calculated from the viscosity of bi-disperse suspensions and the viscosity of small particles before adding the large particles. Then, if a suspension of large particles is considered instead a fine particles suspension, and more large particles are added, the viscosity of the suspensions of large particles is as follows,

$$G_m(\varphi_c) = \frac{\eta_{rel(mc)}}{G_m(\varphi_f)} \quad (5.7)$$

where m stands for mono-disperse system and c for large particles. $G_m(\varphi_c)$ and $G_m(\varphi_f)$ vary as the ratio of the fraction of both, large and small particles, changes. The difference between $G_m(\varphi_c)$ and $G(\varphi_c)$ is only due to the presence of small particle in the system and this difference can be normalize by,

$$J(\varphi_f) = \frac{G(\varphi_c)}{G_m(\varphi_c)} \quad (5.8)$$

where $J(\varphi_f)$ is a function the fraction of small particles for bi-modal suspension and it can be obtained a fit of the experimental data. A more detailed explanation of this model can be found in the paper by Zaman and Moudgil.⁴⁷

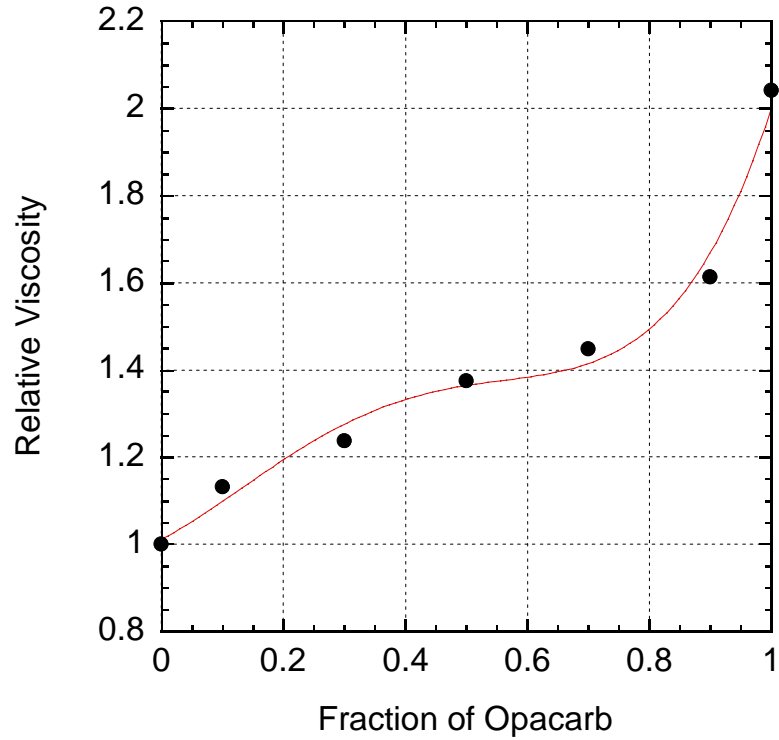


Figure 5.35 Model for the Prediction of Viscosity Values at Volume Fraction of 0.48 at 1420 s^{-1}

By using a fourth order polynomial the data can be adjusted. The equation to determine the viscosity of the mixture of Opacarb and Albagloss XL at 0.46 volume fraction of bi-modal dispersion at different Opacarb mixture volume fractions is:

$$J(\varphi_f) = 4.94\varphi_f^4 - 6.84E^{-3}\varphi_f^3 + 2.17\varphi_f^2 + 0.71\varphi_f + 1$$

where φ_f is the volume fraction of fine in the coatings mixture.

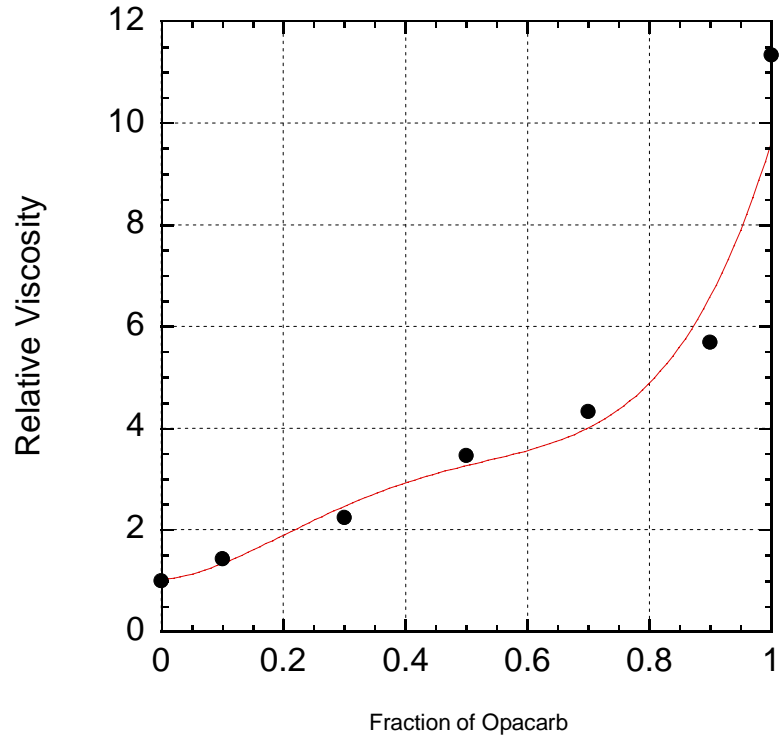


Figure 5.36 Model for the Prediction of Viscosity Values at Volume Fraction of 0.48 at 1.73 s^{-1}

By using a fourth order polynomial the data can be adjusted. The equation to determine the viscosity of the mixture of Opacarb and Albagloss XL at 0.48 volume fraction of bi-modal dispersion at different Opacarb mixture volume fractions is:

$$J(\varphi_f) = 42.64\varphi_f^4 - 62.66\varphi_f^3 + 27.61\varphi_f^2 + 1.02\varphi + 1$$

CHAPTER 6

CONCLUSIONS

Previous research has been performed on the rheology of bi-modal suspensions of particles with the same shape (spheres) but different sizes. Due to the well-defined material used in these studies, industrial applicability of the concepts has been extremely limited. In addition, there is a lack of theoretical methods to define the flow behavior of bi-modal suspensions as a function of the different physical and chemical parameters of the system at high solids volume fractions.

The impact of particle size and shape on the viscosity of paper coatings based on PCC was studied. Four different particle sizes and two different shapes were used. The coating formulations were produced by combining two pigments sizes or two different shapes. The flow curves of the coating formulations were measured on a rheometer in a Couette geometry and the experimental data was analyzed at two shear rates commonly encountered in paper coating operations.

It was found that for all combinations, when 10 % by weight of larger particles are added to 90 % by weight of small particles, the viscosity of the suspension undergoes a significant reduction. Utilizing pigments with the same shape, the decrease on viscosity is dependent on size ratio and is largest for the bi-modal coating of Albagloss

S:Albagloss XL. As size ratio increases, so does hysteresis between consecutive flow curves. The most interesting observation arrived when different pigment shapes were mixed. When 10 % by weight of Albagloss XL was added to 90 % by weight of Opacarb the most dramatic decrease in viscosity of all coatings was observed. By adding 10% of large particles the viscosity dropped by 50 ± 4 % at 1.73s^{-1} and by 21 ± 3 % at 1420s^{-1} . Higher packing fraction was the key factor causing the change in viscosity because of the higher fluidity that it represents. Packing fraction can be inferred from dry particles packing, thus, our hypothesis of a higher packing fraction was supported by the glossiness, porosity, roughness, and brightness tests performed on samples of paper coated with the experimental coatings. There was a significant positive impact on glossiness and coated paper porosity for the mixture of Albagloss XL and Opacarb. Since there is no model that can predict the behavior of all bi-disperse suspensions due to all the physical and chemical parameters encountered, an empirical fit can be performed to the obtained results at a determined volume fraction. The empirical model obtained from the fit can then be used for predicting the behavior of the same mixture at different volume fraction of solids.

The relevance of this project lies in the fact that the developed techniques can immediately be implemented by the industry due to commercial availability of the materials used. The implementation would lead to a decrease of manufacturing cost by avoiding machine down-times and promoting energy savings, thus, increasing the efficiency of the coating processes.

CHAPTER 7

FUTURE RESEARCH

Based on the results obtained, further research can be performed on finding the maximum packing fractions of the used coatings and coatings based on the combination of existent pigments with new pigments being developed with larger aspect ratios (i.e. MD 1074 PCC – Calcite see Figure 7.1). MD1074 has an aspect ratio of approximately 4 to 6 and size distribution of $D_{20}=0.25\mu\text{m}$ $D_{50}=0.4\mu\text{m}$ $D_{90}=0.8\mu\text{m}$. Since Opacarb and MD1074 have approximately the same size distribution, from the aspect ratio can be expected that MD1074 will show a higher viscosity as a single pigment coating in comparison to the previous single pigment coatings in this research. A combination of Albagloss XL with MD1074 could potentially have a higher packing fraction than the mixture of Albagloss XL and Opacarb. The higher packing is suggested by the larger aspect ratio that could allow particles of MD1074 to fill in the void spaces between Albagloss XL particles with higher efficiency; research should be performed to confirm this hypothesis.

In addition, based on the work done by D’Haene and Mewis, modeling of the results obtained in this study can be performed. D’Haene and Mewis considered the bi-modal dispersion as a suspension of coarse spheres in a “quasi-continuum” suspension formed by small particles in a Newtonian fluid.⁴⁹ Results from modeling would not be expected

to be accurate based on the fact that D'Haene and Mewis considered size ratios larger than the actual size ratios of our PCC, used spherical particles, and had a Newtonian suspending fluid. Since our particles do not have a spherical shape and the suspending fluid is non-Newtonian due to the latex and starch components. Therefore, it is expected an implementation of a parameter accounting for size ratio, aspect ratio, and non-Newtonian suspending fluid could be added. In the results modeling a first attempt to account for the effects due to particle shape was performed but more experimentation concerning viscosity of the coatings at different volume fractions of solids needs to be performed.

Furthermore, a study of the PCC-based coatings used here at higher shear rates by using capillary rheometers or high shear rate Couette cylinder rheometers would yield interesting results relevant to the industry at high shear rates not covered by this study. When comparing the viscosity of single pigment coatings with coating mixtures, i.e. pure Opacarb and a 90/10 mixture of Opacarb and Albagloss XL, it is suggested that as shear rate increases, the change in viscosity from the single to the bi-disperse coating will be minimum. This potentially small change has to be quantified to establish the significance of its impact in the rheology of the system, thus, its impact on the coated paper manufacturing process. Other effects that can be studied by analyzing higher shear rates is the shear thickening behavior encounter also in coating machine operations.

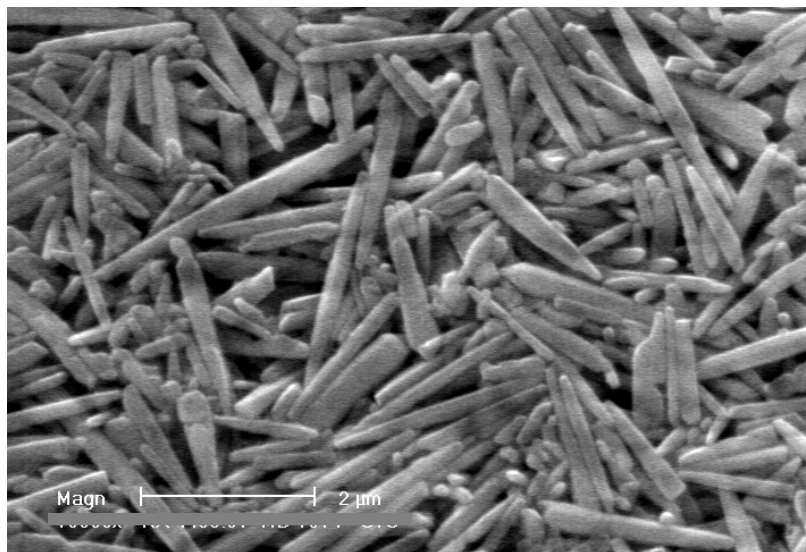


Figure 7.1 MD1074 PCC (Calcite)

Another interesting potential area of expansion of this research is the study of the de-watering kinetics of suspensions, in particular paper coatings. Observations and formulation of concepts on how viscosity changes with a progressive increase of volume fraction of solids can be very valuable to understand the rheological behavior of coatings caused by the de-watering of the suspension right after the metering and through out the drying section in the coating machine. Since porosity could be one of the driving factors, packing fraction could be the mechanism governing or highly influencing the de-watering since it affects the presence of pores. This research can be performed by utilizing an immobilization cell from Paar Physica (see Figure 7.1) that uses a vacuum and a filter to subtract only the water from the suspension in study.

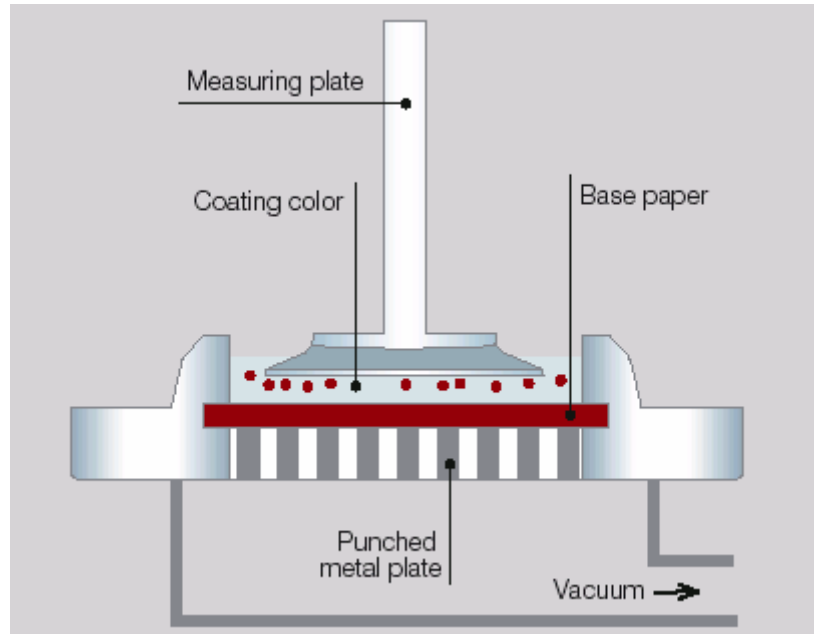


Figure 7.2 Immobilization Cell from Paar Physica

The study of the de-watering kinetics can lead to process and product optimization by improving the rheology of paper coatings through a better understanding of coating components interactions while the volume fraction of solids increases progressively.

REFERENCES

- ¹ Clark, David **“Globalization, Changing Markets and the Challenge to Paper coating Technology”** TAPPI Coating Conference, pp.1 Toronto May 1999
- ² Paulapuro, Hannu Et al. **“Papermaking Science and Technology: Pigment Coating and Surface Sizing of Paper”** Vol. 11 Ch. 1, Esa Lehtinen Helsinki University of Technology, 2000
- ³ Eklund, R. W. **“Trouble-Shooting Coater Runnability Defects”** TAPPI Coating Conference pp.271, May 1999
- ⁴ Carreau, P. J. Ghosh, T. Lavoie, P. **“Rheology of Coatings Colors and Their Runnability on a Cylindrical Laboratory Coater”** TAPPI Coating Conference Proceedings, pp.303, May 1996
- ⁵ Chonde, Y. Roper, J. Salminen, P. **“A Review of Wet Coating Structure: Pigment/Latex/Co-binder Interaction and its Impact on Rheology and Runnability”** Coatings Fundamentals Symposium, Book 1 pp. 57, TAPPI Proceedings 1995
- ⁶ Mezger, Thomas G. **“The Rheology Handbook: for Users of Rotational and Oscillatory Rheometers”** Chapter 2 pp. 21, Hannover: Vincentz Verlag 2002
- ⁷ Einstein, A. **Correction to my paper: “A New Determination of Molecular Dimension”** Annalen der Physik, Vol. 34 pp.591-592, 1911
- ⁸ Batchelor, G. K. **“The Effect of Brownian Motion on the Bulk Stress in a Suspension of Spherical Particles”** Journal of Fluids Mechanics, Vol. 83, part 1 pp. 97-117, 1977
- ⁹ Barnes, H. A. **“A Handbook of Elementary Rheology”** Ch.15 pp.123, University of Wales Institute of Non-Newtonian Fluid Mechanics, Aberystwyth, 2000

- ¹⁰ Anderson, L. G. **“The Coating Processes: Typical Coating Components”** Ch. 2 Section 1 pp.9 TAPPI Press 1993
- ¹¹ Newberry, V. F. **“Introduction to Coating Formulations”** Coating Materials: Pigments, Binders and Additives Short Course pp.1 , TAPPI Press, 1999
- ¹² Welch, L. J. **“Pigments for Coated Papers and Some Interrelationships with Coating Binders”** Coating Binders Short Course, pp. 19 TAPPI Press 1994
- ¹³ Riggin, M. W. **“The Nature of Coating Clays”** Coating Materials: Pigments, Binders, and Additives Short Course pp. 13 TAPPI Press 1999
- ¹⁴ Osterhuber, E. J. **“Precipitated Calcium Carbonate for Paper Coating”** Coating Materials: Pigments, Binders, and Additives Short Course pp. 111-121, TAPPI Press 1999
- ¹⁵ Michel-Sanchez, Enrique **“Pervaporation Using Hydrophilic Membranes”** B.S. Thesis, Ch.5 pp.25, Universidad Popular Autonoma del Estado de Puebla, 2003
- ¹⁶ Vincent, E. M. **“Binders Overview”** Ch. 1, TAPPI Coating Binders Short Course, TAPPI Press 1996
- ¹⁷ Hagemeyer, R.W., **“Pigment Coating”** Pulp and Paper, Chemistry and Chemical Technology, Vol. 4 pp.216-217, J.P. Casey, Ed., 3rd edition., John Wiley & Sons, New York, 1983
- ¹⁸ Kearney, Robert L. **“Starch and Starch Products in Paper Coating”** pp.1, TAPPI PRESS 1990
- ¹⁹ Walter, Jan C. **“The Coating Processes”** pp. 15, TAPPI PRESS 1993
- ²⁰ Chaplin, M. **“Water Structure and Behavior: Starch”**
www.martin.chaplin.btinternet.co.uk/hysta.html accessed October 2004

- ²¹ Department of Polymer Science, University of Mississippi, **“Polymers Up-Close and Personal: Cellulose”**, <http://www.psrc.usm.edu/macrog/cell.htm> 1996, Accessed on October 2004
- ²² Brander, J. Thorn, I. Bacquet, G. Isoard, J.-C. **“Surface Application of Paper Chemicals”** Ch. 3 Section 1 pp.48-49, Blackie Academic and Professional 1997
- ²³ Van Gilder, R. **“High Solids Latex Coating Rheology and Performance”** Papieri Ja Puu pp. 39-40, 1989
- ²⁴ Heiser, E. **“Review of Latex Binder Formulations, Effects on Coated Paper Properties”** Pulp & Paper 1981
- ²⁵ Kane, R. J. **“Paper Coating Additives”** Ch. 1 pp. 5, TAPPI Press 1995
- ²⁶ Roper III, J. A. **“An Introduction to the Rheology of Paper Coatings”** TAPPI Coating Binders Short Course Ch. 3 Section 2, TAPPI Press 1996
- ²⁷ Tadros, Th. F. **“Colloidal and Rheological Phenomena in High Solids Dispersions”** Symposium on Paper Coating Fundamentals, pp. 1-13, TAPPI Press 1991
- ²⁸ Shapiro, A. P. Probst, R. F. **“Random Packing of Spheres and Fluidity Limits of Monodisperse and Bisperse Suspensions”** Physical Review Letters Vol. 68 No. 9 pp. 1422-1425, March 1992
- ²⁹ Metzner, A. B. **“Rheology of Suspensions in Polymeric Liquids”** Journal of Rheology, 29 (6), 739-775, 1985
- ³⁰ Krieger, I. M. **“Structure-Rheology Relations in Dispersions”** Symposium on Paper Coating Fundamentals pp.35-39, 1991
- ³¹ Toivakka, M., Eklund, D. **“Prediction of Suspension Rheology Through Particle Motion Simulation”** Coating Fundamentals Symposium pp. 161-177, 1995

- ³² Hoffman, R. L. **“Factors Affecting the Viscosity of Unimodal and Multimodal Colloidal Dispersions”** Journal of Rheology 36 (5), July 1992
- ³³ Chang, C., Powell, R. L. **“Effect of Particle Size Distributions on the Rheology of Concentrated Bimodal Suspensions”** Journal of Rheology 38 (1), 1994
- ³⁴ Donev, A. et al., **“Improving the Density of Jammed Disordered Packings Using Ellipsoids”** Science 303, pp. 990-993, 2004
- ³⁵ Weitz, D. A. **“Packing in the Spheres”** Science 303, pp. 968-969, 2004
- ³⁶ Lindhjem, C. E. **“Particle Packing and Shape Effects on the Rheological Characteristics of Paper Coating Pigments”** Coating Conference Proceedings Ch. 3 Section 3 pp. 131-142, May 1991
- ³⁷ Kline, J. **“Coatings Formulation”** Coating Materials: Pigments, Binders, and Additives Short Course, Session 22, April 1999
- ³⁸ Nakano, T. Ochi, T. **Personal Communication** Materials R&D Research Group of Nippon Paper Industries, Tokyo, Japan August 2005
- ³⁹ Imerys, Premier Kaolin Clay
- ⁴⁰ Dow Chemical Company, Latex CP 620 NA (co-polymer: Styrene-Butadiene)
- ⁴¹ National Starch & Chemicals, Cationic Starch CAT02A
- ⁴² Schaepe, Michael **Personal Communication** IPST Atlanta Georgia, April 2005
- ⁴³ TAPPI Standards, Method T 480 om-99
- ⁴⁴ TAPPI Standards, Method T 538 om-01

⁴⁵ TAPPI Standards, Method T 452 om-02

⁴⁶ Farris, R. J. **“Prediction of the Viscosity of Multimodal Suspensions from Unimodal Viscosity Data”** Transactions of the Society of Rheology 12(2) pp. 281-301, 1968

⁴⁷ Zaman, A. A., Moudgil, B. M. **“Rheology of Bidisperse Aqueous Silica Suspensions : A new Scaling Method for the Bidisperse Viscosity”** Journal of Rheology 42 (1) pp. 21-39, 1998

⁴⁸ Dames, B. Morrison, B.R., Wilenbacher, N. **“An Empirical Model Predicting the Model of Highly Concentrated Bimodal Dispersions with Colloidal Interactions”** Rheologica Acta 40, pp.434, 2001

⁴⁹ D’Haene, P. D. Mewis, J. **“Rheological Characterization of Bimodal Colloidal Dispersions”** Rheologica Acta 33, pp. 165-174, 1994